

14P
Final Report U9-832400-F

VHF NAVIGATION EXPERIMENT



John F. DuBose, et al
TEXAS INSTRUMENTS, INCORPORATED
Equipment Group
13500 North Central Expressway
P O Box 6015
Dallas, Texas 75222

May 1971

Final Report for Period from September 1969 to December 1971

Prepared for

GODDARD SPACE FLIGHT CENTER
Greenbelt, Maryland 20771

FACILITY FORM 602	<u>N71-35770</u>	
	(ACCESSION NUMBER)	(THRU)
	<u>156</u>	<u>G3</u>
	(PAGES)	(CODE)
	<u>CR-121927</u>	<u>21</u>
	(NASA CR OR TMX OR AD NUMBER)	(CATEGORY)

Reproduced by
**NATIONAL TECHNICAL
INFORMATION SERVICE**
Springfield, Va 22151

1 Report No	2 Government Accession No	3 Recipient s Catalog No	
4 Title and Subtitle VHF NAVIGATION EXPERIMENT FINAL REPORT		5 Report Date May 1971	
		6 Performing Organization Code	
7 Author(s) John F DuBose, et al		8 Performing Organization Report No U9 832400 F	
9 Performing Organization Name and Address Texas Instruments Incorporated 13500 North Central Expressway Dallas, Texas 75222		10 Work Unit No	
		11 Contract or Grant No NAS 5-21079	
		13 Type of Report and Period Covered Type III Final Report September 1969--December 1970	
12 Sponsoring Agency Name and Address National Aeronautics & Space Administration Goddard Space Flight Center Greenbelt, Maryland 20771 Tech Officer C N Smith, Code 752		14 Sponsoring Agency Code	
15 Supplementary Notes			
16 Abstract This report documents the results of an experiment to determine the accuracy that could be obtained in locating the position of an aircraft when using sidetone ranging signals relayed by two synchronous satellites, ATS-1 and ATS-3. A real-time display system was developed by Texas Instruments that allowed the aircraft position, as derived by the satellite system, to be compared with that derived from an airport surveillance radar. The experiment demonstrated that the use of differential position location techniques, could provide location accuracy of approximately 3 nautical miles, further processing reduced the error to 2 nautical miles. Recommendations are made that would improve the system accuracy to approximately 1 nautical mile.			
17 Key Words Satellite Air Traffic Control Satellite Navigation Sidetone Ranging Differential Position Location		18 Distribution Statement	
19 Security Classif (of this report) Unclassified	20 Security Classif (of this page) Unclassified	21 No of Pages 156	22 Price

PREFACE

The objective of this experiment was to determine the accuracy that could be obtained in computing the position of an aircraft when using sidetone ranging measurements between a ground station, Application Technology Satellites ATS-1 and ATS-3, and the aircraft

The ground station employed for this experiment was the Omega Position Location Equipment (OPLE) Control Center (OCC). The OCC was modified to communicate with two satellites, simultaneously, and to generate a 941-Hz sidetone. Two identical VHF transponders were constructed, one for use as a reference terminal, and the other for use as an aircraft terminal.

Texas Instruments provided, as a company-funded effort, a real-time display system which displayed the aircraft position as tracked by both the satellite tracking system and a Texas Instruments airport surveillance radar system (ASR-7).

The experiment demonstrated that an aircraft could be located in real time within approximately 3 nautical miles, further reduction of the data improved this accuracy to 2 nautical miles.

The following recommendations are made for future satellite position location systems, using sidetone ranging:

- 1 A frequency be chosen that is subject to less interference
- 2 Time division multiplexing should be used
- 3 A higher sidetone frequency should be chosen

If these recommendations are adopted, position location accuracies on the order of 1 nautical mile can be achieved.

CONTRIBUTORS

In addition to the Project Engineer, J F DuBose, the following persons contributed to this report

R A Wheeldon
J L Coates
C B Wason
R L Clark
J O Battle
B L Lowe

TABLE OF CONTENTS

<i>Section</i>	<i>Title</i>	<i>Page</i>
I	INTRODUCTION	1-1
A	Program Description	1-2
B	Experiment Description	1-4
II	SUMMARY OF RESULTS	2-1
A	Position Location Results	2-1
B	Results of RF Link Measurements	2-2
1	Link Losses	2-3
2	Satellite Characteristics	2-3
3	System Carrier to Noise Power Density	2-4
III	SYSTEM DESCRIPTION	3-1
A	Major System Component Description	3-1
B	Position Determination Techniques	3-1
1	Absolute Ranging/Absolute Position Determination	3-3
2	Absolute Ranging/Differential Position Determination	3-5
3	Differential Ranging/Absolute Position Determination	3-5
IV	HARDWARE DESCRIPTION	4-1
A	Ground Control Center Description	4-1
B	Transponder Description	4-1
C	Real Time Position Display Equipment	4-4
1	Radar Subsystem	4-4
2	Ground Control Center Subsystem	4-8
V	DESCRIPTION OF THE EXPERIMENT	5-1
A	Subsystem Checkout Phase	5-1
1	Dorne Margolin Aircraft Antenna Pattern	5-1
2	VHF Helical Antenna Pattern	5-1
3	VHF Link Measurements	5-3
4	Satellite Power Transfer Measurements	5-5
B	System Performance	5-5
1	On-Line Position Location and Display	5-5
2	Off-Line Analysis	5-6
VI	ANALYSIS OF EXPERIMENTAL RESULTS	6-1
A	Position Location	6-1
1	Comparison of Position Location Techniques	6-1
2	Comparison of Measured and Expected Errors	6-2
B	RF Link Measurements	6-5
1	Link Losses	6-5
2	Satellite Characteristics	6-6
3	System Carrier-to Noise Power Density	6-9
VII	CONCLUSIONS AND RECOMMENDATIONS	7-1

TABLE OF CONTENTS (Continued)

<i>Section</i>	<i>Title</i>	<i>Page</i>
APPENDIXES		
A—	Ground Control Center Description	
B—	Software Description	
C—	Transponder Description	
D—	Position Error Analysis	
E—	RF Link Analysis	
REFERENCES		

LIST OF ILLUSTRATIONS

<i>Figure</i>	<i>Title</i>	<i>Page</i>
1-1	VHF Navigation Experiment Program Schedule	1-3
2-1	ATS-1 Power Transfer Curve	2-5
2-2	ATS-3 Power Transfer Curve	2-6
3-1	VHF Range/Range Experiment Configuration	3-2
3-2	GCC Receiver Assignments	3-4
4-1	Ground Control Center, Simplified Block Diagram	4-2
4-2	VHF Transponder	4-3
4-3	Transponder, Simplified Block Diagram	4-3
4-4	Real Time Position Display Equipment, Simplified Block Diagram	4-5
5-1	Aircraft Antenna Pattern Measurement Configuration	5-2
5-2	VHF Antenna Pattern Measurement Configuration	5-3
5-3	VHF Link Measurement Configuration	5-4
5-4	Satellite Power Transfer Measurement Configuration	5-6
5-5	On-Line Position Location and Display System, Block Diagram	5-7
6-1	Real Time Display of Flight Experiment Data, File 2	6-3
6-2	Real Time Display of Flight Experiment Data, File 12	6-4
6-3	ATS 1 Power Transfer Curve	6-7
6-4	ATS-3 Power Transfer Curve	6-8

LIST OF TABLES

<i>Figure</i>	<i>Title</i>	<i>Page</i>
2-1	Position Location Errors	2 1
2 2	Comparison of Experimental and Predicted Position Location Errors for Differential Ranging	2-2
2 3	Link Losses	2-3
2-4	Pilot Tone Carrier-to Noise Power Densities	2-7
2-5	Ranging Tone Carrier-to Noise Power Densities	2 7
4-1	Transponder Characteristics	4-7
6-1	Position Location Errors	6-1
6-2	Comparison of Experimental and Predicted Position Location Errors for Differential Ranging	6-2
6-3	Link Losses	6-5
6-4	Pilot Tone Carrier to Noise Power Densities	6 10
6 5	Ranging Tone Carrier to Noise Power Densities	6 10

TEXAS INSTRUMENTS INCORPORATED
EQUIPMENT GROUP
13500 North Central Expressway
P O Box 6015
Dallas, Texas 75222

May 1971

VHF NAVIGATION EXPERIMENT
FINAL REPORT
U9-832400-F

SECTION I
INTRODUCTION

Texas Instruments was selected by NASA Goddard Space Flight Center (GSFC) to conduct the VHF Navigation Experiment (also known as the VHF Range/Range or VHF R/R Experiment) The purpose of the experiment was to determine the accuracy that could be obtained in computing the position of an aircraft, flying at known altitude, using sidetone range measurements between a ground station, the Applications Technology Satellites ATS-1 and -3 and the aircraft The ground station that was used was the OPLE Control Center (OCC), and the self-check feature of this equipment was modified to provide a sidetone range measurement capability using a 941-Hz tone A VHF transponder was also designed and two were constructed, one to function as a reference terminal and the other as the aircraft flight terminal

It was the intent of the contract to use the modified OCC to compute the phase angles associated with the various range measurements and to then perform the position location computations off-line Early in the experiment, however, Texas Instruments recognized the need for on-line (or real-time) position location and display for two reasons First, real-time measurements of the system parameters were essential to simplify checkout during integration and testing Second, it was considered that a real-time demonstration of position location with comparative radar ground truth data would be most effective in showing the utility of satellites to en route surveillance of air traffic Texas Instruments decided, therefore, to support the program with company funding and provided the following items

- Real-time display equipment and software
- Real-time radar data from an ASR-7 airport surveillance radar
- A motion-picture documentation of the real-time position location system

As a result of subsequent schedule conflicts for the FAA aircraft which was originally planned for the flight portions of the experiment, Texas Instruments also donated the use of a DC-3 aircraft, and several successful flight tests were performed in November and December of 1970

The result of this NASA contract, and the funding contributed by Texas Instruments, was a real-time demonstration of aircraft position location using satellites in which an accuracy of

approximately 2 nautical miles was obtained using the differential position location techniques. It is believed that this represented the first real-time demonstration of a basic aircraft surveillance system.

A Program Description

As shown on the accompanying schedule, Figure 1-1, the program was structured in two phases. The first phase dealt primarily with system design, modification/checkout of the OPLE Control Center available at NASA/GSFC from the OPLE Contract (NAS 5-10248), and development of a reference terminal ranging transponder. The second phase option was exercised by NASA in January 1970, and involved developing a ranging transponder for the aircraft, testing the transponders, and experiment flight testing following installation of the transponders.

The schedule shows a number of other tests performed using the ground station in its OPLE mode to accommodate other agencies in evaluating such systems as Position Location by Orbital Tracking (PLOT), and Global Rescue Alarm Net (GRAN). As these tests were not part of the present contract they are not discussed here, but are noted on the schedule to show some of the overlap of usage of the OPLE Control Center.

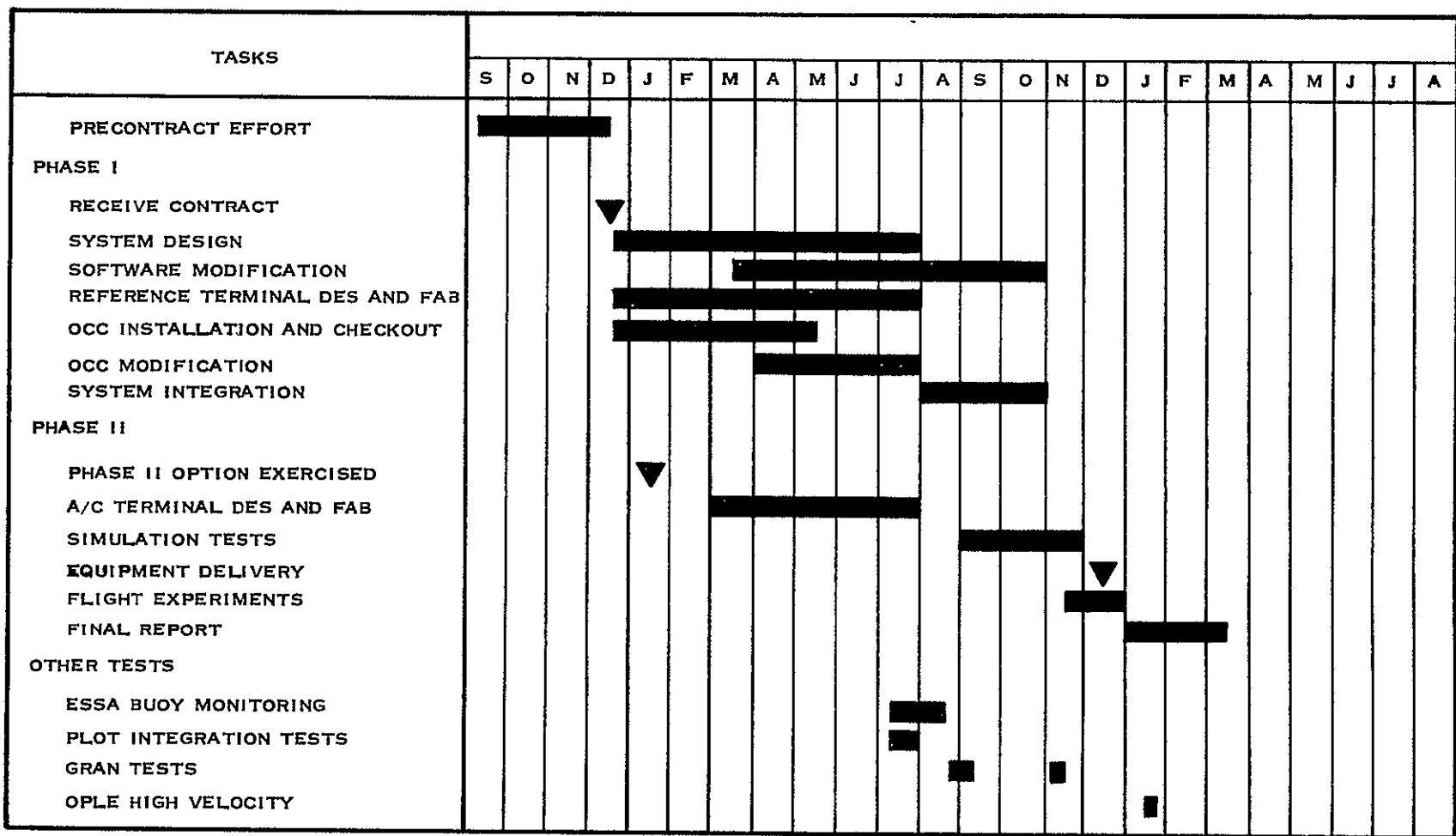
During integration of the system it was established that the link estimates made in the original proposal were optimistic, and that a number of system parameters would require modification to allow the system to acquire lock. The major sources of additional link loss were:

- Aircraft voice communications interference in the frequency band at 135.6 MHz during daylight hours. (It was established that this interference was caused by direct radiation from aircraft in the Dallas area.)
- Capture of a significant part of the ATS-3 satellite transponder power as a result of continuous interference from ground radio sources.

To improve the performance of the satellite communications links, experiments were scheduled late in the evening to minimize the possibilities of interference from the above two causes. To provide additional margin, the aircraft and reference terminal transmitter powers were increased from 5 watts to 20 watts, and the acquisition bandwidth of the OCC phase-locked loops was decreased from 150 Hz to 50 Hz.

As a result of the relatively narrow sweep range of the phase-locked loops in the OCC, it was also necessary to establish high-frequency accuracy (± 100 Hz) in both the pilot tone channel and the ranging signal transmission and receiving channels. The pilot tone channel had previously been incorporated into the OCC during the OPLE experiment to remove phase jitter in the transponded signal induced by one-way passage of a signal through the ATS-3 satellite. Once these factors were incorporated into the system, integration was completed and the flight and static experiments were performed.

The data from a number of tests were then computer analyzed off-line (during the Final Report task of Phase II) to determine the rms, mean and deviation position errors, and to compare the deviation errors with predicted errors. The results obtained for both the static and flight tests show very good agreement between predicted and measured errors.



124067

Figure 11 VHF Navigation Experiment Program Schedule

B Experiment Description

The method used for determining the position of the aircraft involved measuring the ranges of the aircraft from ATS-1 and ATS-3, and then knowing the aircraft altitude, solving for the two points of intersection of the three spheres centered on each satellite and the center of the earth and choosing the solution in the northern hemisphere. The ranges of the aircraft to both satellites are determined in essentially two ways. In the first method, called absolute ranging, the range from the control center to the aircraft and back through the appropriate satellites is computed using (1) the differences in phase between that measured over the path and that measured in the calibration mode using the reference terminal, and (2) the known range from the reference terminal to the satellite at the time of making the calibration measurement. In the second method, called differential ranging, the ranges of the aircraft to the satellites are determined in a similar manner except that effectively new calibration measurements through the reference terminal were used for each measurement obtained from the aircraft. In this way, common mode errors caused by changes in the satellite position and equipment drift were significantly reduced.

Although the computer in the OCC was programmed in the OPLE experiment to compute phase measurements only, the program was enlarged to solve the position location algorithm from the phase data, and to convert radar range and bearing information into latitude and longitude. The digital outputs from the computer were then converted to analog voltages and used in a time multiplexed manner, to control the position of the display spot of a TV monitor. A scale map of the Dallas area was provided as a transparent overlay on the screen.

In performing a real-time experiment, the aircraft flight began approximately one-half hour before the assigned satellite time and the equipment would be checked out. At the beginning of satellite time, a calibration test was made at the OCC with all four of the OPLE receivers, or phase measurement receivers, assigned to receive signals relayed by ATS-3 from the reference terminal. The OCC was then placed in the acquisition mode and two phase measurement receivers assigned to each of the aircraft terminal and to the reference terminal. In each pair, one receiver would receive signals relayed by ATS-3 and one would receive signals relayed by ATS-1.

A frequency check would then be performed to realize the required tolerance for acquisition. Any corrections found necessary were accomplished using the synthesizers in the down-conversion system. Once these corrections were made, the system would lock and the real-time position determination could proceed.

SECTION II

SUMMARY OF RESULTS

This section presents a summary of the experimental results. A detailed analysis of these results is provided in Section VI.

A Position Location Results

A large number of checkout flights and experiment flights were made during the course of the VHF Range/Range Experiment using the ATS-1 and ATS-3 satellites, the modified OPLE Control Center, and a Texas Instruments airport surveillance radar (as a source of ground track truth data). These flights were made with a Texas Instruments DC-3 and limited to a range of 70 miles from Dallas.

Because of the large number of data points taken during each experiment, an off-line software program was written and used to analyze the data for two of the flights and two static tests. Table 2-1 gives a comparison of the rms latitude and longitude errors for the three methods of position location employed (discussed in Section III). Both the differential ranging and differential position location techniques proved to be superior to the absolute ranging technique. This is particularly well illustrated in Flight Data File 2 where the latitude error is approximately 10 times greater in the absolute mode than in the differential modes.

TABLE 2-1 POSITION LOCATION ERRORS

Experiment Description	No Samples	Absolute Ranging		Differential Position		Differential Ranging	
		Latitude Error (nmi)	Longitude Error (nmi)	Latitude Error (nmi)	Longitude Error (nmi)	Latitude Error (nmi)	Longitude Error (nmi)
Flight Data							
File 2	177	18.29	2.64	1.70	3.05	1.63	3.22
File 12	91	5.34	6.11	4.38	2.15	4.14	2.21
Static Data							
File 5	116	4.34	2.46	4.51	1.23	4.27	1.38
File 6	140	3.65	5.07	2.92	1.85	2.57	2.03

The data presented in Table 2-1 includes bias errors which are not common-mode effects in the differential position location modes, as well as random error sources. The error sources include:

- Part of the propagation errors caused by the ionosphere and troposphere
- Measurement errors caused by system noise and ground processor inaccuracies
- Delay errors caused by uncompensated delays of aircraft transponder, reference transponder, satellite transponders, and the ground processor
- Satellite position uncertainty

As shown in Table 2-1, the position location error using the differential techniques are approximately 3 nautical miles (nm). To illustrate that improved accuracy can be obtained, the data was analyzed to separate the mean error and the error deviation from the mean. The results obtained from this analysis are shown in Table 2-2, where they are compared with the predicted results.

TABLE 2-2 COMPARISON OF EXPERIMENTAL AND PREDICTED POSITION LOCATION ERRORS FOR DIFFERENTIAL RANGING

Description	Experimental Results						Predicted Results	
	Latitude Error (nmi)			Longitude Error (nmi)			Latitude Error (nmi)	Longitude Error (nmi)
	rms	Mean	Deviation	rms	Mean	Deviation		
Flight Data								
File 2	1.63	0.22	1.61	3.22	2.97	1.23	2.75	1.75
File 12	4.14	-3.49	2.44	2.21	1.53	1.59	2.75	1.75
Static Data								
File 5	4.27	4.13	1.09	1.38	1.08	0.86	1.50	0.93
File 6	2.57	-2.06	1.53	2.03	1.83	0.88	1.50	0.93

Agreement between the predicted and measured deviation errors is very good. The longitude deviation errors for the static tests of Files 5 and 6 are 0.86 and 0.88 nm, respectively, as compared with a predicted error of 1.50 nm.

A comparison of the predicted and measured deviation errors for the flight tests shows that the actual errors are consistently less than the predicted errors. For example, the predicted latitude error is 2.75 nm, but the measured results for Files 2 and 12 are 1.6 nm and 2.44 nm, respectively. The predicted longitude error is 1.75 nm, while the measured results were 1.23 nm and 1.59 nm for Files 2 and 12, respectively.

In summary, the VHF Range/Range Experiment demonstrated that VHF sidetone ranging using synchronous satellites for relay of signals can produce position accuracy on the order of 3 nm using differential ranging techniques. If bias errors are taken into account, the location accuracy can be improved to better than 2 nm. A more optimum implementation of the ranging tones would improve the position location accuracy to approximately 1½ nm.

B Results of RF Link Measurements

As discussed in the introduction, it became necessary during the experiment to optimize the various system transmitted signal levels to achieve satisfactory results. Although the RF link measurements were not included in the original goal of the experiment, a considerable effort was expended in gathering and analyzing these measurements. A summary of these measurements is presented in following paragraphs; detail discussion of these measurements is located in Sections V and VI.

1 Link Losses

The procedure used to measure the down-link losses is described in Subsection V A 3. The experimentally determined up-link losses were derived from the measured down-link losses by taking into consideration the theoretical difference in free space losses, and cable and diplexer losses. Over a 2-month period, several measurements were made for each of the link losses and the values tabulated in Table 2-3 are an average of these measurements. The predicted values are derived in Appendix E.

TABLE 2-3 LINK LOSSES

Link	Predicted (dB)		Measured (dB)
	Nominal	Worst Case	
GCC-to-ATS-3	-157	-161.2	-159
Aircraft-to-ATS 3	-171.3	-178.5	-170
Aircraft-to-ATS 1	-171.3	-178.5	-170
Reference-to-ATS 3	-172.3	-176.5	-169
Reference to-ATS-1	-172.3	-176.5	-174
ATS-3-to-GCC	-155.7	-159.7	-158
ATS-3-to-Aircraft	-171.2	-178.2	-170
ATS-3 to-Reference	-170.7	-174.7	-168
ATS-1-to-GCC	-154.2	-158.2	-160

As shown in Table 2-3, with the exception of the ATS-1-to-GCC loss, the measured and predicted nominal link losses agree to within approximately 3 dB. The discrepancy in the predicted and measured ATS-1 link loss was most likely caused by the relatively low elevation angle (21 degrees) of the satellite at the time the measurements were made.

As was anticipated, the signal levels at the aircraft showed considerable multipath related variations. These signal fluctuations were on the order of 4 dB. This should be considered only as a nominal multipath effect because larger variations can be encountered if the aircraft is flying toward or away from the satellite. The effects were especially pronounced during the time that the aircraft was ascending or descending.

2 Satellite Characteristics

Power transfer curves for ATS-1 and ATS-3 VHF repeaters were experimentally determined (as described in Subsection V A 4) by varying the power of the pilot tone transmitted to the satellite under test and measuring the received signal level at the GCC. Theoretical transfer curves were generated and compared with the experimental data to verify the link losses and power sharing at the satellites.

The resulting power transfer curves for ATS-1 and ATS-3 are shown in Figures 2-1 and 2-2, respectively. Comparison of the two experimental satellite power transfer curves shows that ATS-3 was approaching saturation with the GCC transmitting 50 dBm of pilot tone power while ATS-1 was still several decibels below saturation. This difference reflects the higher link loss between the GCC (ATS-3 antenna) and ATS-1. The satellite transfer characteristics are essentially linear for transmitted levels less than 42 dBm because the predominant satellite input power is

the relatively constant noise power. For GCC transmitted levels greater than 42 dBm, the received pilot tone signal at the satellite is a significant component of the total input power and the slope of the transfer curve begins to decrease.

Comparison of the experimental and predicted curves shows a 1-dB-maximum deviation for the ATS-1 data and a 2-dB-maximum deviation for the ATS-3 data. Because the predicted and experimental transfer curves approach saturation at the same GCC transmitter power level, it can be concluded that if the link losses are correct, then the assumed -113-dBm satellite noise power is also valid. This is true because the slope of the transfer curve begins to decrease rapidly when the received signal is on the same order of magnitude as the noise power. The discrepancy between the measured and predicted ATS-3 power transfer curve is most likely caused by the one-way link loss being approximately 1 dB greater during the test than the values used for the theoretical curve. If this 1-dB error existed for both the up and down links, then the net result would be an experimentally determined curve which is down by 2 dB from the predicted curve.

3 System Carrier-to-Noise Power Density

The details of the techniques employed in this experiment to determine the signal-to-noise power densities at the various receivers are discussed in Subsection V A 3. During each experiment, data from the meters used for this purpose was recorded at specified intervals while chart recorders provided a continuous record of received signal strengths.

As discussed in Appendix E, the carrier-to-noise power density at any receiver is partially determined by the link losses between each repeater. Monitoring of the ATS-3 retransmitted pilot tone signal at the GCC and the transponders provided data for verification of power sharing at ATS-3. The predicted and measured pilot tone C/N_0 values are listed in Table 2-4 and 2-5. The predicted data is derived in Appendix E.

Chart recordings at the reference transponder showed that the received signal was relatively constant during an experiment period. With the exception of local or satellite interference, signal variations in excess of 3 dB rarely occurred. The received pilot tone signal at the GCC also remained relatively free of short term fluctuations. The received signals at the aircraft, however, did exhibit frequent short term fluctuation of a larger magnitude than observed at the reference transponder. These signal strength variations were caused by local interference and multipath effects. During periods of heavy interference, the aircraft transponder would frequently lose lock. Because of this problem, the experiments were scheduled for a later time at night.

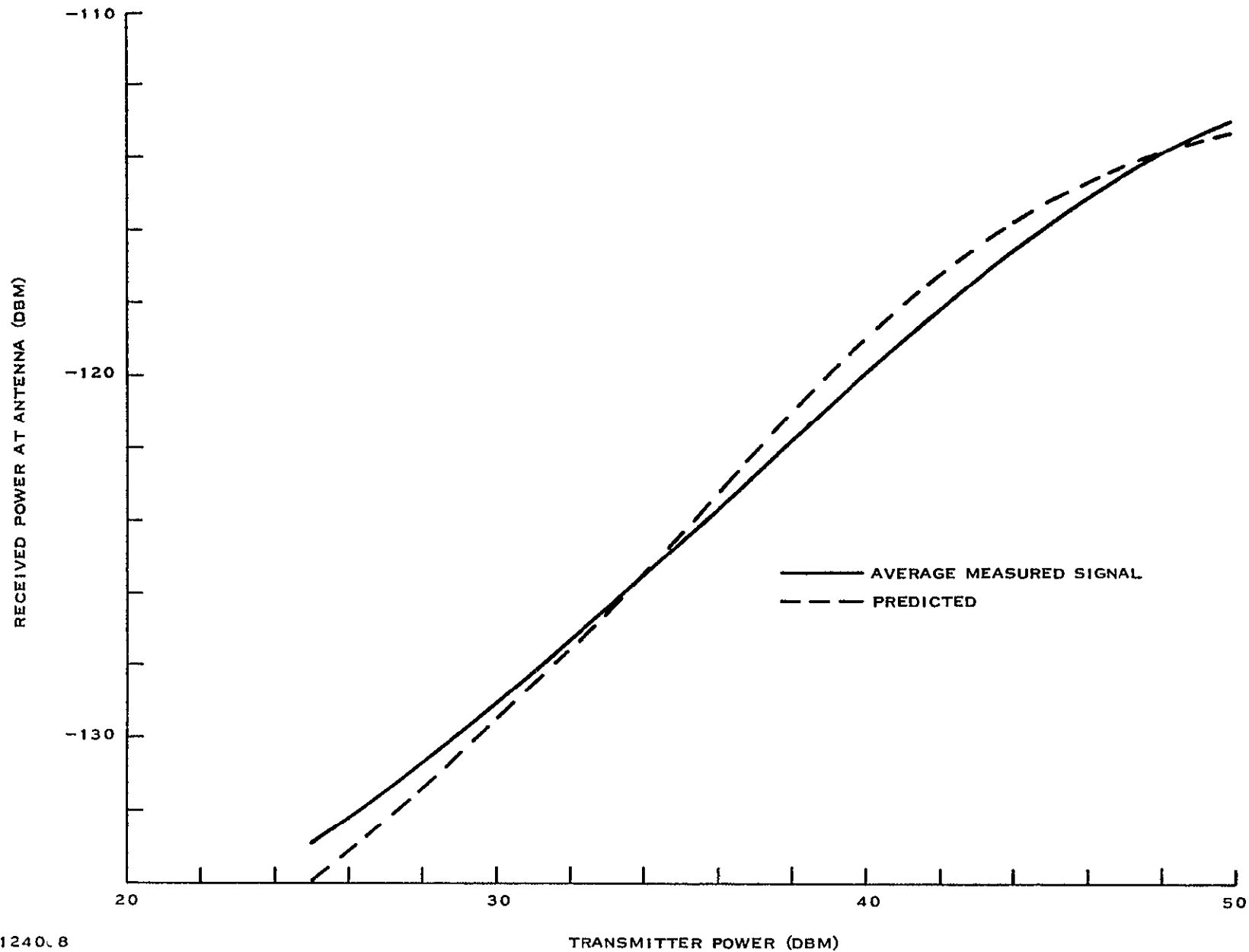
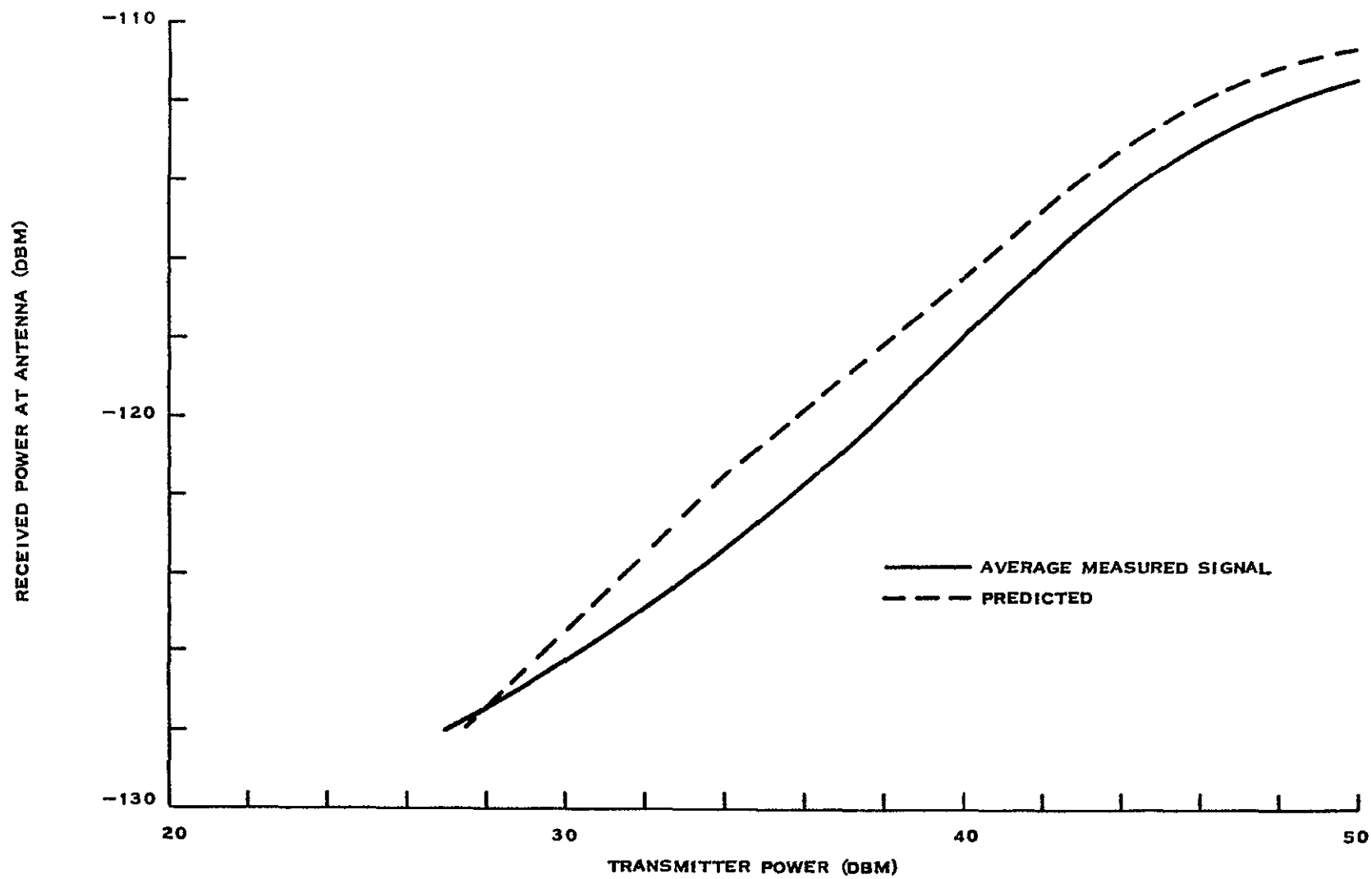


Figure 2-1 ATS-1 Power Transfer Curve



124069

Figure 2-2 ATS 3 Power Transfer Curve

TABLE 2-4 PILOT TONE CARRIER-TO-NOISE POWER DENSITIES

Receiver	Predicted		Measured			
	Nominal (dB Hz)	Worst Case (dB Hz)	Maximum* (dB Hz)	Average* (dB Hz)	Maximum† (dB-Hz)	Average† (dB-Hz)
GCC	48.3	43.1	47.2	46.2	51.8	51
Aircraft	36.8	28.2	34	33.6	39.4	36.4
Reference	37.3	31.7	41	34.9	39	37.8

* Early evening, moderate interference

† Late evening/early morning, low interference

TABLE 2-5 RANGING TONE CARRIER-TO NOISE POWER DENSITIES

Receiver	Predicted	Measured			
	(dB Hz)	Maximum* (dB Hz)	Average* (dB Hz)	Maximum† (dB Hz)	Average† (dB Hz)
1	28.7	29.7	26.2	29	25.5
2	27	28.9	27.4	32	28.3
3	30	29.9	27.9	30.2	28.8
4	28.3	30.7	27.5	30.6	31.1

SECTION III

SYSTEM DESCRIPTION

This section describes the major system components comprising the VHF Range/Range Experiment, the differential ranging techniques utilized, and the subsequent determination of position. A more detailed description of the system hardware is presented in Section IV and the appendixes, a detailed analysis of the algorithm utilized to determine position is also presented in the appendix material.

A Major System Component Description

The major components comprising the VHF Range/Range Experiment are depicted in Figure 3-1 and consist of the Ground Control Center (GCC), reference transponder, aircraft transponder, ATS-1 satellite, and the ATS-3 satellite. Another vital component in the experiment itself was Texas Instruments ASR-7 airport surveillance radar which is also depicted in Figure 3-1. The radar unit was utilized to provide truth measurements of the aircraft location against which VHF Range/Range determined position could be compared.

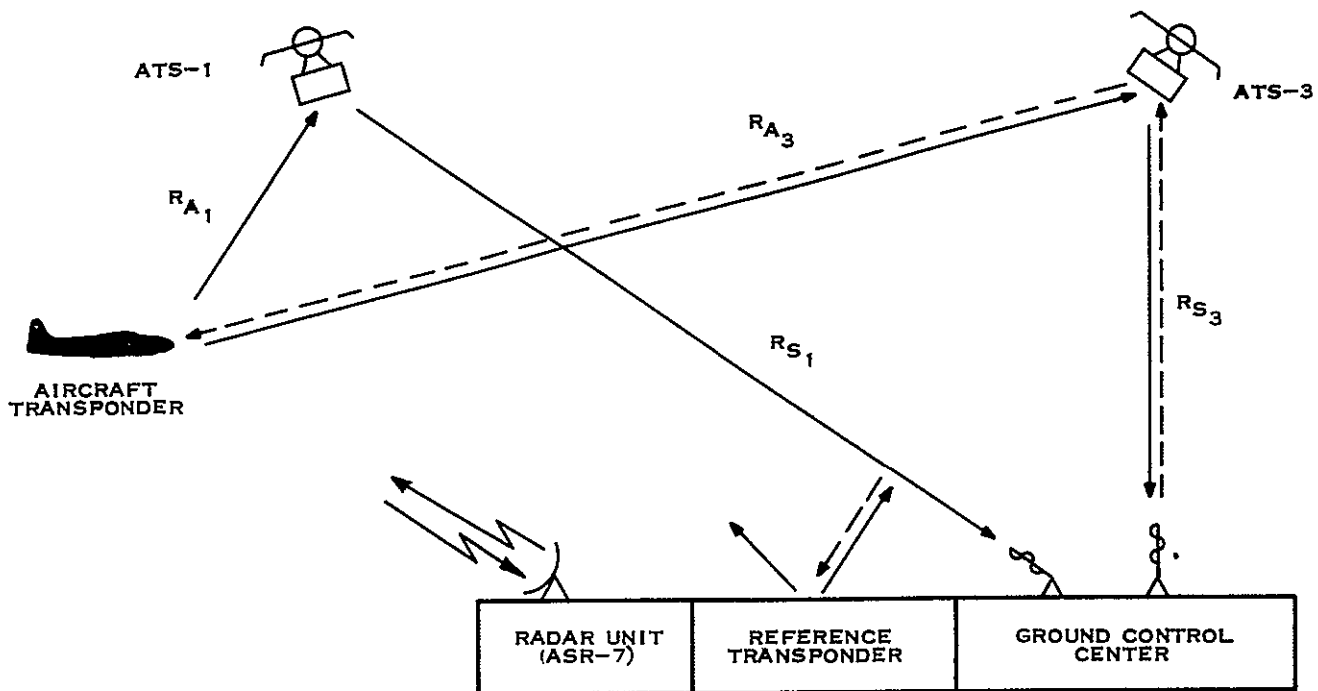
The ground control center was located in the North Building of Texas Instruments Dallas plant. Housed in the same room with the GCC was the reference transponder. The aircraft transponder was mounted onboard a DC-3 aircraft which flew within a 35-mile radius of the location of the GCC. At the time the experiment was conducted, the ATS-1 satellite was located approximately 0° latitude and 150° west longitude and the ATS-3 satellite was located approximately 0° latitude and 45° west longitude.

Each satellite serves as a transponder which receives in a 100-kHz frequency band centered at 149.22 MHz and transmits in a 100-kHz frequency band centered at 135.6 MHz. The ATS-3 satellite receives from and transmits to both the GCC and the transponders, whereas the ATS-1 satellite only receives from the transponders and transmits to the GCC. Thus the ATS-3 satellite is termed the "master" satellite in that it transmits the ranging tones to the transponders, whereas the ATS-1 satellite is termed the "slave" satellite in that it merely relays the transponded ranging tones from the transponders back to the GCC.

The aircraft and reference transponders receive at 135.6 MHz and transmit at 149.22 MHz. The required ranging tones are generated at the Ground Control Center, relayed via the ATS-3 satellite to the aircraft and the reference transponders, retransmitted by the transponders on two different frequency channels to the GCC via both the ATS-1 and ATS-3 satellites, and processed at the GCC to determine the path lengths from the remote terminals to the satellites. A more detailed description of the position determination techniques utilized, in particular the concept of differential ranging, is presented in the following subsection.

B Position Determination Techniques

The position of the remote or aircraft transponder is defined by the intersection of three spheres of position, each of which includes the aircraft terminal's position. One sphere is concentric with the earth's surface and has a radius defined by the known altitude of the aircraft.



124070

Figure 3 1 VHF Range/Range Experiment Configuration

transponder plus the earth's radius. A second sphere is centered at the ATS-1 satellite position and has a radius equal to the measured range from the transponder to the satellite (R_{A1}). Similarly, a third sphere of position is defined by the measured range from the transponder to the ATS-3 satellite (R_{A3}). The distance from each satellite to the aircraft terminal can be determined by measuring the phase differences between the tones transmitted by the GCC and the tones received from the aircraft terminal via both the ATS-1 and ATS-3 satellites. The mathematics and coordinate system involved in transforming the phase measurements to distance measurements, and the subsequent calculation of position, is presented in detail in Appendix B.

In determining the phase differences, and making the subsequent position location calculations, there are basic sources of error with which to contend. These sources are ionospheric effects, drifts in satellite position, bulk equipment delays, and drifts in the bulk equipment delays. These error sources can be reduced to a second-order effect by establishing some form of a differential technique utilizing a reference transponder. However, the use of a reference transponder is complicated by the receive system in the GCC being a frequency division multiplex rather than a time division multiplex system. The aircraft and reference transponders have to be assigned to two different transmit frequency channels and subsequently received by two different receive channels in the GCC whose bulk delay differs. This problem can be resolved by utilizing a "calibration run" where all receive channels in the GCC are assigned to the reference transponder.

To determine the effectiveness of reducing the above-mentioned error sources, three different algorithms were utilized in making the position location calculations. These three methods

are

Position location using absolute ranging

Differential position location using absolute ranging

Position location using differential ranging

Each of these methods will be discussed in detail in the paragraphs that follow

1 Absolute Ranging/Absolute Position Determination

Figure 3-2 depicts the receiver assignments utilized for all three of the above-listed methods, the phase measurements, ϕ_n , from each of the four receivers contain the following ranging information

$$\phi_1 \rightarrow 2R_{s_3} + 2R_{A_3} + \epsilon_1$$

$$\phi_2 \rightarrow 4R_{s_3} + \epsilon_2$$

$$\phi_3 \rightarrow R_{s_3} + R_{A_3} + R_{A_1} + R_{s_1} + \epsilon_3$$

$$\phi_4 \rightarrow 2R_{s_3} + 2R_{s_1} + \epsilon_4$$

The nomenclature utilized here is consistent with that depicted in Figure 3-1. In a true absolute ranging/absolute position location determination scheme, the phase error terms ϵ_1 and ϵ_3 would be ignored, and the ranges R_{A_1} and R_{A_3} would be determined by

$$R_{A_3} = \frac{K\phi_1 - 2R_{s_3}}{2}$$

$$R_{A_1} = K\phi_3 - R_{s_3} - R_{s_1} - R_{A_3}$$

where K is a phase delay-to-distance conversion constant. However, it was found that the bulk delays, especially in the GCC receivers, were too great to allow any reasonable results to be obtained. Hence, a calibration run was utilized to reduce the bulk delays to a second-order effect. To aid in describing the usefulness of a calibration run, the error terms ϵ_n will be examined more closely.

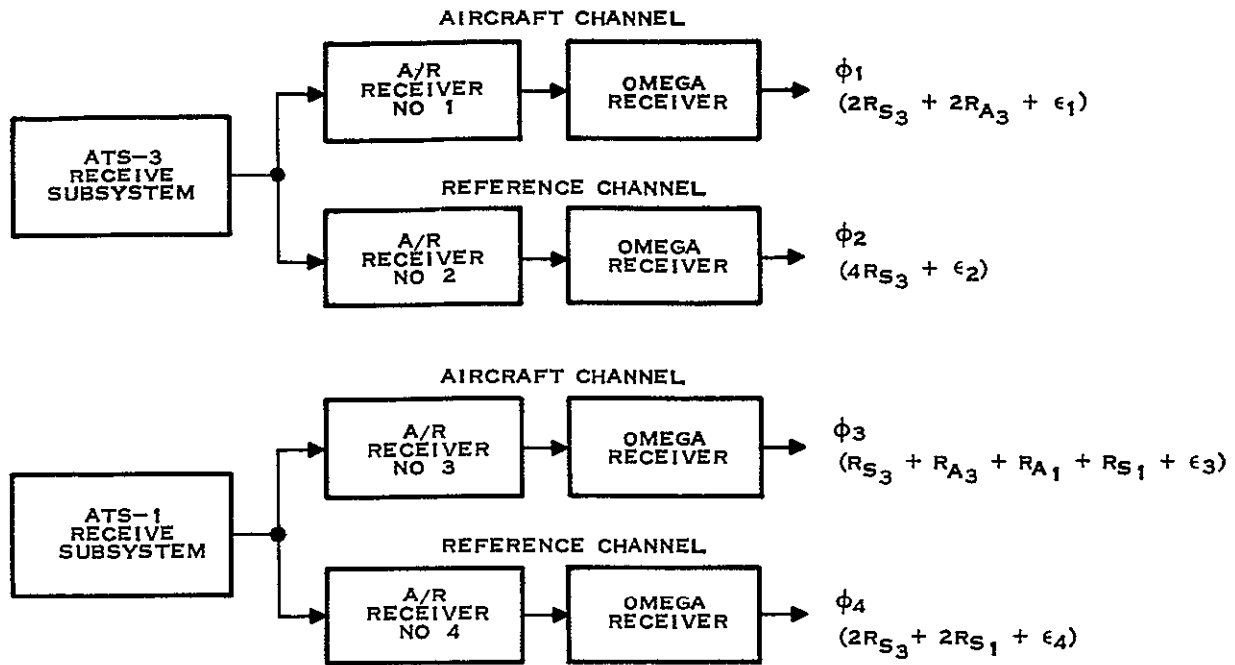
Each error term ϵ_n is composed of a common mode error and a receiver error, or more definitively

$$\epsilon_1 = 2\epsilon_{cm_3} + \epsilon_{R_1}$$

$$\epsilon_2 = 2\epsilon_{cm_3} + \epsilon_{R_2}$$

$$\epsilon_3 = \epsilon_{cm_3} + \epsilon_{cm_1} + \epsilon_{R_3}$$

$$\epsilon_4 = \epsilon_{cm_3} + \epsilon_{cm_1} + \epsilon_{R_4}$$



124071

Figure 3-2 GCC Receiver Assignments

where

ϵ_{cm_3} = common mode error in path from GCC to ATS-3 satellite to transponder, or vice versa

ϵ_{cm_1} = common mode error in path from transponder to ATS-1 satellite to GCC

ϵ_{R_n} = error associated with particular A/R tone and Omega receiver chain at GCC

It is assumed in the above definitions of the error terms that the aircraft transponder and reference transponder were located close enough to one another that the errors derived in going to or from a given satellite to either the reference or aircraft transponder were identical

In the calibration run all four GCC receivers are assigned to the reference transponder. The resulting phase measurements (ϕ_{n_c}) contain the following ranging information

$$\phi_{1_c} \rightarrow 4R_{s_3} + 4\epsilon_{cm_3} + \epsilon_{R_1}$$

$$\phi_{2_c} \rightarrow 4R_{s_3} + 4\epsilon_{cm_3} + \epsilon_{R_2}$$

$$\phi_{3_c} \rightarrow 2R_{s_3} + 2R_{s_1} + 2\epsilon_{cm_3} + 2\epsilon_{cm_1} + \epsilon_{R_3}$$

$$\phi_{4_c} \rightarrow 2R_{s_3} + 2R_{s_1} + 2\epsilon_{cm_3} + 2\epsilon_{cm_1} + \epsilon_{R_4}$$

Subtracting the calibration measurements from the phase measurements would reduce all fixed, time-invariant, phase error terms to a second-order effect. The subtraction of calibration data from the phase data, and the subsequent determination of position is defined in this report as the absolute ranging/absolute position determination method, although it is a method in which time-invariant error sources are reduced to a second-order effect.

2 Absolute Ranging/Differential Position Determination

This method attempts to reduce to a second-order effect the time-variant errors caused by equipment delay drifts and drifts in the satellite positions. In this method, GCC receivers 2 and 4 are utilized to calculate, by the absolute ranging/absolute position determination method, the location of the reference transponder. Since the position of the transponder is known a priori, Δ latitude and Δ longitude errors can be determined and applied to the aircraft latitude and longitude readings. This method assumes that the time-variant errors in the phase measurements can be linearly reduced to a second-order effect by subtracting position measurements resulting from the phase measurements.

3 Differential Ranging/Absolute Position Determination

This method also attempts to reduce to a second-order effect the time-variant errors. In this method, however, the time-variant phase errors are reduced to a second-order effect at the phase measurement level, rather than the position determination level. In this method, the ranges R_{A_1} and R_{A_2} are determined by the following equations:

$$R_{A_2} = R_{s_3} \frac{(\phi_2 - \phi_{c_2}) - (\phi_1 - \phi_{c_1})}{2}$$

$$R_{A_2} = R_{s_1} + (\phi_3 - \phi_{c_3}) + \frac{(\phi_2 - \phi_{c_2}) - (\phi_1 - \phi_{c_1})}{2}$$

The advantage of this method over the absolute ranging/differential position determination method is that the time-variant phase errors are linearly reduced to a second-order effect before being applied to the quadratic position determination equations.

As previously mentioned, the mathematics and coordinate system involved in transforming the phase measurements to distance measurements, and the subsequent calculation of position, is presented in detail in Appendix B. However, Appendix B only describes the on-line position determination software utilized in the GCC data processor, and thus does not cover the differential ranging/absolute position determination method. The data for this method was obtained off-line in a separate computer program utilizing the raw phase data stored on magnetic tape by the on-line GCC software.

SECTION IV

HARDWARE DESCRIPTION

A Ground Control Center Description

The Ground Control Center (GCC) utilized in the VHF Satellite Navigation Experiment consists of the OPLE Control Center modified to meet the requirements of the VHF Navigation Experiment. The modifications were made in such a way that the equipment can be readily converted to either an OPLE Experiment configuration or a VHF Range/Range configuration. This section will briefly describe the function of the GCC in the VHF Range/Range Experiment. Description of the component parts of the GCC, the modifications made to the equipment, and the software developed for the VHF Range/Range Experiment are provided in Appendix A.

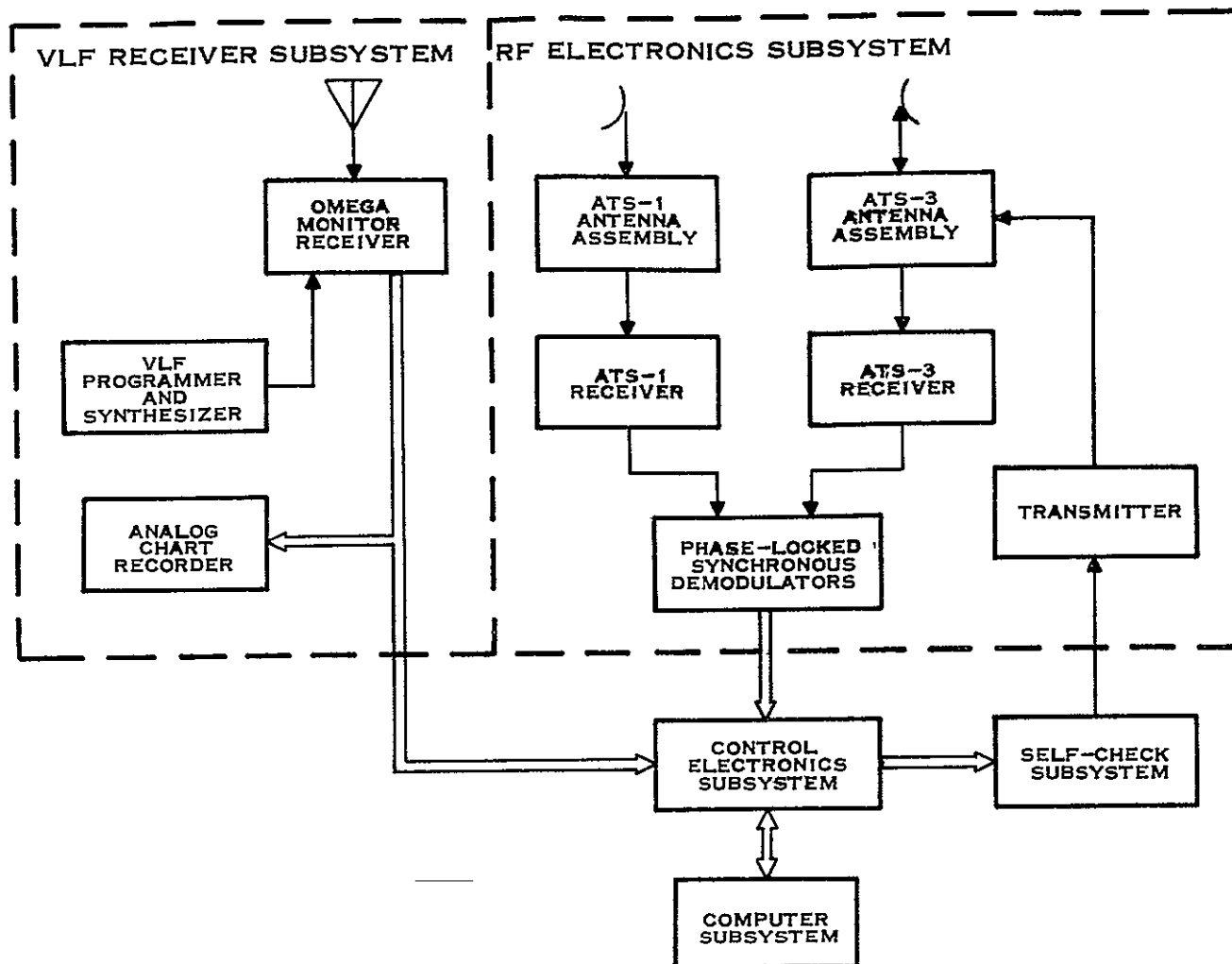
The GCC, as shown in the simplified block diagram in Figure 4-1, generates the ranging tones (in the self-check subsystem) and transmits them to the ATS-3 satellite. The returned ranging tones are received from the ATS-1 and ATS-3 satellites, coherently demodulated, and processed in the data processor.

The ranging tones and the Acquisition/Reference (A/R) tone output of the self-check subsystem are up-converted to approximately 10.78 MHz and summed with the output of the Pilot Tone Transmit synthesizer. The resulting output of the summing amplifier is then up-converted to approximately 149.2 MHz, amplified, passed through the ATS-3 VHF diplexer, and transmitted to the ATS-3 satellite. The received signal from the ATS-3 satellite is passed through the ATS-3 diplexer to the preamplifier and down-converted to 5 MHz in the ATS-3 NEMS-CLARKE VHF receiver. The pilot tone phase-lock loop acquires phase lock to the received pilot tone which is included in the 5-MHz IF output of the VHF receiver. Then, via the pilot tone phase-lock loop feedback input to the VHF receiver, the frequency jitter introduced by the ATS-3 satellite on the return link from the transponders is tracked out. The 5-MHz output of the ATS-3 VHF receiver is also applied to the A/R tone phase-lock loops No. 1 and No. 2, which provide the capability for receiving two separate ranging tone channels from the ATS-3 satellite. One channel is assigned to the aircraft transponder, and the other channel is assigned to the reference transponder or a second aircraft transponder.

A pilot tone phase-lock loop is not required on the ATS-1 NEMS-CLARKE VHF receiver. The transponders remove the frequency jitter introduced by the ATS-3 satellite on the link to the terminal, and frequency jitter is not introduced by the ATS-1 satellite on the return link to the GCC. The 5-MHz output of the ATS-1 VHF receiver is applied to the A/R tone phase-lock loops No. 3 and No. 4. Again, one channel is assigned to the aircraft transponder and the other channel is assigned to the reference transponder or a second aircraft transponder.

B Transponder Description

The transponder developed for the VHF Navigation Experiment functions as a transponder for the ranging signals as received from ATS-3. Two of the transponders were constructed, one for use as a reference terminal at the GCC, and one for use as an aircraft terminal in the aircraft being tracked during the experiment. Both of these transponders were identical (except for transmit frequency) and were packaged in a standard 1/2 long Austin Trumbell Radio (ATR).



124072

Figure 4-1 Ground Control Center, Simplified Block Diagram

case as shown in Figure 4-2. The following paragraphs provide a brief description of the transponder, a more detailed description is provided in Appendix C.

The transponder, as shown in Figure 4-3, consists of a dual conversion receiver (containing a pilot tone phase-lock loop), a transmitter and a diplexer. The incoming signal, as received from ATS-3, includes a pilot tone and a set of ranging tones (one Acquisition/Reference tone and one sidetone spaced 941 Hz away from the A/R tone).

The receiver converts the incoming signal (at 135.6 MHz) to a first IF frequency of 70 MHz. At that point the signal is converted to second IF frequencies of 10.7 MHz and 10.665 MHz, which are the IF frequencies of the pilot zone and ranging signals, respectively. The pilot tone phase-lock loop locks the incoming pilot tone to an internal reference oscillator (at 10.7 MHz).

Although the main function of this phase-lock loop is to remove low frequency phase jitter (imparted by ATS-3) from the ranging signal, it also centers the ranging signals in the 10 665-MHz IF filter

The ranging signal spectrum, after being filtered and amplified at 10 665 MHz, is up-converted to 149 2 MHz and amplified for transmission to a 4-watt level. The 149 2-MHz signal then passes through the diplexer (which isolates the transmitter and receiver) before being sent to the antenna.

During the experiment, it was determined that the transponder output power needed further amplification to a 30-watt level. As an expedient, Texas Instruments provided a commercial vacuum tube linear amplifier (Gonset Model 903A) for each of the two transponders. The Gonset linear amplifier was driven by the solid-state power amplifier in the transponder, the Gonset's output was connected to the transmit part of the diplexer in place of the normal (internal) solid-state power amplifier's output.

Table 4-1 describes the operating characteristics of the transponder.

C Real-Time Position Display Equipment

The real-time position display equipment was developed by Texas Instruments on internal funds for on-line system checkout purposes. This equipment proved invaluable in system debugging in that an on-line display of the position computation was available for immediate analysis, rather than having to take the system off-line to verify the data. A block diagram of the real-time position display equipment is shown in Figure 4-4.

The equipment is basically divided into two sections or subsystems, one subsystem being located at the radar facility and the other subsystem at the Ground Control Center. The subsystem at the radar facility counts azimuth and range pulses until a target with a predetermined window on the planned position indicator (PPI) has been recognized. At this time the azimuth and range counts are transmitted via telephone lines to the subsystem at the Ground Control Center. At the Ground Control Center the received data is input into the DMI Data-620 computer via the control electronics subsystem. The position location data, both radar and VHF Range/Range determined, is output from the 620 computer via the control electronics subsystem to a bank of registers and digital-to-analog converters. The analog signals are multiplexed and then presented on a Hewlett-Packard 1300A X-Y display unit. Each of the two subsystems comprising the real-time position display equipment are discussed in detail in the following subsections.

1 Radar Subsystem

The subsystem at the radar site interfaces with a Texas Instruments type ASR-7 Airport Surveillance Radar. Definitions of the signals from the ASR-7 radar utilized by the radar system are:

ACP—Azimuth change pulse, 4096 of these pulses occur in 360 degrees

ARP—Azimuth reference pulse, pulse that occurs when the radar antenna is pointing true north

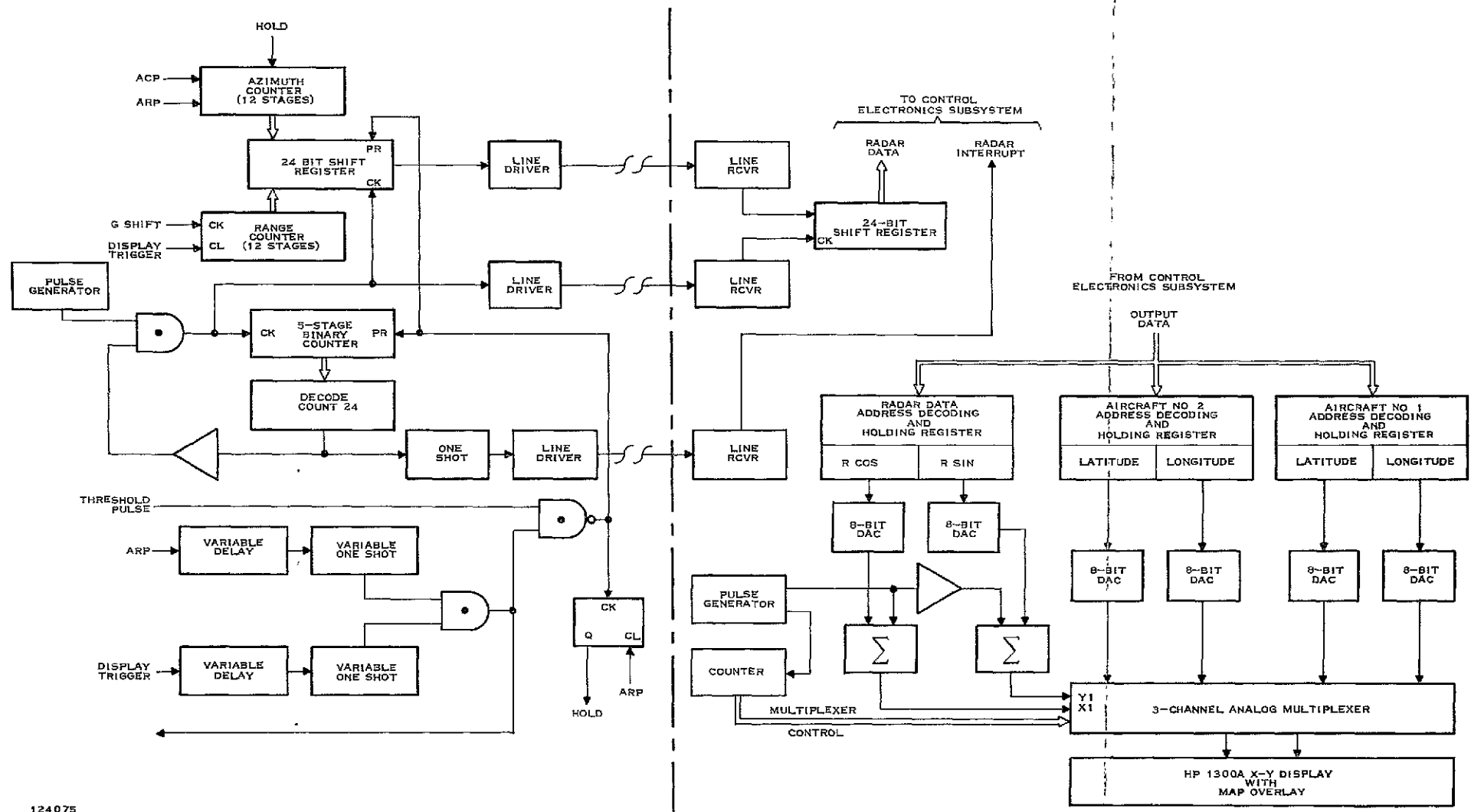


Figure 4-4 Real Time Position Display Equipment, Simplified Block Diagram

TABLE 4-1 TRANSPONDER CHARACTERISTICS

A Operating Frequencies	
1	Receive (ranging tones) 135 60125 MHz ± 1.0 kHz
2	Receive (pilot tone) 135 56625 MHz ± 1.0 kHz
3	Transmit (ref terminal) 149 20843 MHz ± 1.5 kHz
4	Transmit (aircraft) 149 23123 MHz ± 1.5 kHz
B Transmitter	
1	Power Output 4.0 watts minimum
2	Nominal antenna impedance 50 $\pm j0$ ohms
3	Maximum permissible VSWR 1.8
4	Spurious outputs (harmonically related) -30 dB
5	Spurious outputs (nonharmonically related) -70 dB (this does not include P.A. linearity)
C Receiver	
1	Noise figure (overall, including duplexer) 6 dB
2	Cross modulation 1% maximum cross modulation for -30 dB interfering signal with 30% modulation
3	Spurious response rejection rejects all signals below -70 dBm
4	IF bandwidth 6 kHz
5	IF shape factor 3.0
D Phase-Lock Loop	
1	Pull in range ± 2.0 kHz
2	Hold in range ± 4.0 kHz
3	Lock up time 10 seconds maximum
4	Loop noise bandwidth 200 Hz
E Power Requirements	
1	+12V $\pm 1\%$ at 0.3 amperes
2	-12 V $\pm 1\%$ at 0.3 amperes
3	+13V $\pm 1\%$ at 1.7 amperes
F Power Supplies—Laboratory supplies operated from 110V 60 Hz AC	
G Other Specifications	
1	AGC dynamic range 60 dB maximum
2	AGC time constant 0.01 second
3	Platform phase error contribution ± 10 degrees maximum
4	Linearity Intermodulation Distortion Products Suppression > 20 dB
H Mechanical Description	
1	Size $\frac{1}{2}$ ATR, 19 $\frac{1}{2}$ inches long, 5 inches wide, 7 $\frac{1}{4}$ inches high
2	Weight 16 pounds

G Shift—Range pulses, 1200 pulses occur for every 60 nautical miles

Display Trigger—Pulse that marks the firing of the radar transmitter (0-nautical mile range)

Threshold Pulse—Pulse that indicates the returned radar signal has exceeded a predetermined level, thereby indicating a target has been found

The subsystem consists of an azimuth counter, a range counter, a 24-bit holding register, a bit rate clock circuit which generates only 24-bit clocks, and a window or aperture circuit

The window or aperture circuit serves to allow the recognition of targets only within the window itself. The APR pulse and the display trigger pulse are first delayed through delay lines which can accommodate varying amounts of delay. The outputs of the delay lines service one-shot multivibrators whose outputs can be varied in pulse duration. The outputs of the two

one-shots are then ANDed together to generate a pulse which serves as a window within which a target can be recognized. Should a threshold pulse occur when the window pulse is present, a flip-flop is set (HOLD) to indicate the desired target has been located.

Also, on the occurrence of ARP pulse and the display trigger pulse, the azimuth counter and range counter are respectively cleared. These counters then begin counting azimuth and range pulses until the signal HOLD becomes true. At this time, the counts in the azimuth and range counters are input into the 24-bit holding register. At the same time, the 24-count bit rate clock circuit is enabled. The 24-bit clocks serve to serially shift the data into the 24-bit holding register in the subsystem located at the Ground Control Center. After the occurrence of the 24th bit clock, the bit clock circuit is disabled and a data available pulse is sent to the subsystem located at the Ground Control Center to serve as a computer interrupt.

2 Ground Control Center Subsystem

The subsystem at the GCC provides an interface for both inputting the raw radar data into the GCC processor and outputting both the radar and VHF Range/Range position location data to the Hewlett-Packard 1300A X-Y display. The circuitry for inputting the raw radar data into the GCC simply consists of a 24-bit holding register. The circuitry for outputting the radar and VHF Range/Range position location data to the display unit consists of address decoding and holding registers, six 8-bit digital-to-analog converters, modulation circuitry for modulating the analog-converted radar data, a three-channel analog multiplexer, and a Hewlett-Packard 1300A X-Y display.

Each position-located calculation that is output from the OPLE Control Center (OCC) processor must be prefaced with an address to indicate whether the data was computed from the raw radar data, raw phase data from the airborne transponder, or raw phase data from the reference transponder. The three holding registers are each equipped with address decoding logic to allow steering of the data on the common processor bus into the appropriate register. Each holding register consists of two 8-bit sections, one section containing the latitude or Y-data and the other section containing the longitude or X-data. Each 8-bit section is assigned to an 8-bit digital-to-analog converter to convert the digital data to an analog format for presentation to the display unit via the multiplexer. The modulation circuitry consists of a sine-wave generator whose output and complement are summed with the radar's longitude and latitude, respectively. The resultant modulated latitude and longitude signals will produce a circular position location display rather than a dot. The outputs of the D/A converters are multiplexed in a three-channel, two-pole multiplexer whose channel selection is governed by a three-count counter driven from the same generator that provided the modulating sine wave. The output of the multiplexer is presented to the Hewlett-Packard 1300A X-Y display. A transparent area map overlay was made, with the OCC at the center point of the overlay, to correlate the display with actual geographic location.

SECTION V

DESCRIPTION OF THE EXPERIMENT

The VHF Range/Range Experiment was conducted by Texas Instruments in two separate phases. Each phase, and the subsequent experiments within each phase, involves different configurations of the Ground Control Center and the transponders. The advantage of this approach was that system parameters, such as satellite-to-ground VHF link measurements, could be measured without having the system in its final configuration.

The first phase was essentially a system checkout phase. The parameters determined in this phase were the VHF helical antenna patterns and the antenna pattern of the Dorne and Margolin Satcom Antenna DMC33-2, the satellite-to-ground and satellite-to-aircraft VHF links, and the transfer characteristics of both the ATS-1 and ATS-3 satellites. The second phase was a system performance phase which consisted of the on-line position computation and display of resulting position and an off-line analysis of the resulting data. Each phase of the experiment is discussed in detail as follows.

A Subsystem Checkout Phase

1 Dorne-Margolin Aircraft Antenna Pattern

The purpose of this experiment was to determine the characteristics of the Dorne-Margolin Satcom Antenna DMC33-2 as mounted on the Texas Instruments DC-3 aircraft. The configuration of the equipment used to determine the characteristics of the aircraft antenna is shown in Figure 5-1.

The sequence of the experiment was as follows:

ATS-3 satellite was saturated to serve as a beacon by a single tone transmitted from the Mojave Ground Station.

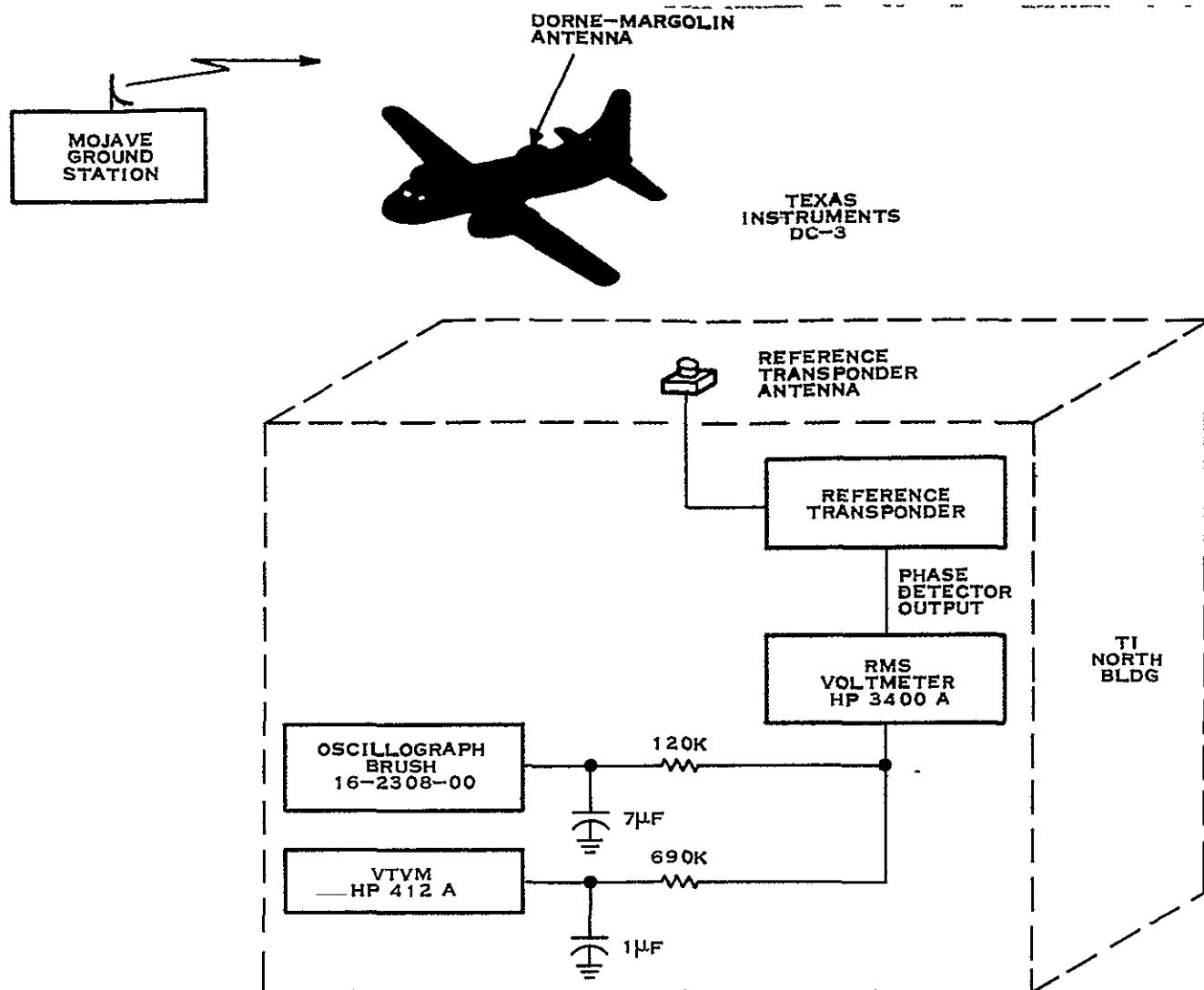
Signal-to-noise measurements were made at aircraft transponder for various aircraft headings and orientations. The signal-to-noise measurements were made by measuring the phase detector output noise and comparing this measurement against predetermined signal-to-noise calibration data. An oscillograph was also used to enable postanalysis of the data.

Signal-to-noise measurements were made concurrently at reference transponder, in the same manner as described above, to normalize the aircraft signal-to-noise measurements.

2 VHF Helical Antenna Pattern

The purpose of this experiment was to determine the characteristics of both the ATS-1 and ATS-3 helical antennas. The configuration of the equipment used to determine the characteristics of the VHF helical antennas is shown in Figure 5-2. The sequence of the experiment was as follows:

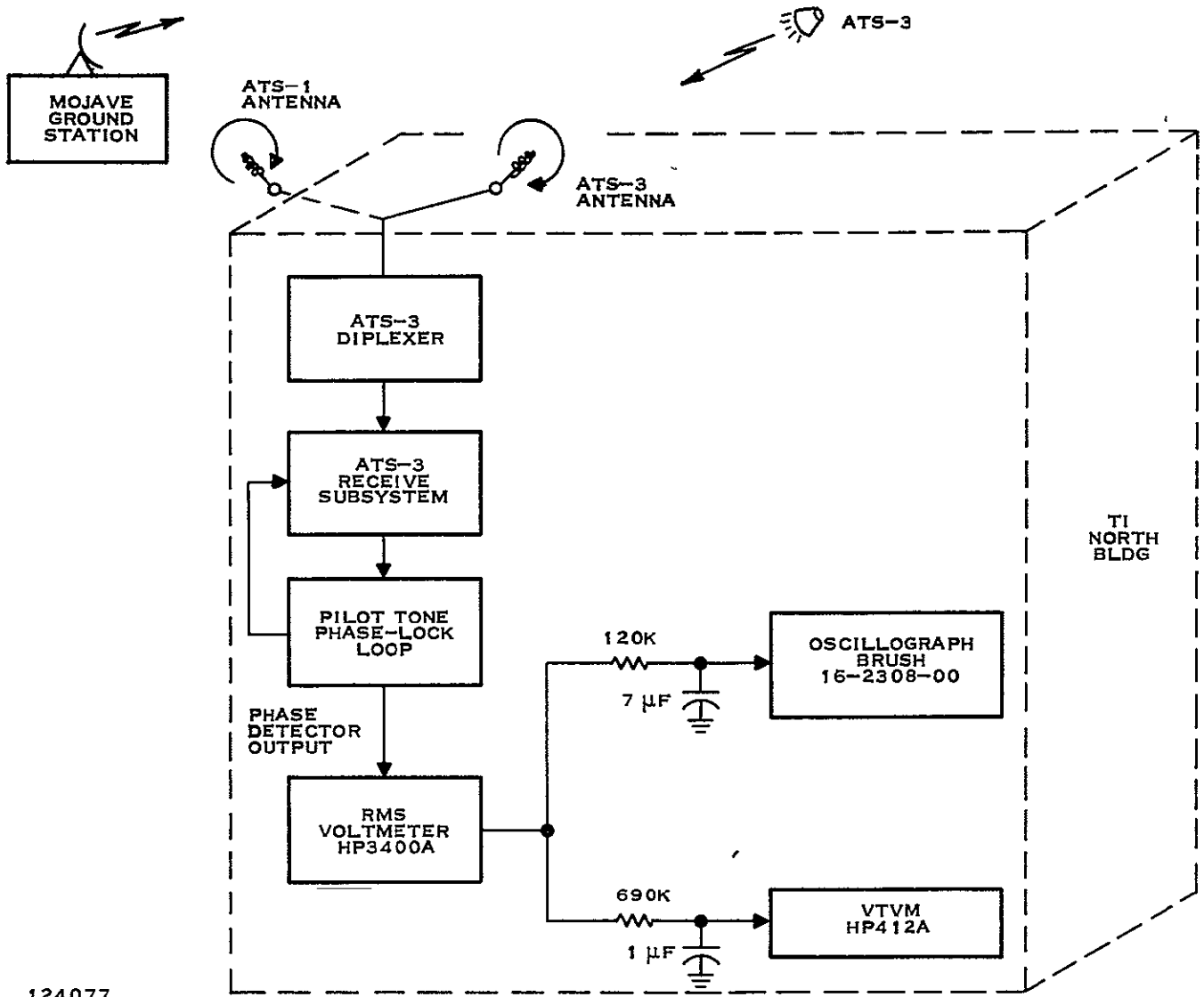
ATS-3 satellite was saturated to serve as a beacon by a single tone transmitted from the Mojave Ground Station.



124076

Figure 5 1 Aircraft Antenna Pattern Measurement Configuration

Signal-to-noise measurements were made at Ground Control Center for various ATS-1 or ATS-3 VHF helical antenna orientations. The ATS-3 receive subsystem was alternately connected to the ATS-1 and ATS-3 VHF antennas. The signal-to-noise measurements were made by measuring the phase detector output noise of the pilot tone phase-lock loop and comparing the measurement against predetermined signal-to-noise calibration data. An oscilloscope was also used to enable postanalysis of the data.



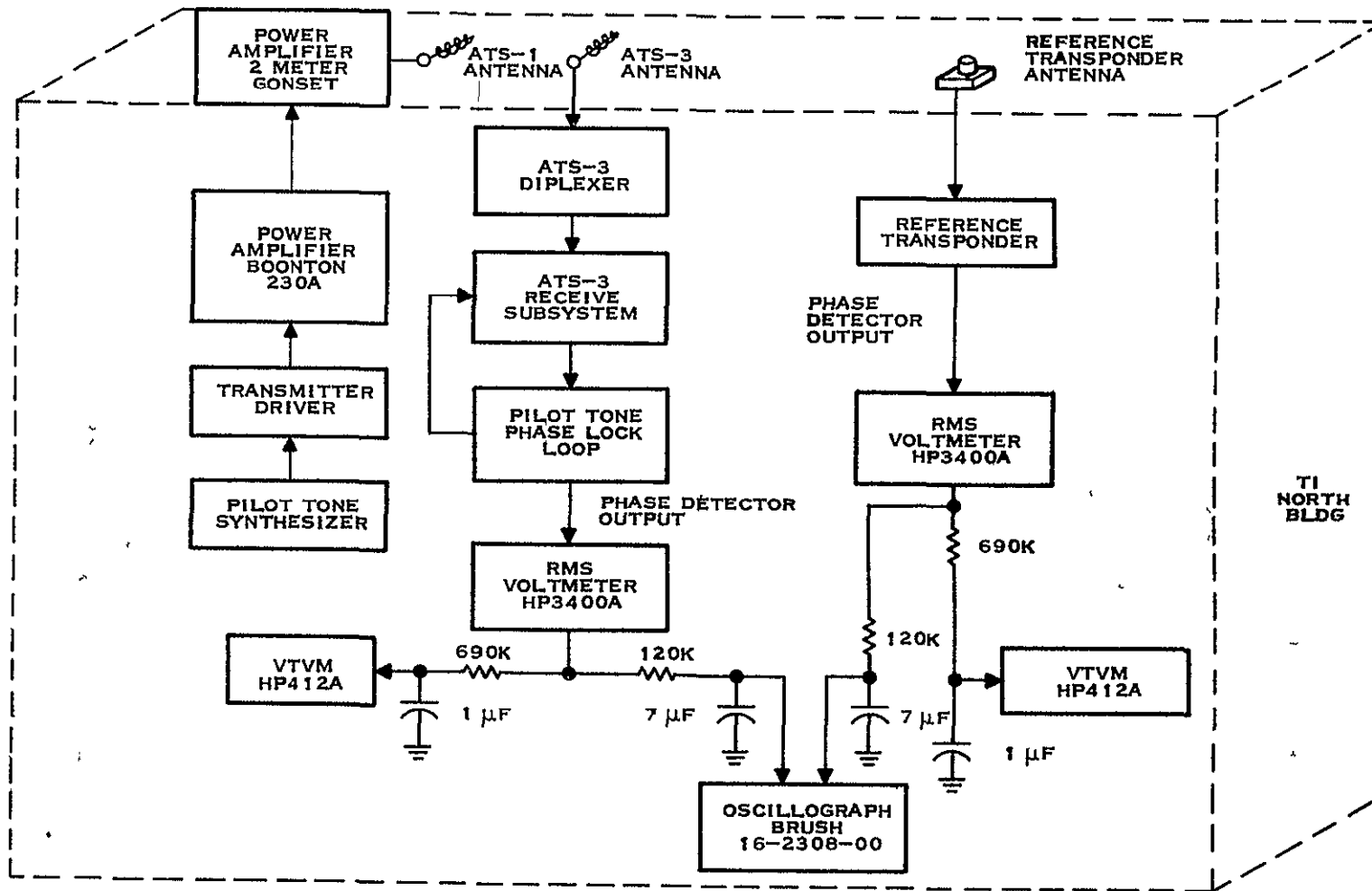
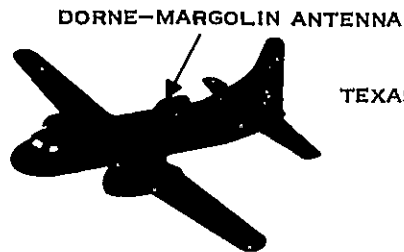
124077

Figure 5-2 VHF Antenna Pattern Measurement Configuration

3 VHF Link Measurements

The purpose of this experiment was to determine the satellite-to-aircraft VHF link losses. The configuration of the equipment used to determine the link losses is shown in Figure 5-3. The sequence of the experiment was as follows:

ATS-3 was saturated by transmitting the pilot tone at approximately 2000-W ERP from the ATS-1 antenna. This amount of power was obtained by amplifying the transmitter driver output by a Boonton power amplifier and then amplifying the resultant by a Gonset 2-meter, 200-W power amplifier located on the roof of the North Building next to the ATS-1 antenna.



124078

Figure 5-3 VHF Link Measurement Configuration

The return signal-to-noise was measured at both the aircraft and reference transponder and the Ground Control Center using the same procedure described in the preceding subsections. Knowing the received signal strength from the signal-to-noise measurements, and assuming a +46-dBm signal from the ATS-3 satellite, the link losses can be determined. This test was repeated for the ATS-1 satellite, again assuming a +46-dBm signal from the ATS-1 satellite.

4 Satellite Power Transfer Measurements

The purpose of this experiment was to determine the power transfer characteristics of the ATS-1 and ATS-3 satellites. The configuration of the equipment used to determine the power transfer characteristics of ATS-3 is shown in Figure 5-4. The sequence of the experiment was as follows:

- A controlled and variable amount of pilot tone signal was transmitted first to the ATS-1 and then to the ATS-3 satellite. The return signal-to-noise from the ATS-1 or ATS-3 satellite was measured at the Ground Control Center via the pilot tone phase-lock loop as described in Subsections V A 1 and V A 2.
- A plot was constructed of transmitted power versus received signal-to-noise at the Ground Control Center. Having previously measured the ATS-1 and ATS-3 VHF link losses, the transmitted power can be converted to satellite received power and the received signal-to-noise at the Ground Control Center can be converted to transmitted satellite signal power.

B System Performance

1 On-Line Position Location and Display

The system configuration utilized in conducting the on-line position location experiment is depicted in Figure 5-5. The major components consist of the modified Ground Control Center, reference transponder, aircraft transponder and the ATS-1 and ATS-3 satellites. Texas Instruments-funded equipments consisted of the ASR-7 radar unit, radar interface equipment, real-time position display equipment, use of Texas Instruments DC-3 aircraft with a Dorne and Margolin DMC33-2 VHF aircraft antenna, and a NARCO radio telephone to provide voice communications with the aircraft.

The Ground Control Center, reference transponder, and aircraft transponder, in conjunction with the ATS-1 and ATS-3 satellites and the Texas Instruments DC-3 aircraft, provided the VHF Range/Range position-location data. The ASR-7 radar unit provided "truth" measurements of the aircraft position in terms of slant range and bearing. The real-time position display equipment provided a means of displaying on-line the position of the aircraft as determined by both the ASR-7 radar and the VHF Range/Range equipment. Finally, the NARCO radio equipment provided voice communications with the aircraft to enable effective coordination and verification of the flight plan in use. In addition to displaying the position data, the raw phase data as well as the radar and VHF Range/Range position data was stored on magnetic tape for subsequent off-line processing.

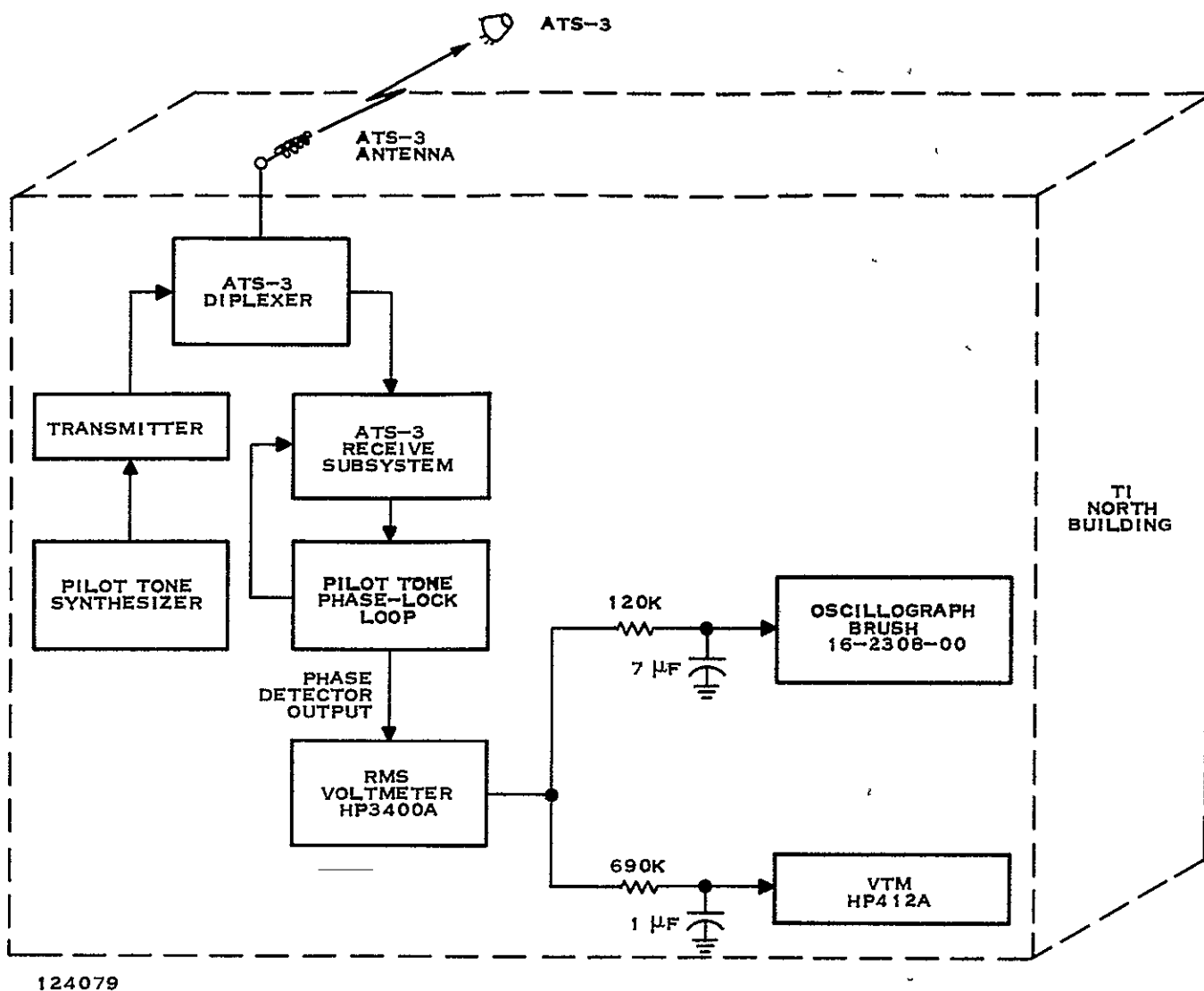


Figure 5-4 Satellite Power Transfer Measurement Configuration

2 Off-Line Analysis

The first step in the off-line data analysis program was to recompute the aircraft position from the raw VHF Range/Range phase data by three different position determination techniques

Absolute Ranging and Position Determination

Differential Ranging and Position Determination

Absolute Ranging and Differential Position Determination

Each of these three techniques is discussed in more detail

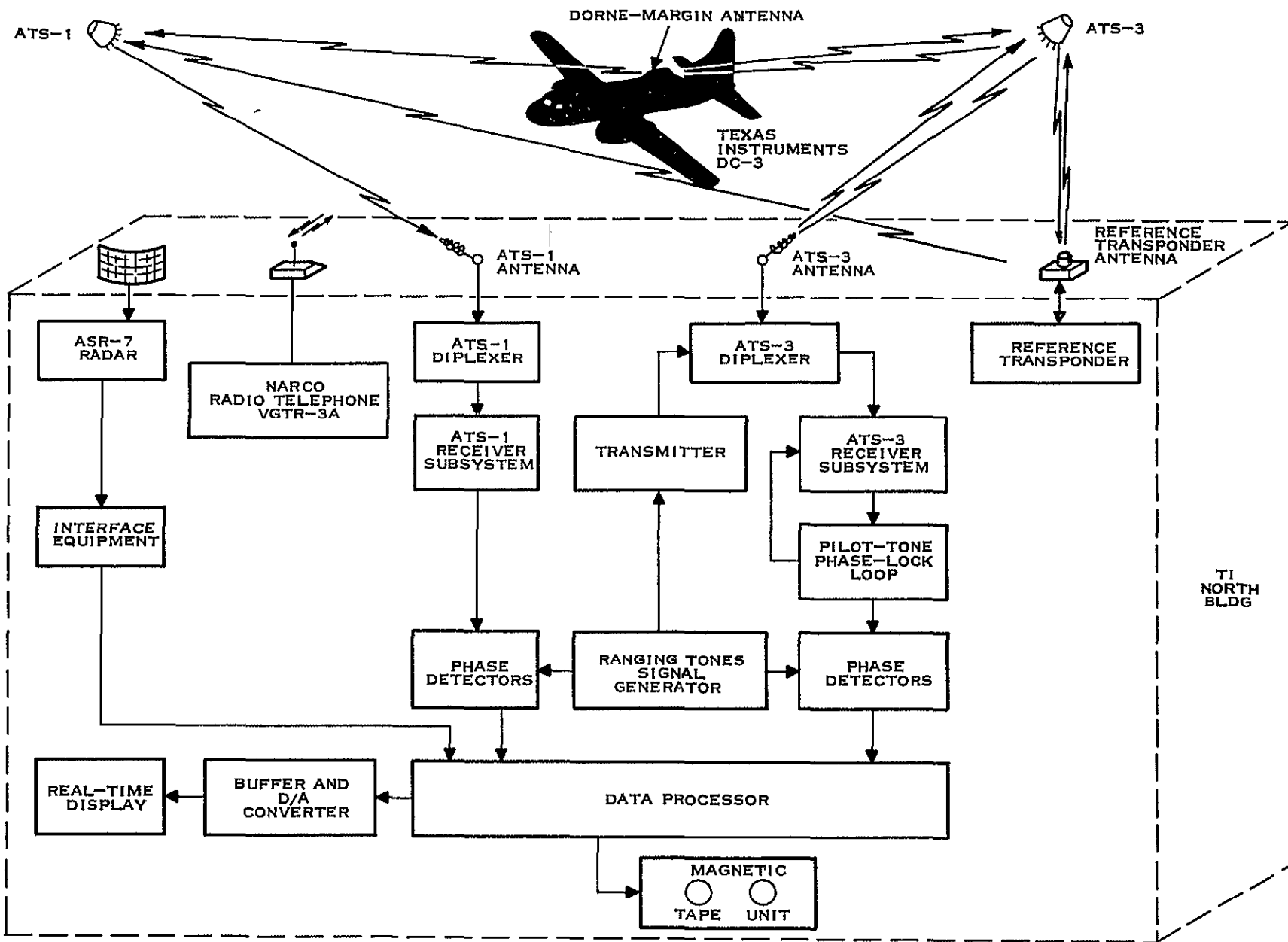


Figure 5-5 On Line Position Location and Display System, Block Diagram

Subsection III B presented a somewhat detailed discussion of the second technique listed above. The purpose behind tone ranging is to determine the range from the ATS-1 and ATS-3 satellites to the aircraft transponder. It was also concluded in Subsection III B that by simultaneously ranging to a reference transponder at a known location, the common mode error sources (some of which vary with time) can be canceled to a first-order approximation. However, the calibration run, which was used to cancel the error sources associated with using different receive channels at the Ground Control Center, can also be used to cancel to a first-order approximation those common mode error sources which are constant over a short-term time period such as 30 minutes. The equations for the absolute ranging technique, using the same phase-lock loop receiver assignments as presented in Figure 3-2 are as follows:

$$R_1 = \frac{\phi_1 - \phi_{1c}}{2} + R_{s_1}$$

$$R_2 = \phi_3 - \phi_{3c} - \frac{\phi_1 - \phi_{1c}}{2} + R_{s_2} \quad (5-1)$$

Having determined R_1 and R_2 by the absolute ranging technique, the position of the aircraft transponder can be calculated.

Note in Equation (5-1) that the phase-lock loop receivers 2 and 4, which are assigned to the reference transponder via the ATS-3 and ATS-1 satellites, respectively, are not utilized. By using the phase information in receivers 2 and 4 in the same manner as the phase information in receivers 1 and 3 were used in Equation (5-1), a determination of the range error caused by time-varying common mode error sources can be made. Furthermore, this range error can be converted to X- and Y-coordinate position error and subtracted from the position determined from the absolute ranging and position determination technique. This technique is referred to as the absolute ranging and differential position determination technique.

Having determined the position of the aircraft transponder by each of the three techniques discussed above, it is now necessary to determine the error associated with each of the three techniques. In conducting the on-line VHF Range/Range experiment, two different modes of operation with respect to the aircraft transponder mounted on board the Texas Instruments DC-3 were used. In one case, the DC-3 was stationary on an airport runway, thereby enabling static position determination tests to be made. In the other case, the DC-3 was airborne at approximately 5000 feet. For the static case, the following error analysis was made:

- Mean offset in X-direction (east-west) from known position
- Mean offset in Y-direction (north-south) from known position
- RMS offset in X-direction from known position
- RMS offset in Y-direction from known position
- Variance in X-direction
- Variance in Y-direction

For the airborne case, the following error analysis was made:

Mean offset in X-direction from radar-determined position
Mean offset in Y-direction from radar-determined position
RMS offset in X-direction from radar-determined position
RMS offset in Y-direction from radar-determined position
Variance in X-direction
Variance in Y-direction

SECTION VI

ANALYSIS OF EXPERIMENTAL RESULTS

The major objective of the experiment was to evaluate the performance of the alternate position location techniques and to compare the accuracy of the differential ranging technique with its predicted performance. To establish reasonable estimates for the predicted position location error, extensive measurements were also made of the RF link performance. This data is also summarized in this report.

A Position Location

During the course of this contract, a number of real-time comparative flight demonstrations and experiments were performed using the satellite system and a Texas Instruments airport surveillance radar as a source of ground truth data. Aircraft flights were made within a range of approximately 70 miles of Dallas, Texas. The details of the experimental implementation are given in Section V. In this section the performance obtained during four experiments is analyzed and discussed. Two experiments were actual flight tests and two were static tests performed with the aircraft on the ground. The data presented represents a large number of data prints taken during each experiment.

1 Comparison of Position Location Techniques

Table 6-1 shows a comparison of the rms latitude and longitude errors for the three methods of position location described in Section III. Both of the differential ranging techniques are superior to the absolute ranging technique. This is particularly well illustrated in Flight Data File 2 where the latitude error is approximately 10 times greater in the absolute mode than in the differential modes.

TABLE 6-1 POSITION LOCATION ERRORS

Experiment Description	No Samples	Absolute Ranging		Differential Position		Differential Ranging	
		Latitude Error (nmi)	Longitude Error (nmi)	Latitude Error (nmi)	Longitude Error (nmi)	Latitude Error (nmi)	Longitude Error (nmi)
Flight Data							
File 2	177	18.29	2.64	1.70	3.05	1.63	3.22
File 12	91	5.34	6.11	4.38	2.15	4.14	2.21
Static Data							
File 5	116	4.34	2.46	4.51	1.23	4.27	1.38
File 6	140	3.65	5.07	2.92	1.85	2.57	2.03

The position location results derived in the flight experiments are also depicted in Figures 6-1 and 6-2 which show the flight paths of the aircraft, as determined by the satellite system and radar, for the trials recorded on Flight Files 2 and 12. A number of factors should be noted in these results:

- Very large position errors that occur for short durations (such as in File 2) represent drop-out of the phase-locked loops caused by interference due to VHF aircraft voice communications
- Discontinuities in the radar coverage are due to the maximum and minimum range limitations of the radar
- Noticeable bias errors exist between the radar and satellite determined positions

The bias errors are discussed in Appendix D and are considered in more detail in the next subsection where the measured and expected errors are compared.

2 Comparison of Measured and Expected Errors

The experimental results obtained for position location using the differential ranging technique were analyzed, as described in Appendix B, to determine the rms error, the bias error, and deviation from the mean. These results are shown in Table 6-2 for the static and flight tests. Also included are the predicted deviation errors which were derived in Appendix D from an analysis of the various error sources and the Geometric Dilution of Precision (GDOP) effect.

TABLE 6-2 COMPARISON OF EXPERIMENTAL AND PREDICTED POSITION LOCATION ERRORS FOR DIFFERENTIAL RANGING

Description	Experimental Results						Predicted Results	
	Latitude Error (nmi)			Longitude Error (nmi)			Latitude Error (nmi)	Longitude Error (nmi)
	rms	Mean	Deviation	rms	Mean	Deviation		
Flight Data								
File 2	1.63	0.22	1.61	3.22	2.97	1.23	2.75	1.75
File 12	4.14	-3.49	2.44	2.21	1.53	1.59	2.75	1.75
Static Data								
File 5	4.27	4.13	1.09	1.38	1.08	0.86	1.50	0.93
File 6	2.57	-2.06	1.53	2.03	1.83	0.88	1.50	0.93

Agreement between the predicted and measured deviation errors for the static tests is very good. The longitude errors for File 5 and File 6 are 0.86 nmi and 0.88 nmi, respectively, and the predicted error is 0.93 nmi. The latitude errors for File 5 and 6 are 1.09 nmi and 1.53 nmi, respectively, as compared with a predicted error of 1.50 nmi. It should be noted that the mean square deviation in latitude for Files 5 and 6 is 1.33 nmi, which is also very close to the predicted result.

A comparison of the predicted and measured deviation errors for the flight tests shows that the actual errors are consistently less than the predicted errors. The predicted latitude error is 2.75 nmi, but the measured results for Files 2 and 12 are 1.61 and 2.44 nmi, respectively. The predicted longitude error is 1.75 nmi while the measured results were 1.23 and 1.59 nmi for Files 2 and 12, respectively. As a result of the good agreement obtained in the static tests, the

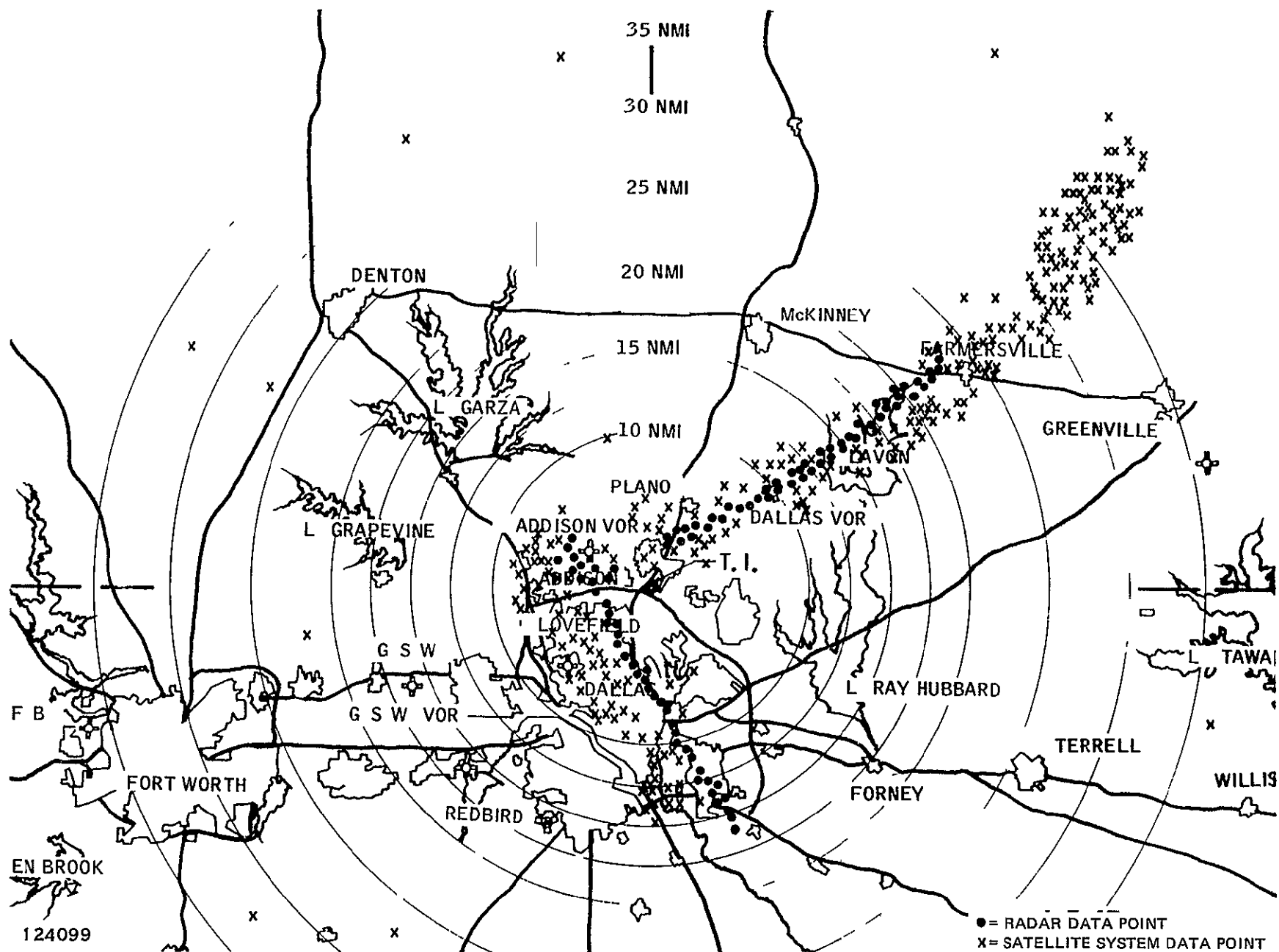


Figure 6 1 Real Time Display of Flight Experiment Data, File 2

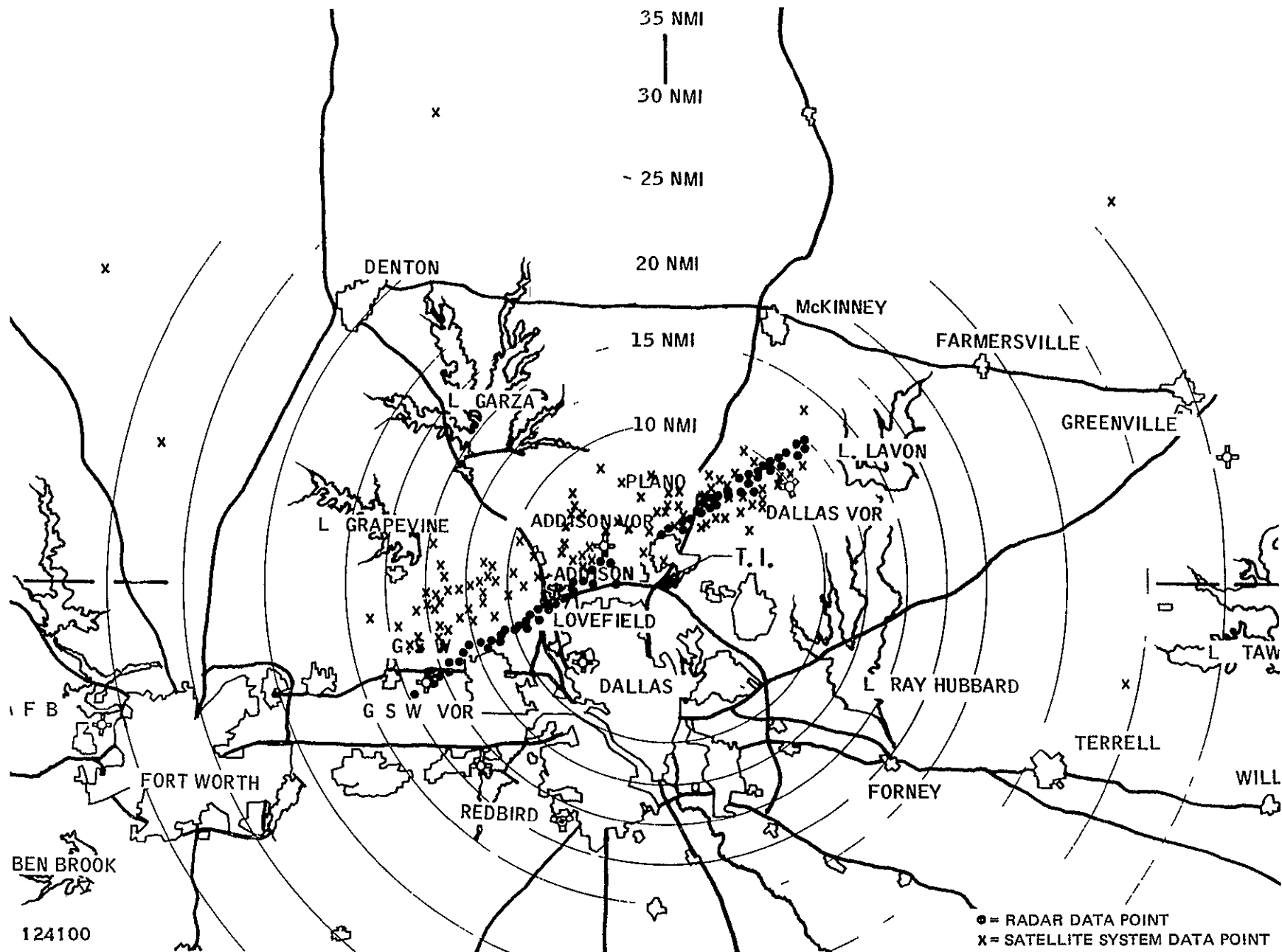


Figure 6 2 Real Time Display of Flight Experiment Data, File 12

lack of agreement obtained in the flight tests is most likely due to inaccurate estimation of the two additional error sources which are the ionospheric effect and the multipath effect

As a result of the differential ranging measurements made between the aircraft and the reference terminal, and the relative proximity of the aircraft and reference terminals during this experiment, it may be inferred that the error contribution of 1.8 km caused by the ionosphere (Table D-6 of Appendix D) is excessive. If this error source is essentially eliminated, then the predicted latitude and longitude errors become 2.4 and 1.5 nm, respectively. These results are in better agreement with the experimental data, although still larger. It appears, therefore, that the multipath contribution assigned in Appendix D may also be too large.

It should be noted that the bias errors in the experimental data in Table 6-2 show no particular trend. Bias errors can be caused by a number of effects which include instrumentation bias error and ground truth error. The bias errors introduced by the GCC are due to errors in phase measurement caused by the phase detector and by phase shifts associated with the use of a frequency division multiplexed system for the detection and measurement of the various ranging signals.

B RF Link Measurements

1 Link Losses

The procedure used to measure the down-link losses is described in Subsection V A 3. The experimentally determined up-link losses were derived from the measured down-link losses by taking into consideration the theoretical difference in free-space losses, and cable and diplexer losses. Over a 2-month period, several measurements were made for each of the link losses and the values tabulated in Table 6-3 are an average of these measurements. The predicted values are derived in Appendix E.

The stabilization spin imparted to both satellites in conjunction with the individual phasing of the signals fed to each satellite antenna results in a constant sinusoidal variation in the signal strength. The frequency of this spin modulation is approximately 13 Hz and the peak-to-peak excursions for the ATS-1 and ATS-3 satellites are 2 and 6 dB, respectively. The effect of spin modulation on the measured losses was included by considering the median received signal level.

TABLE 6-3 LINK LOSSES

Link	Predicted (dB)		Measured (dB)
	Nominal	Worst Case	
GCC-to ATS-3	-157	-161.2	-159
Aircraft-to ATS-3	-171.3	-178.5	-170
Aircraft to ATS-1	-171.3	-178.5	-170
Reference to ATS-3	-172.3	-176.5	-169
Reference-to-ATS-1	-172.3	-176.5	-174
ATS-3 to-GCC	-155.7	-159.7	-158
ATS-3 to Aircraft	-171.2	-178.2	-170
ATS-3 to Reference	-170.7	-174.7	-168
ATS-1 to GCC	-154.2	-158.2	-160

As shown in Table 6-3, with the exception of the ATS-1-to-GCC loss, the measured and predicted nominal link losses agree to within approximately 3 dB. The discrepancy in the predicted and measured ATS-1 link loss is most likely caused by the relatively low elevation angle (21 degrees) of the satellite at the time the measurements were made.

As was anticipated, the signal levels at the aircraft showed considerable multipath related variations. These signal fluctuations were on the order of 4 dB. This should be considered only as a nominal multipath effect because larger variations can be encountered if the aircraft is flying toward or away from the satellite. The effects are especially pronounced during the time that the aircraft is ascending or descending.

2 Satellite Characteristics

Power transfer curves for ATS-1 and ATS-3 VHF repeaters were experimentally determined as described in Subsection V A 4 by varying the power of the pilot tone transmitted to the satellite under test and measuring the received signal level at the GCC. Theoretical transfer curves were generated and compared with the experimental data to verify the link losses and power sharing at the satellites.

For each measured transmitted signal level, a scattered group of received signal levels was recorded. These data points were plotted and a curve was drawn connecting the maximum received signal-level points while another was drawn connecting the minimum signal-level points. A third curve was drawn between the maximum and minimum curves so that approximately half of the data points were above this average measured signal curve.

The resulting power transfer curves for ATS-1 and ATS-3 are shown in Figures 6-3 and 6-4, respectively. Comparison of the two experimental satellite power transfer curves shows that ATS-3 was approaching saturation with the GCC transmitting 50 dBm of pilot tone power while ATS-1 was still several decibels below saturation. This difference reflects the higher link loss between the GCC (ATS-3 antenna) and ATS-1. The satellite transfer characteristics are essentially linear for transmitted levels less than 42 dBm because the predominate satellite input power is the relatively constant noise power. For GCC transmitted levels greater than 42 dBm, the received pilot tone signal at the satellite is a significant component of the total input power and the slope of the transfer curve begins to decrease.

The predicted power transfer curves were derived by using the basic power sharing equation derived in Appendix E in conjunction with the measured satellite-to-ground link losses. In this particular application, the received pilot tone power (P_R) at the GCC is given by

$$P_R = P_{PT} - L_{GS} + P_S - P_{IS} - L_{SG}$$

where

P_{PT} = GCC transmitted pilot tone power

P_S = satellite output power

P_{IS} = input power to the satellite including noise and interference
and excluding pilot tone

L_{GS} = appropriate ground-to-satellite link loss

L_{SG} = appropriate satellite-to-ground link loss

GCC-to-satellite losses were inferred from the measured down link losses by taking into consideration the difference between the 135.6- and 149.2-MHz theoretical path losses along

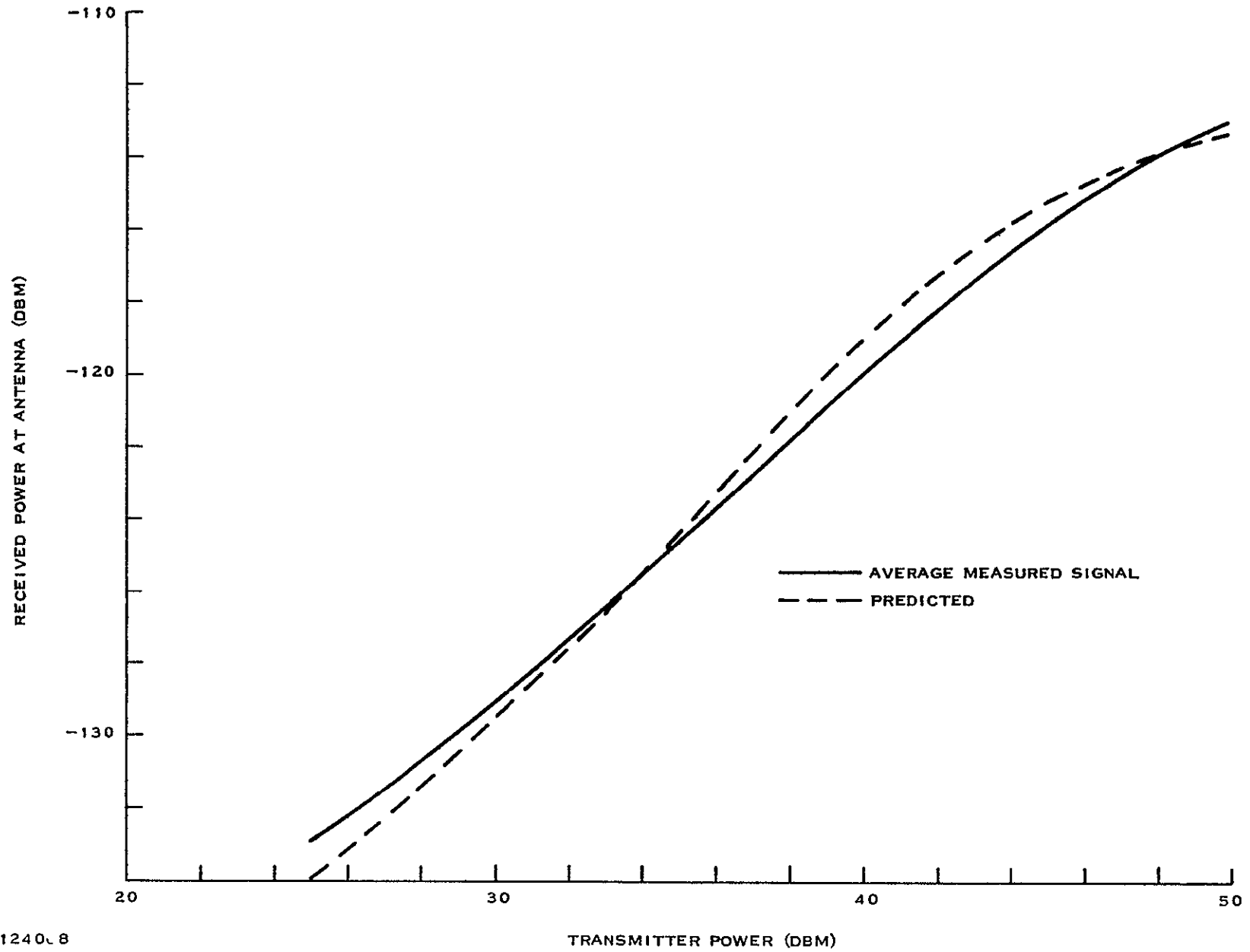
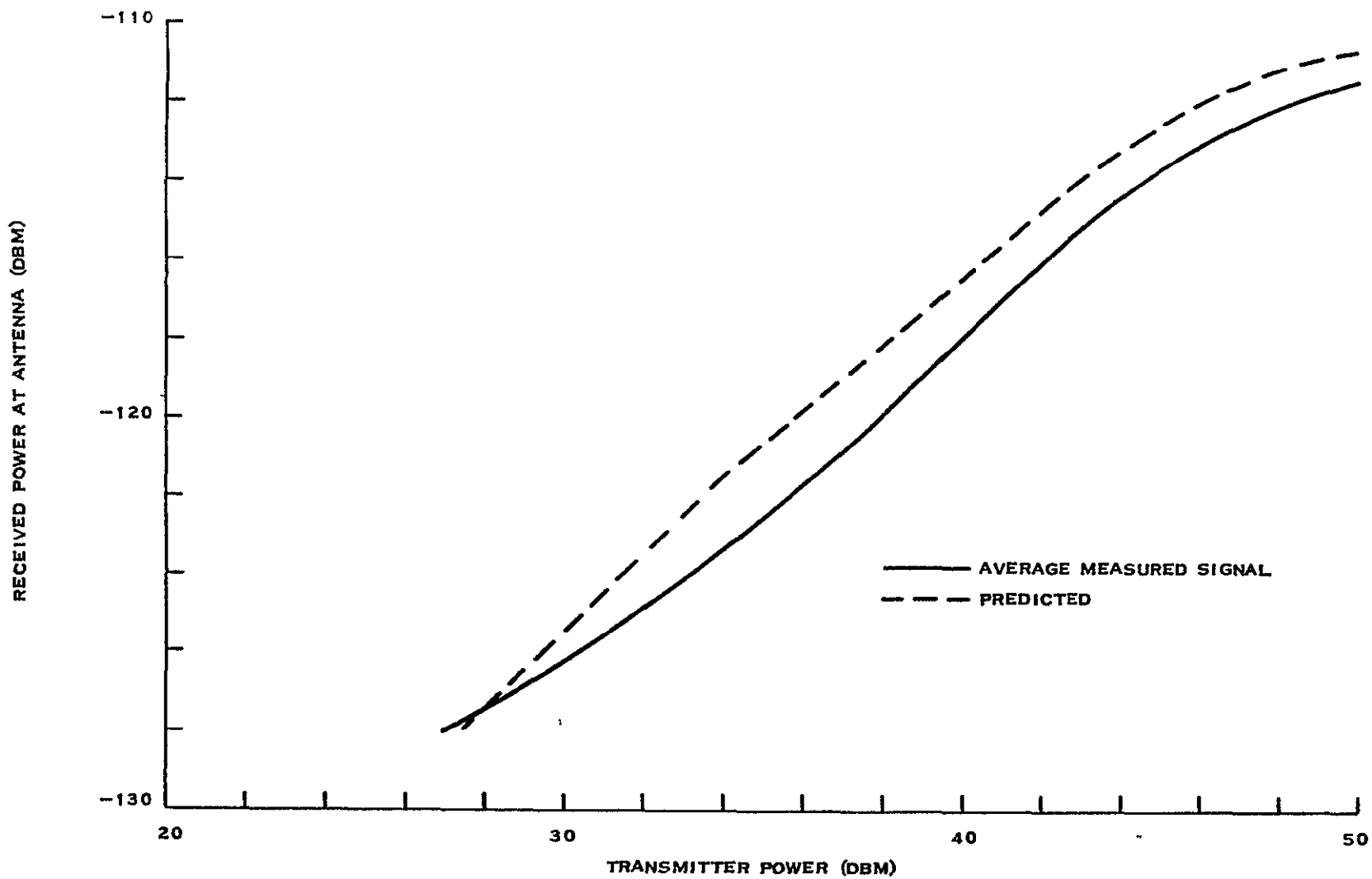


Figure 6 3 ATS-1 Power Transfer Curve



124069

Figure 6-4 ATS-3 Power Transfer Curve

with cable and diplexer losses. The link losses used in determining the theoretical curves are as follows:

ATS-1 (Utilizing GCC ATS-3 Antenna)

ATS-1-GCC	156.5 dB
GCC-ATS-1	162 dB

ATS-3 (Utilizing GCC ATS-3 Antenna)

ATS-3-GCC	154.5 dB
GCC-ATS-3	160 dB

The diplexer losses for the down links are omitted so that the received power is referred to the antenna. The total satellite input power for each transmitted power level was derived from the received pilot tone power and the empirical -113 -dBm noise and interference power.

Comparison of the experimental and predicted curves shows a 1-dB-maximum deviation for the ATS-1 data and a 2-dB-maximum deviation for the ATS-3 data. Because the predicted and experimental transfer curves approach saturation at the same GCC transmitter power level, it can be concluded that if the link losses are correct, then the assumed -113 -dBm satellite noise power is also valid. This is true because the slope of the transfer curve begins to decrease rapidly when the received signal is on the same order of magnitude as the noise power. The discrepancy between the measured and predicted ATS-3 power transfer curve is most likely caused by the one-way link loss being approximately 1 dB greater during the test than the values used for the theoretical curve. If this 1-dB error existed for both the up and down links, then the net result would be an experimentally determined curve which is down by 2 dB from the predicted curve.

3 System Carrier-to-Noise Power Density

The details of the techniques employed in this experiment to determine the signal-to-noise power densities at the various receivers are discussed in Subsection V A 3. During each experiment, data from the meters used for this purpose was recorded at specified intervals while chart recorders provided a continuous record of received signal strengths.

As discussed in Appendix E, the carrier-to-noise power density at any receiver is partially determined by the link losses between each repeater. Monitoring of the ATS-3 retransmitted pilot tone signal at the GCC and the transponders provided data for verification of power sharing at ATS-3. The predicted and measured pilot tone C/No values are listed in Tables 6-4 and 6-5. The predicted data is derived from Appendix E.

Chart recordings at the reference transponder showed that the received signal was relatively constant during an experiment period. With the exception of local or satellite interference, signal variations in excess of 3 dB rarely occurred. The received pilot tone signal at the GCC also remained relatively free of short-term fluctuations. The received signals at the aircraft, however, did exhibit frequent short-term fluctuations of a larger magnitude than that observed at the reference transponder. These signal strength variations were caused by local interference and multipath effects. During periods of heavy interference, the aircraft transponder would frequently lose lock. Because of this problem, the experiments were scheduled for a later time at night.

TABLE 6-4 PILOT TONE CARRIER-TO NOISE POWER DENSITIES

Receiver	Predicted		Measured			
	Nominal	Worst Case	Maximum* (dB Hz)	Average* (dB Hz)	Maximum† (dB Hz)	Average† (dB Hz)
GCC	48.3	43.1	47.2	46.2	51.8	51
Aircraft	36.8	28.2	34	33.6	39.4	36.4
Reference	37.3	31.7	41	34.9	39	37.8

* Early evening, moderate interference

† Late evening/early morning, low interference

TABLE 6-5 RANGING TONE CARRIER-TO NOISE POWER DENSITIES

Receiver	Predicted		Measured		
	(dB Hz)	Maximum* (dB Hz)	Average* (dB Hz)	Maximum† (dB Hz)	Average† (dB Hz)
1	28.7	29.7	26.2	29	25.5
2	27	28.9	27.4	32	28.3
3	30	29.9	27.9	30.2	28.8
4	28.3	30.7	27.5	30.6	31.1

* Early evening, moderate interference

† Late evening/early morning, low interference

SECTION VII

CONCLUSIONS AND RECOMMENDATIONS

This experiment, using some equipment previously developed for NASA, plus the contributions made by Texas Instruments, has yielded a self-contained air traffic surveillance system and has demonstrated

- The utility of synchronous satellites in the master/slave configuration using differential techniques to remove large common mode errors in the ranging measurements
- The capabilities of narrow-band sidetone ranging yielding position location accuracies of approximately 2 nm for a 941-Hz sidetone
- The facility for real-time computation and display of aircraft position, using differential or absolute ranging techniques

The following recommendations are made for future satellite air traffic surveillance systems employing sidetone ranging

- A more usable frequency should be chosen, that is, one not subject to the interference level encountered at 135.6 MHz
- Time division multiplexing would remove some of the delay variation encountered in the frequency division multiplexed system used for this experiment
- A higher sidetone frequency should be chosen

If the above improvements are made, the differential ranging position location techniques can yield improved accuracy on the order of 1 nm. Although this experiment was conducted at VHF, the principles demonstrated are equally applicable at the higher frequencies, such as L-band, more likely to be chosen for use in a satellite air traffic control system.

APPENDIX A

GROUND CONTROL CENTER DESCRIPTION

I. GCC Hardware Description

The Ground Control Center (GCC) consists of five functional subsystems and the necessary power supplies. Each subsystem is packaged in a separate drawer(s) or rack(s) to minimize the number of interconnecting cables. Figures A-1 through A-4 are photographs of the GCC equipment, including the two VHF antennas, and Figure A-5 is a functional block diagram of the GCC. Brief descriptions of the five functional subsystems are provided in the following paragraphs.

A. Computer Subsystem

The computer subsystem consists of a Data Machines Incorporated (DMI) Data-620 computer, a Teletype Corporation Model ASR-35 teletypewriter, and an Ampex Corporation Model TM-7 magnetic tape recorder. In the OPLE Experiment configuration the computer subsystem controls the Platform Electronics Package (PEP) interrogation data timing and sequencing, collects and stores the various OPLE Experiment data, formats and reads out the OPLE Experiment data, and processes the raw phase data from the PEP's and the Omega monitor receiver. In the VHF Range/Range Experiment configuration the computer subsystem controls the sidetone and Acquisition/Reference (A/R) tone transmission, collects and stores the VHF Range/Range Experiment data, processes the raw phase data, calculates on-line position-location data and outputs the position location data for a real-time display unit, collects and processes radar data for outputting to a real-time display unit, and outputs the entire VHF Range/Range Experiment data, including radar data, onto magnetic tape for further off-line processing.

B. Control Electronics Subsystem

The control electronics subsystem consists of the control console, the multiplexer/ADC, the 2.7-MHz rms frequency synthesizer, the 1-MHz frequency standard, and the logic drawer. In addition to interfacing the computer subsystem with the remainder of the GCC, the control electronics subsystem performs numerous timing and control functions, provides special-purpose address decoding and ambiguity-resolving circuitry for digital transmission, and accumulates radar data for presentation to the computer subsystem.

C. RF Electronics Subsystem

The RF electronics subsystem is composed of an ATS-3 VHF antenna assembly, an ATS-1 VHF antenna assembly, a VHF transmitter section, an ATS-3 VHF Receiver group including a pilot-tone phase-lock loop to track out phase jitter introduced by the ATS-3 satellite transponder, an ATS-1 VHF Receiver group, and four phase-locked synchronous demodulators (channel selectors). The RF electronics subsystem utilizes interrogation and tone data from the self-check subsystem and timing and control signals provided by the remainder of the GCC in generating the VHF signals to be transmitted. The incoming VHF signals are received and demodulated by the RF electronics subsystem, and the resulting data is applied to other subsystems in the OCC for processing.

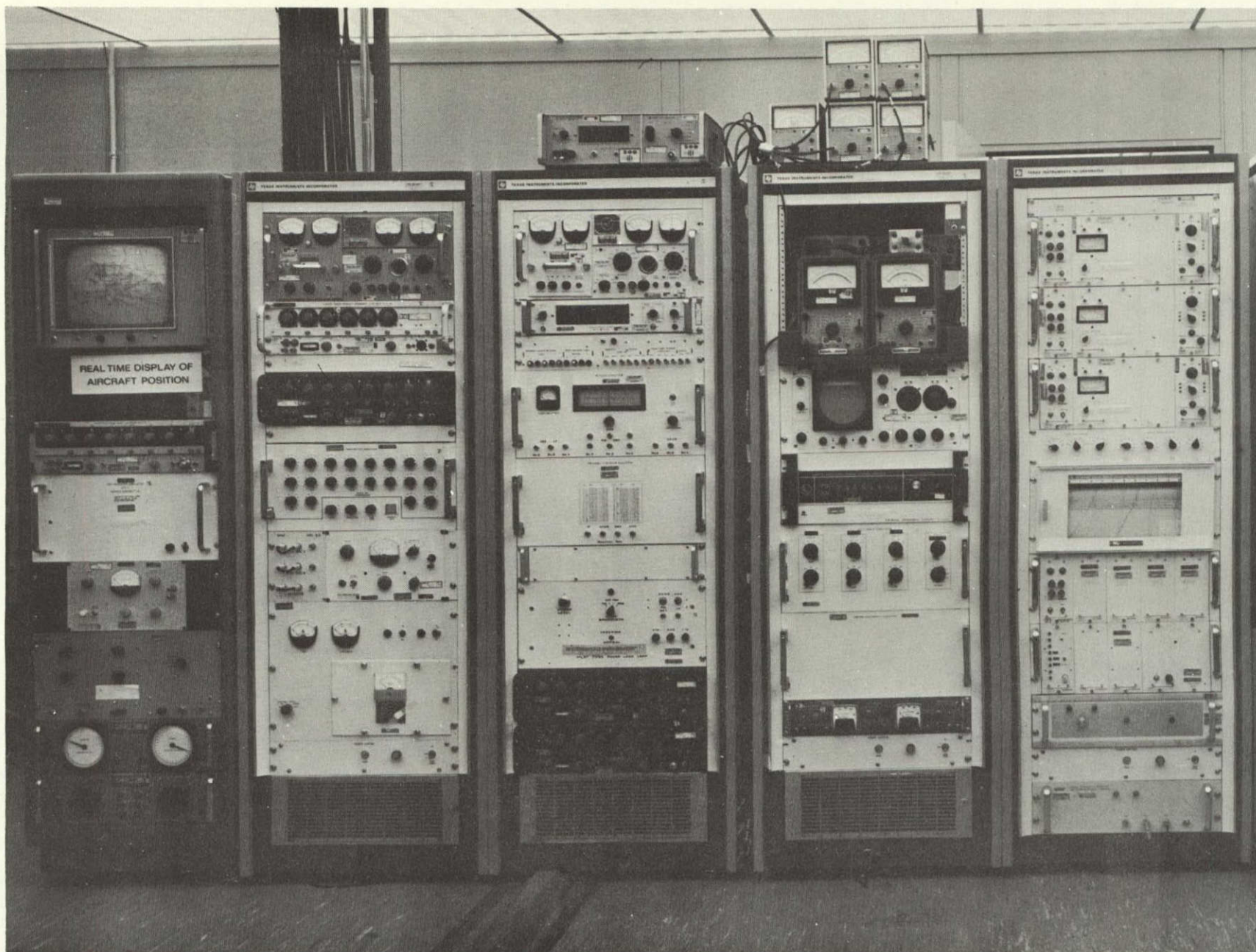


Figure A-1. Ground Control Center Receive Subsystem, Transmit Subsystem, and Real-Time Display

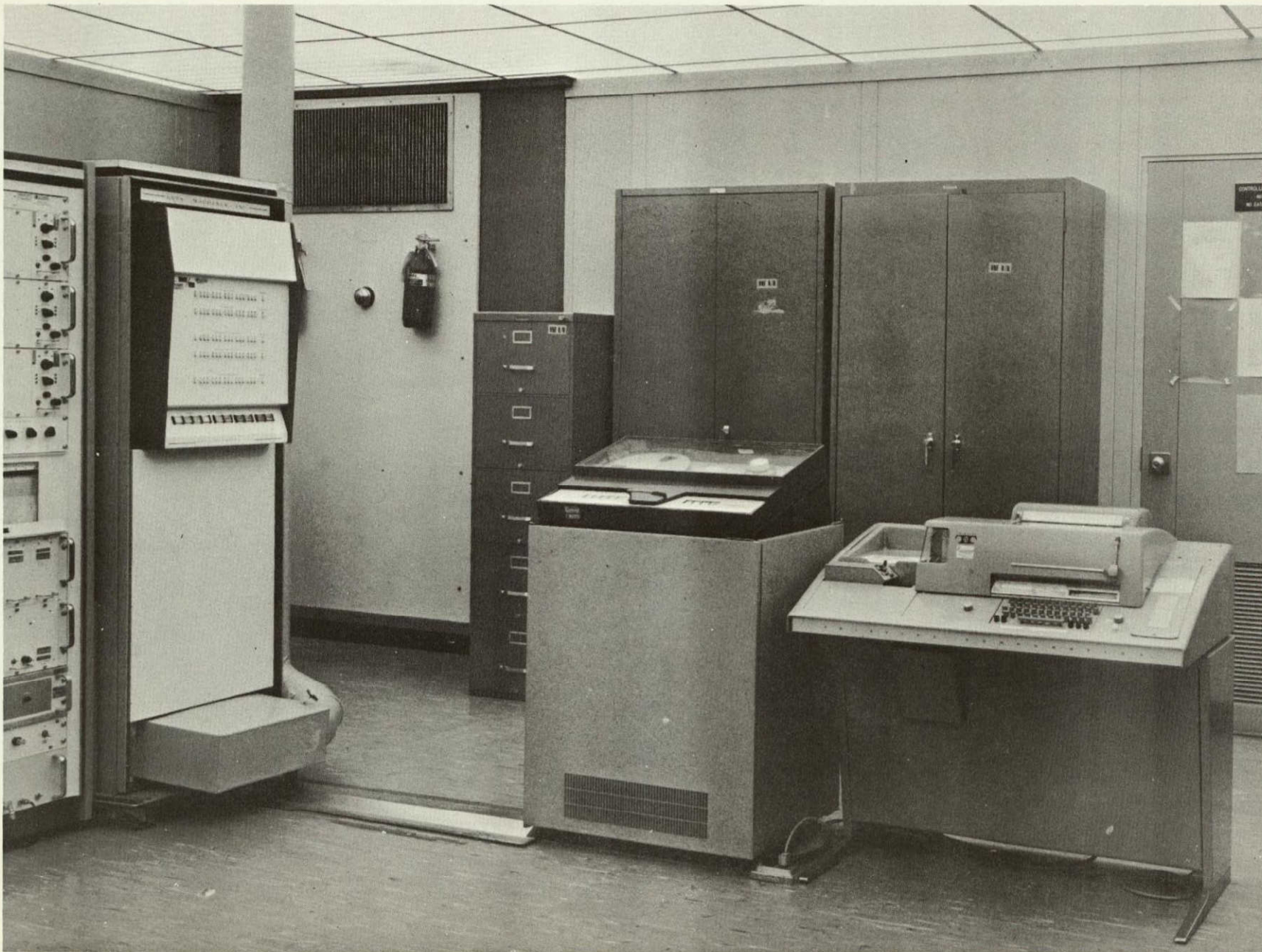


Figure A-2. Ground Control Center Data Processor



Figure A-3. Ground Control Center Control Console

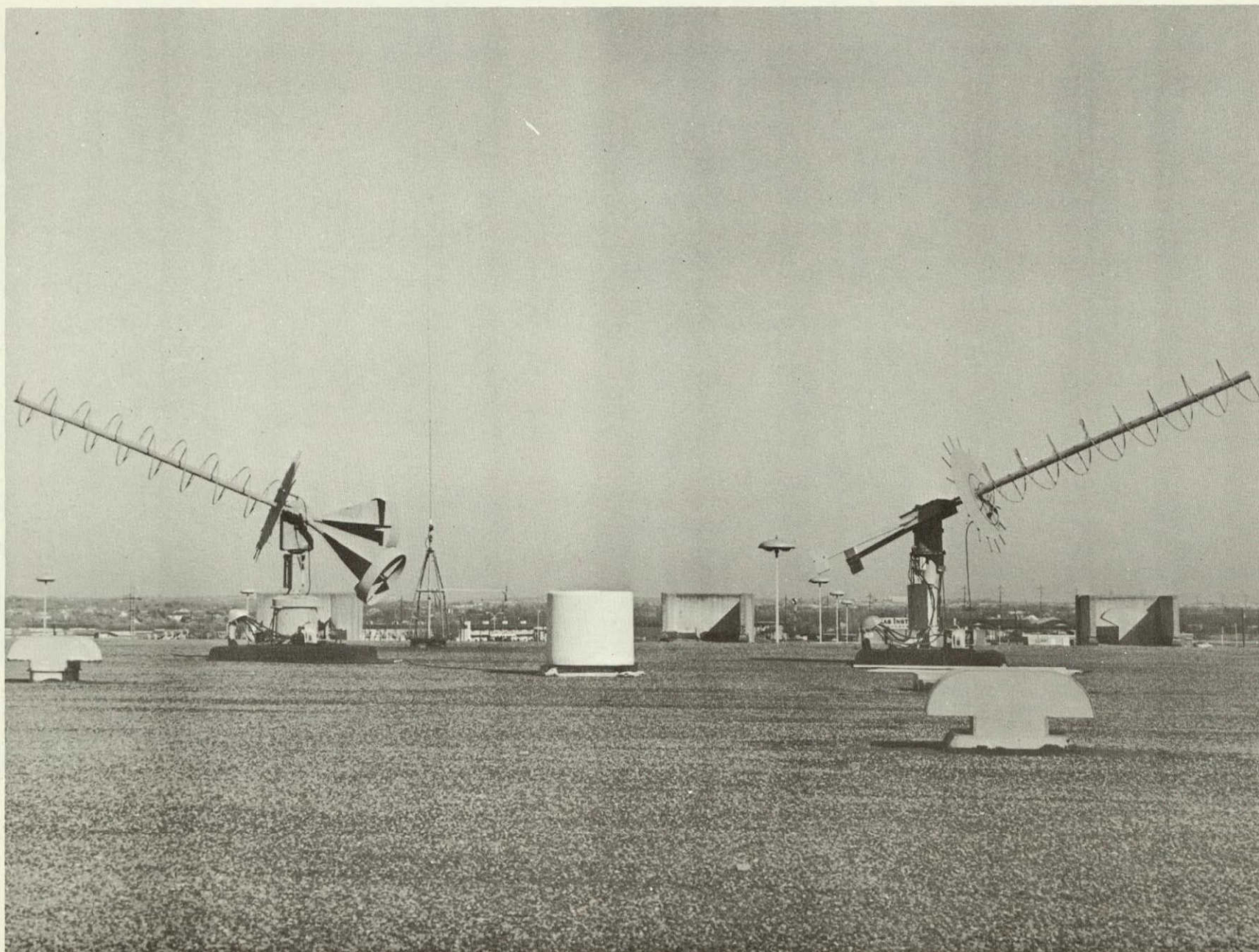


Figure A-4. Ground Control Center Antenna Configuration

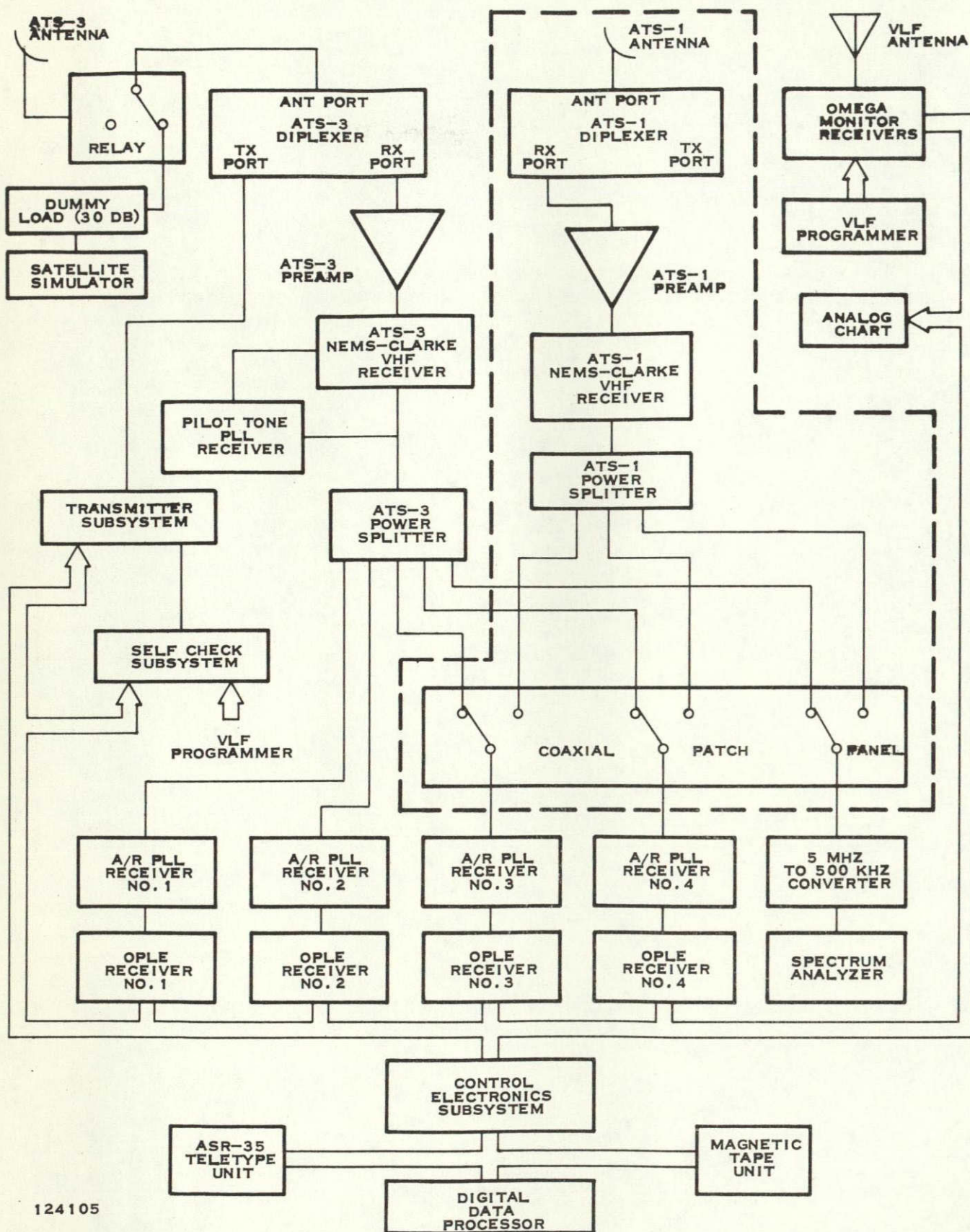


Figure A-5. OPLE-VHF Range/Range Ground Control Center, Block Daigram

D. Self-Check Subsystem

In the OPLE Experiment configuration, the self-check subsystem simulates OPLE PEP data, which consists of an A/R tone and OMEGA-sequenced sidetones, and generates PEP interrogation data. In the VHF Range/Range Experiment configuration, the self-check subsystem provides a continuous transmission of A/R tone and sidetones.

E. VLF Receiver Subsystem

The VLF receiver subsystem, manufactured by Tracor Incorporated, processes the data that is provided by the phase-locked synchronous demodulators and the OMEGA monitor signals that are received directly from the Omega transmitters. The processed Omega monitor data and the processed phase data from the phase-locked synchronous demodulators are output to the control electronics subsystem for digitization. The Omega monitor data is also displayed by means of an analog chart recorder.

II. OCC Modifications

A. General

The modifications to the OPLE Control Center necessary to provide the functions required of the GCC in the VHF Satellite Navigation Experiment consisted of relatively simple wiring changes and equipment additions. These modifications were implemented in such a way as to render the equipment readily convertible to either an OPLE Experiment configuration or a VHF Range/Range Experiment configuration. The required modifications to the OPLE Control Center are as follows:

- Addition of an ATS-1 receive subsystem consisting of a VHF helical antenna, VHF diplexer, preamplifier, and NEMS-CLARKE Receiver

- Addition of a coaxial patch panel to enable assigning A/R tone phase-lock loop receivers No. 3 and No. 4 to either the ATS-1 or ATS-3 receive subsystems

- Modification of the self-check subsystem to enable continuous rather than Omega-sequenced transmission of tones.

Figure A-5 depicts the configuration of the modified OPLE Ground Control Center. The dotted lines depict the additional equipment required to convert the station to an OPLE-VHF Range/Range Ground Control Center. Basically, the modification to accommodate the VHF Range/Range program consisted of assigning two A/R tone phase-lock loop receivers to an ATS-1 satellite receive subsystem. A list of equipment additions and/or modifications to achieve the VHF Range/Range configuration is given below. A more detailed description of the modifications follows the listing.

- Addition of an ATS-1 receive subsystem consisting of a VHF helical antenna, diplexer, preamplifier, and NEMS-CLARKE VHF receiver

- Addition of coaxial patch panel to enable assigning A/R tone phase-lock loop receivers No. 3 and No. 4 to either the ATS-1 Receive Subsystem or the ATS-3 receive subsystem

Modification of the self-check subsystem to enable continuous rather than OMEGA-sequenced transmission of tones. The function of the three sidetone AMPL and PHASE switches on the front panel of the self-check subsystem drawer for both the OPLE mode and VHF Range/Range mode is presented in Table A-1.

TABLE A-1. FUNCTION OF SIDETONE AMPL AND PHASE SWITCHES

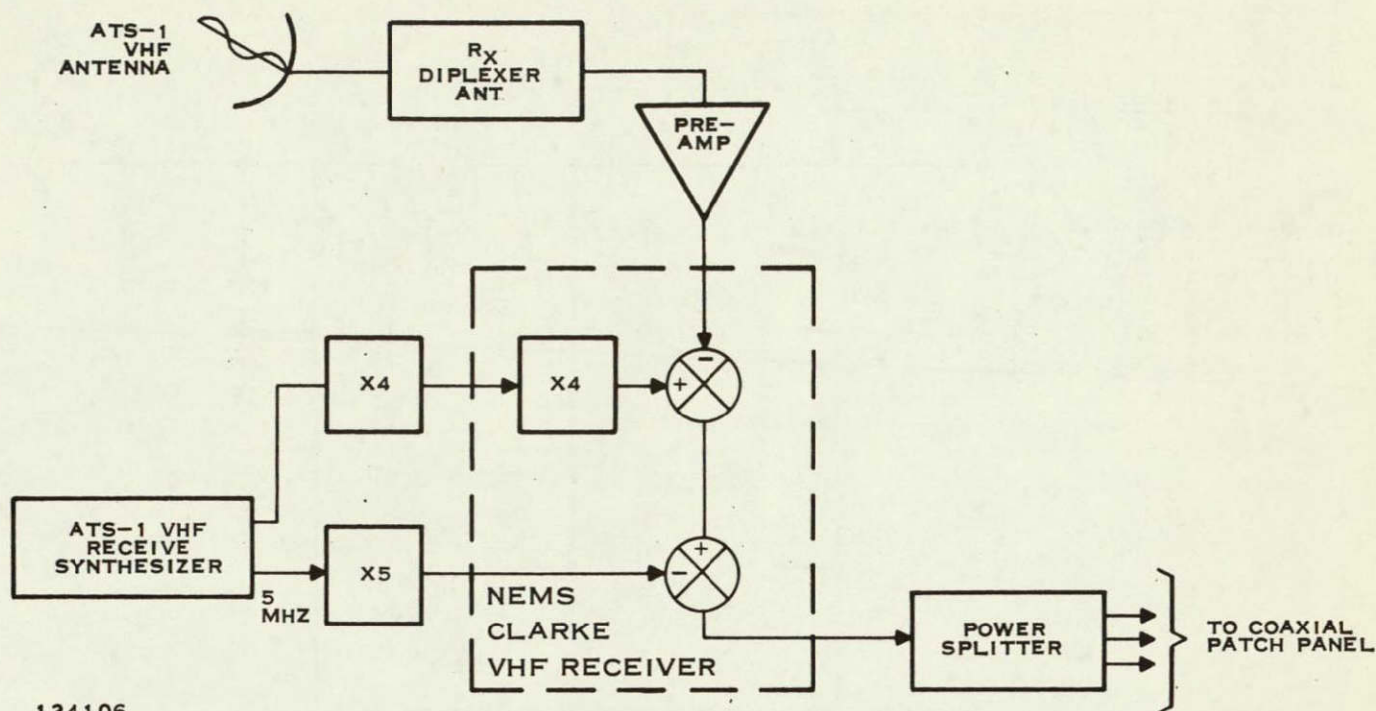
Switches	VHF Range/Range	OPLE
STATION A AMPL and PHASE switches	Adjusts amplitude and phase of the 941-Hz (13.6-kHz) sidetone.	Adjusts amplitude and phase of the sidetone transmissions associated with Station A.
STATION B AMPL and PHASE switches	Adjusts amplitude and phase of the 426-Hz (10.2-kHz) sidetone.	Adjusts amplitude and phase of the sidetone transmissions associated with Station B.
STATION D AMPL and PHASE switches	Adjusts amplitude and phase of the 707-Hz (11.3-kHz) sidetone.	Adjusts amplitude and phase of the sidetone transmissions associated with Station D.

B. ATS-1 Receive Subsystem Modifications

Figure A-6 is a block diagram of the added ATS-1 receive subsystem. The ATS-1 antenna is a Fairchild helical antenna with positioner. Because of the physical proximity of the ATS-1 antenna to the ATS-3 antenna (approximately 33 feet), it was found necessary to install a diplexer to protect the ATS-1 VHF receiver preamplifier from being saturated by transmitted signals from the ATS-3 antenna. The diplexer is a Microlab-FXR model (Texas Instruments Drawing No. SK594097) which was installed with the original OPLE Ground Control Center. The antenna and diplexer were furnished GFE for VHF Range/Range program.

The ATS-1 receiver preamplifier contains a front end FET stage for optimum noise figure. The preamplifier has a gain of approximately 27 dB and a noise figure of 2.5 dB. Because of the low figure afforded by the FET stage an identical preamplifier was installed in the ATS-3 receive subsystem replacing the vacuum tube version (Rantec Corp. EPV904). Figure A-7 is a schematic of the FET preamplifier.

The 135.6-MHz signal from the ATS-1 receiver preamplifier is converted down in the ATS-1 NEMS-CLARKE telemetry receiver (Model 1456A) to 5 MHz and brought out to a power splitter. The first mixing signal for the receiver is provided by a X16 multiplier which receives its input signal from the ATS-1 VHF receive synthesizer. The second mixing signal for the receiver is provided by a 25-MHz multiplier which receives its input signal from the 5-MHz output of the ATS-1 VHF receive synthesizer. The X16 multiplier consists of an external X4 multiplier (Type TD, Texas Instruments Drawing No. SK592235) and a X4 multiplier which is internal to the NEMS-CLARKE receiver. The 25-MHz multiplier is a type TE board (Texas Instruments Drawing No. SK592229). The power splitter, which follows the NEMS-CLARKE receiver, is similar to the one used in the ATS-3 receive subsystem. A schematic of the ATS-1 power splitter is shown in Figure A-8.



124106

Figure A-6. Receive Subsystem Block Diagram

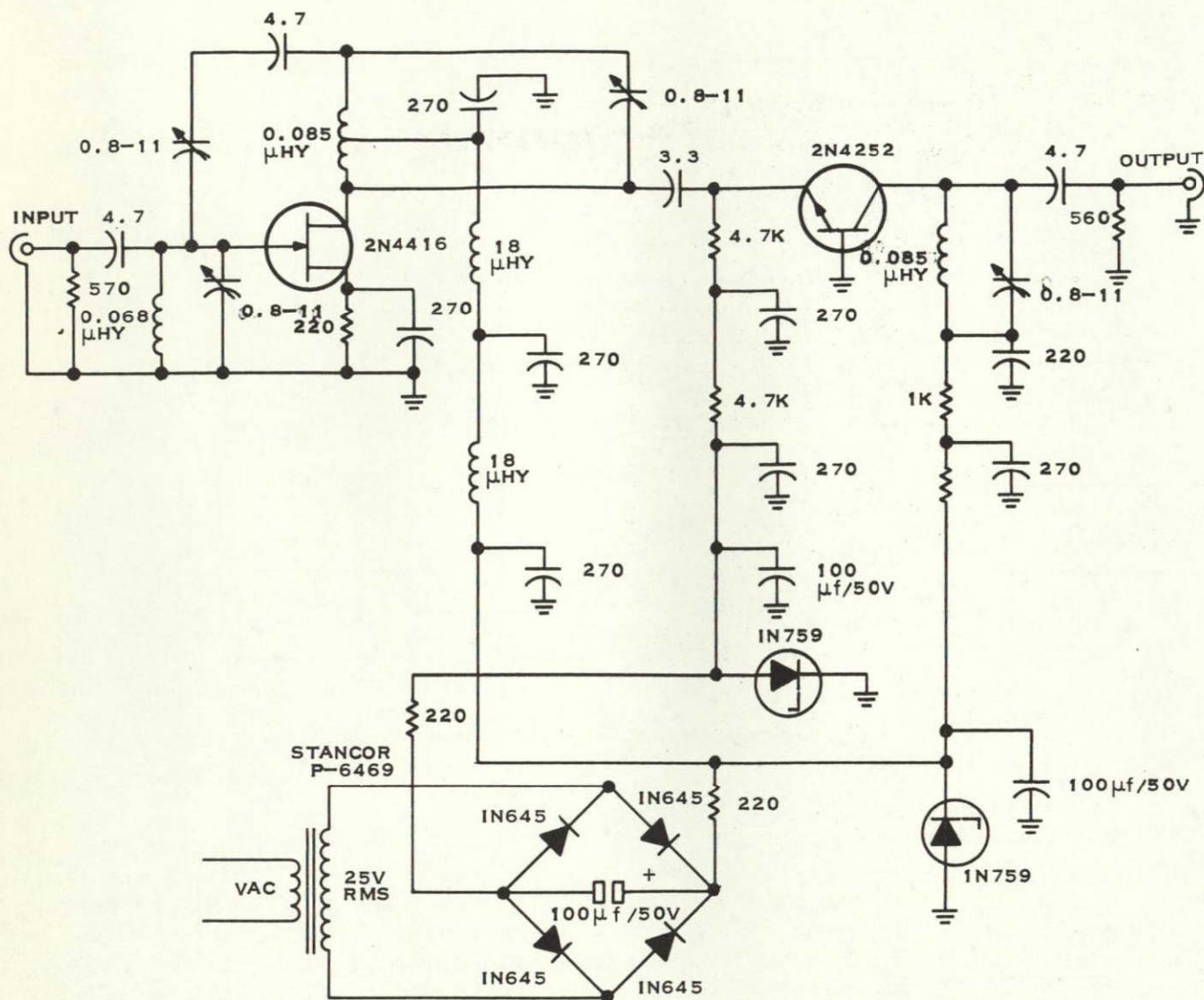
C. Coaxial Patch Panel

The function of the coaxial patch panel is to provide front-panel control in assigning A/R tone phase-lock loop receivers to either the ATS-1 or ATS-3 receive subsystem. Specifically, A/R tone phase-lock loop receivers No. 3 and No. 4 and the monitor circuitry consisting of a spectrum analyzer can be assigned to either the ATS-1 or ATS-3 receive subsystem. A functional schematic of the coaxial patch panel is shown in Figure A-5.

D. Self-Check Subsystem Modifications

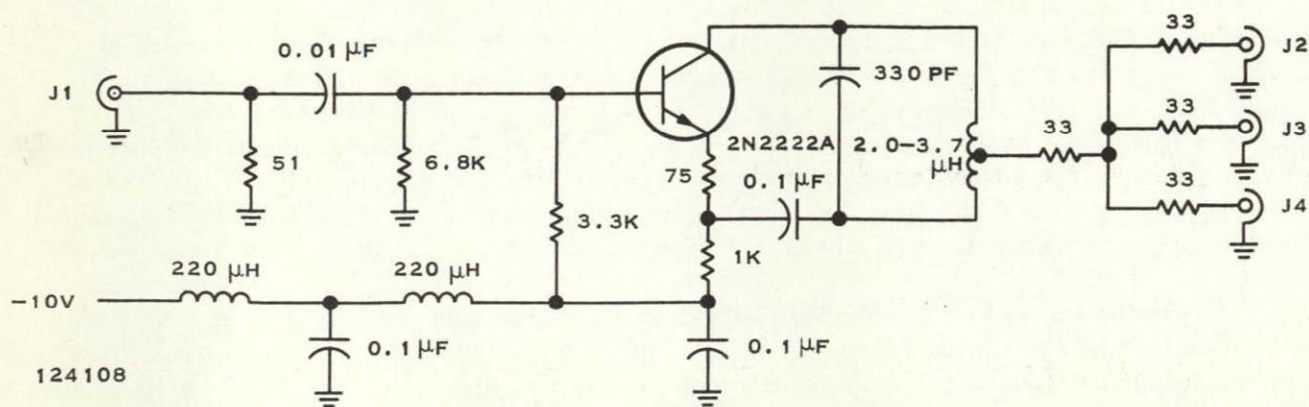
The self-check subsystem modifications provide for continuous rather than the commutated OMEGA sequence transmission of sidetones. An OPLE-VHF R/R switch was installed on the front panel of the self-check subsystem drawer in place of the NOISE-ON-OFF switch (S7). As shown in Figure A-9, in the VHF R/R switch position OMEGA intervals 2 and 6 become PMODE and OMEGA intervals 1, 3, 4, and 5 are shorted to ground. Station B's 426-Hz tone and Station A's 941-Hz tone are generated during interval 2 and Station D's 707-Hz tone is generated during interval 6. Thus, by switching intervals 2 and 6 to the signal PMODE, and shorting to ground all other interval counts, the three sidetones can be continuously transmitted.

One output amplifier was also added to boost the final output level of self-check subsystem drawer. This amplifier was found to be necessary to provide an adequate transmitted power level of A/R tone and sidetone. A schematic of the amplifier is shown in Figure A-10. The gain of the output amplifier can be varied from about +12 dB to about +7 dB.



124107

Figure A-7. FET Preamplifier, Schematic Diagram



124108

Figure A-8. Power Splitter, Schematic Diagram

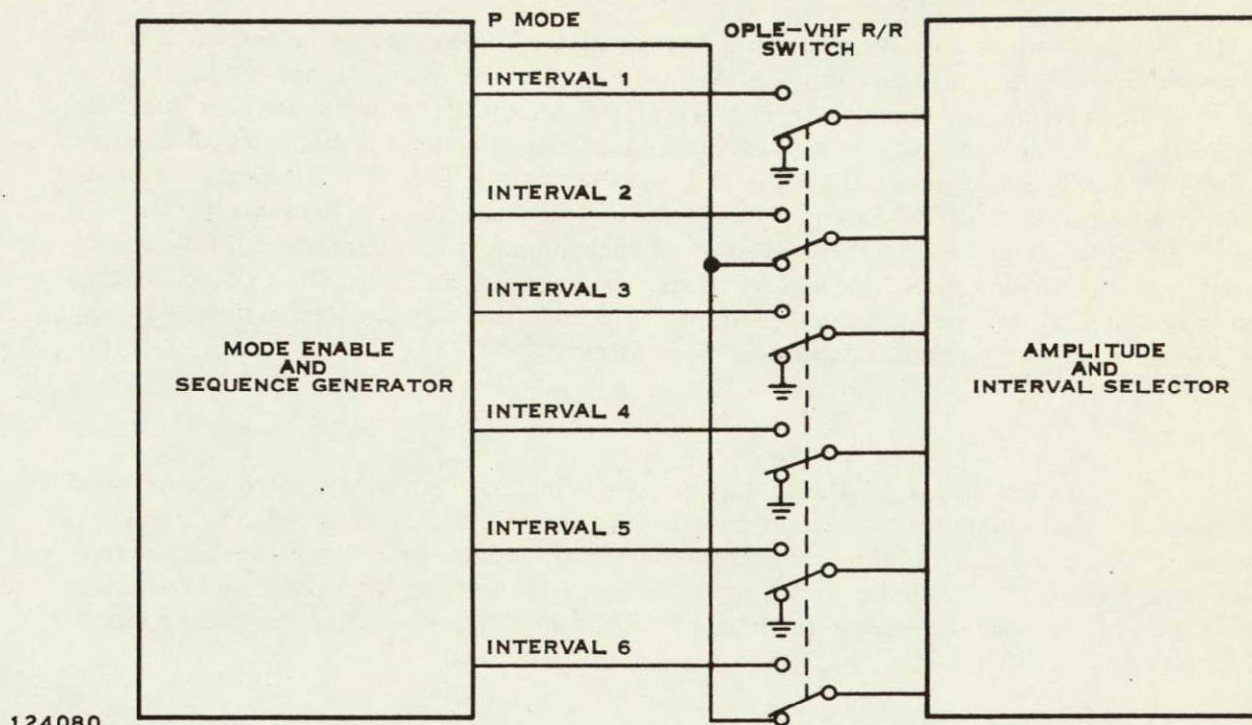


Figure A-9. Self-Check Subsystem Modification, Block Diagram

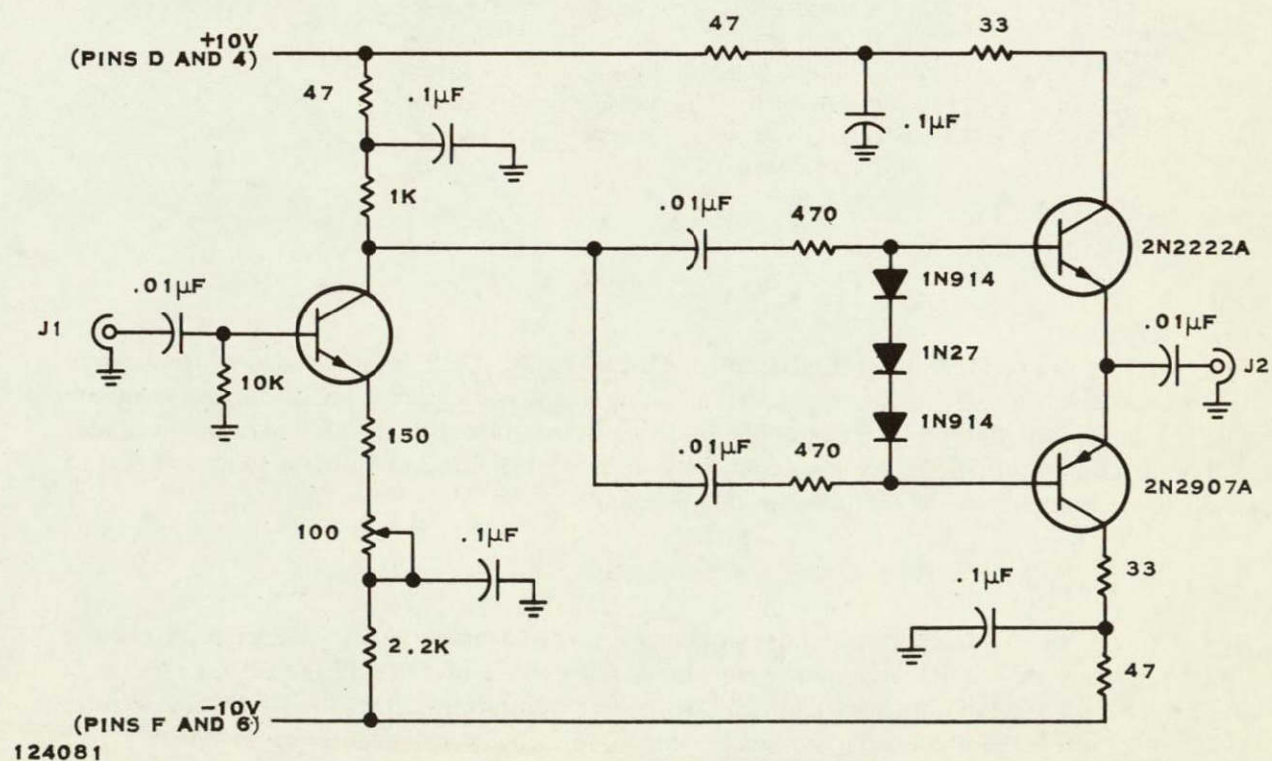


Figure A-10. Self-Check Subsystem Output Amplifier, Schematic Diagram

III. Conversion Procedures

The Omega Position Location Equipment as presently configured can be operated in two different modes: (1) the original OPLE mode, and (2) the VHF Range/Range mode. It is the purpose of this section to describe the conversion and set up of the equipment for the VHF Range/Range mode of operation. A detailed checkout of the equipment in both the OPLE mode and the VHF Range/Range mode is presented in the Acceptance Test—Part I Individual Test for Ground Control Center—VHF Satellite Navigation Experiment (Texas Instruments Drawing No. SK714211). A description of the conversion of the equipment is first presented, followed by a description of the setup of the various frequency synthesizers, calculation of appropriate ephemeris data, and software constants required to render the software compatible with any given geographic location of the Ground Control Center.

A. Conversion

A concise description of the proper switch settings, the required printed circuit board exchange, and the switching of certain cables is presented in the above-mentioned Texas Instruments Drawing No. SK714211. However, the switch settings on the self-check subsystem drawer should be further discussed to distinguish between the settings for a one-tone experiment utilizing the 941-Hz sidetone and a three-tone experiment. Table A-2 gives the proper switch settings for the two different tone package configurations.

TABLE A-2. SWITCH SETTINGS FOR TONE PACKAGES

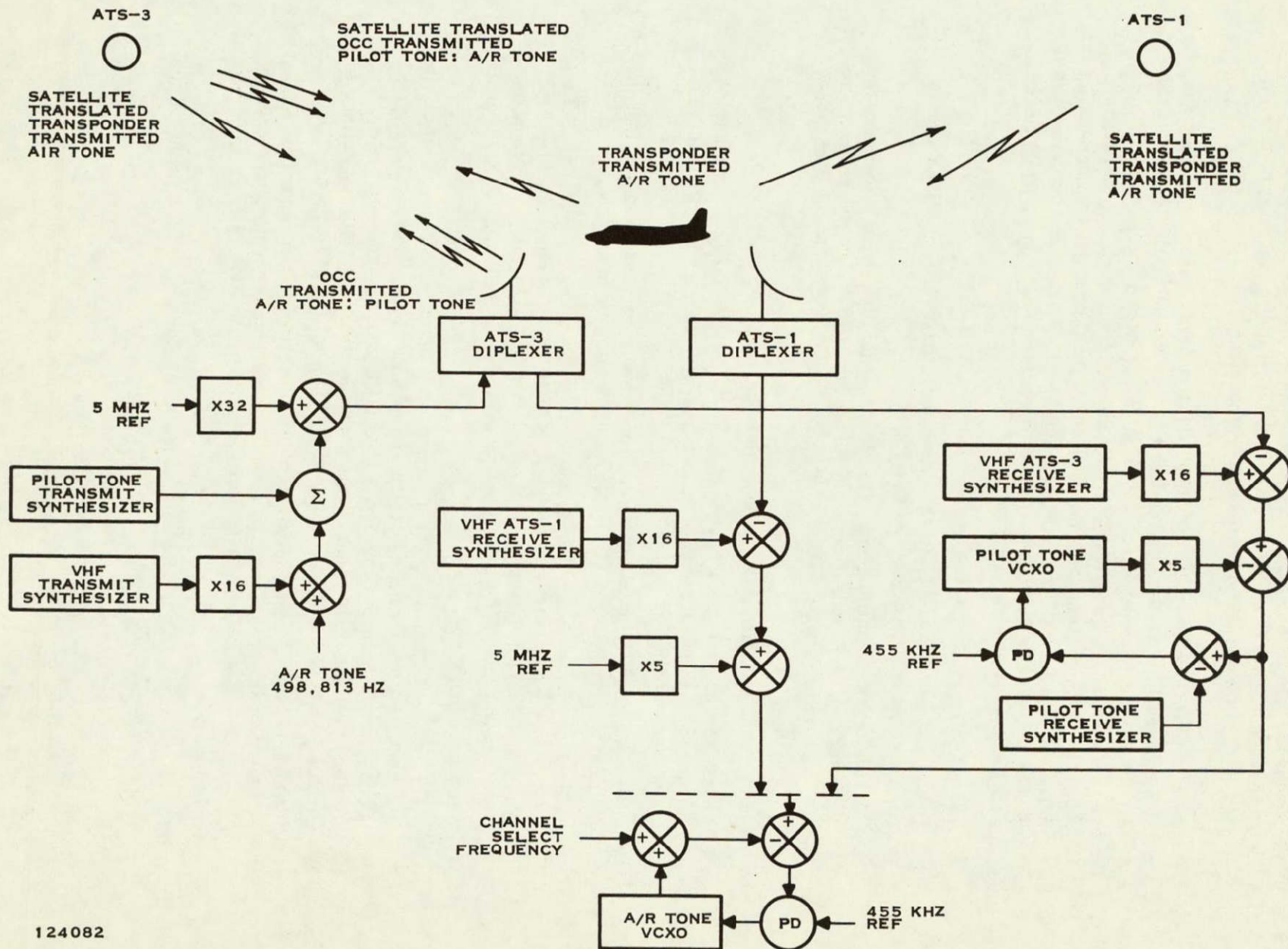
Switch	One Tone	Three Tones
STATION A PHASE switch	0 degree	0 degree
STATION A AMPL switch	Maximum	Maximum
STATION B PHASE switch	0 degree	0 degree
STATION B AMPL switch	Minimum	Maximum
STATION D PHASE switch	0 degree	0 degree
STATION D AMPL switch	Minimum	Maximum

B. Setup

Having converted the Ground Control Center to the VHF Range/Range configuration, it is now necessary to select the proper frequencies for the frequency synthesizers, calculate appropriate ephemeris data, and enter appropriate constants into the on-line software to render the software compatible with the geographic location of the Ground Control Center. Each of three above-mentioned tasks is discussed in detail below.

1. Frequency Settings

A block diagram of the frequencies involved is shown in Figure A-11. If the transmit frequency of the transponders were identical to those of the OPLE PEP's, and if both the ATS-1 and ATS-3 satellites had identical frequency translations, then the frequency settings used for the OPLE configuration would be adequate. However, because of a rather larger



124082

Figure A-11. Frequency Block Diagram

discrepancy in the frequency translations of the ATS-1 and ATS-3 satellites, coupled with the presence of a low received signal level at the Ground Control Center, great care must be taken in selecting the frequency settings for the various frequency synthesizers.

Consider a second order loop containing a pseudo rather than true integrator, which is the type of loop used in both the transponders and the Ground Control Center. It can be easily shown that for a given received signal power at the front-end receiver, the hold-in capability of the loop increases as the frequency of the incoming signal approaches that required to bring the VCXO in the phase-lock loop to its rest frequency. Thus the major consideration in calculating the required frequencies will be to ensure that the incoming frequencies into all phase-lock loops are such to bring the VCXO's to their rest frequency. This consideration can be concisely stated as below:

The received pilot tone at the transponder must be 135,566,250 Hz.

The received A/R tone at the transponder must be 35 kHz above the received pilot tone, or 135,601,250 Hz.

At the Ground Control Center the received pilot tone from ATS-3 and the received A/R tone from both ATS-1 and ATS-3 must be presented to the respective phase-lock loops such that the VCXO's are at their rest frequencies.

The steps involved in calculating the frequency settings are as follows:

- Knowing the translation frequency of the ATS-3 satellite, calculate the frequency setting of the pilot tone transmit synthesizer to ensure the pilot tone as received at the transponder is 135,566,250 Hz.
- Calculate the VHF transmit synthesizer frequency setting to ensure that the transmitted A/R tone is 35 kHz above the transmitted pilot tone.
- Knowing the transmit frequency of the transponder, and the ATS-3 translation frequency, calculate the ATS-3 VHF receive synthesizer frequency setting to ensure the A/R phase-lock loop VCXO's are at their rest frequency (assume in this calculation that the pilot tone phase-lock loop VCXO is at its rest frequency).
- The received pilot tone at the Ground Control Center is identical in frequency to that received at the transponder. Thus knowing the received pilot tone frequency and the ATS-3 VHF receive synthesizer frequency setting, calculate the pilot tone receive synthesizer frequency setting to ensure the pilot tone phase-lock loop VCXO is at its rest frequency.
- Knowing the transmit frequency of the transponder and the ATS-1 translation frequency, calculate the ATS-1 VHF receive synthesizer frequency setting to ensure the A/R phase-lock loop VCXO's are at their rest frequency.

The equations involved in solving the required frequency settings, along with a listing of the nomenclature used, is given in the following.

$$\begin{aligned}
f_{s_3} &= \text{ATS-3 satellite translation frequency} \\
f_{s_1} &= \text{ATS-1 satellite translation frequency} \\
f_{T_x PT} &= \text{pilot tone transmit synthesizer frequency setting} \\
f_{T_x VHF} &= \text{VHF transmit synthesizer frequency setting} \\
f_{R_x ATS-3} &= \text{ATS-3 VHF receive synthesizer frequency setting} \\
f_{R_x ATS-1} &= \text{ATS-1 VHF receive synthesizer frequency setting} \\
f_{R_x PT} &= \text{pilot tone receive synthesizer frequency setting} \\
f_{trans} &= \text{transponder transmit frequency} \\
f_{PTVCXO} &= \text{rest frequency of pilot tone phase-lock loop} \\
&\quad VCXO = 5,000,000 \text{ Hz} \\
f_{A/RVCXO} &= \text{rest frequency of A/R phase-lock loop} \\
&\quad VCXO (4,001,456 \text{ Hz} + \text{channel select frequency}) \\
f_{T_x PT} &= 160,000,000 - (135,566,250 - f_{s_3}) \\
&\quad (160,000,000 - f_{T_x PT} + 35,000) - 498,813 \\
f_{T_x VHF} &= \frac{160,000,000 - f_{T_x PT} + 35,000 - 498,813}{16} \\
f_{R_x ATS-3} &= \frac{[f_{trans} - f_{s_3}] + [f_{A/RVCXO} + 455,000 + 5 f_{PTVCXO}]}{16} \\
f_{R_x PT} &= 16 f_{R_x ATS-3} - 135,566,250 - 455,000 - 5 f_{PTVCXO} \\
f_{R_x ATS-1} &= \frac{[f_{trans} - f_{s_1}] + [f_{A/RVCXO} + 25,455,000]}{16}
\end{aligned}$$

2. Ephemeris Calculations

The ephemeris data required by the on-line software program is listed below:

Distance from Ground Control Center to both ATS-1 and ATS-3 satellites

Distance from center of earth to both ATS-1 and ATS-3 satellites

Direction cosines of both satellites from center of earth (the coordinate system utilized in calculating the direction cosines is presented later in this section)

Distance from center of earth to both reference and aircraft transponder.

The units in which the above-listed items must be entered into the on-line program, and the accuracy to which they must be calculated are given in Table A-3. The coordinate system utilized in deriving the above parameters is shown in Figure A-12. Definition of the nomenclature used is as follows:

θ = longitude of satellite

ϕ = latitude of satellite

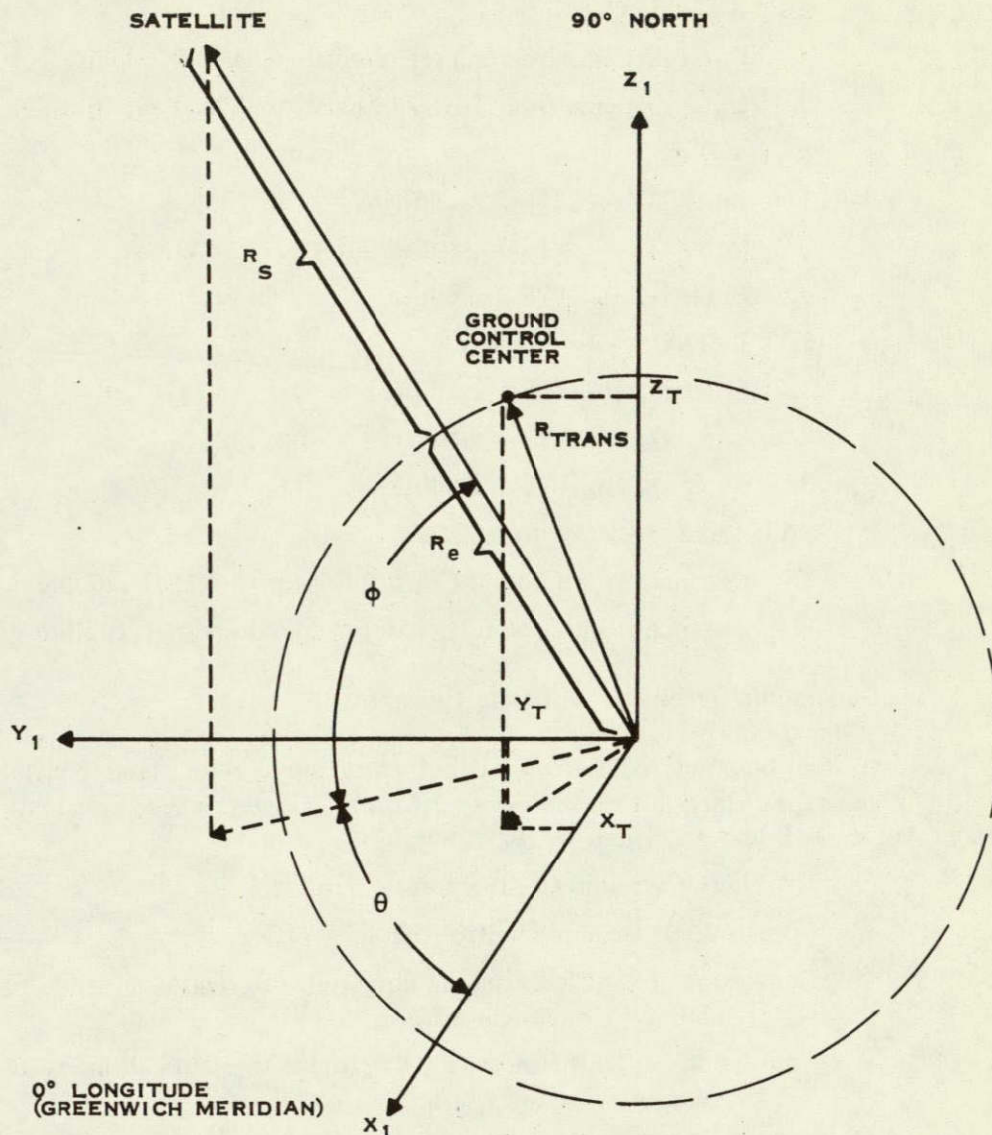
$R_{\text{sat}} = R_s + R_e$ = distance from satellite to center of earth
 R_{Trans} = distance from transponder to center of earth
 D_1 = cosine [angle between R_{sat} and X-axis]
 D_2 = cosine [angle between R_{sat} and Y-axis]
 D_3 = cosine [angle between R_{sat} and Z-axis]
 R_o = distance from Ground Control Center to satellite
 X_T = projection of R_{trans} onto X-axis
 Y_T = projection of R_{trans} onto Y-axis
 Z_T = projection of R_{trans} onto Z-axis.

It should be at once emphasized that in contrast to the accepted convention, the coordinate system used to calculate the ephemeris data is a left-handed rather than a right-handed coordinate system. That is, 50 degrees west in longitude from the Greenwich meridian is considered a positive angle in the coordinate system used. It is necessary to use the left-handed coordinate system in calculating the ephemeris data because the on-line software program utilizes a left-handed coordinate system in the position location algorithm. The equations for the required inputs are given below:

$$\begin{aligned}
 D_1 &= \cos \phi \cos \theta \\
 D_2 &= \cos \phi \sin \theta \\
 D_3 &= \sin \phi \\
 R_o &= [(R_{\text{sat}} D_1 - X_T)^2 + (R_{\text{sat}} D_2 - Y_T)^2 + (R_{\text{sat}} D_3 - Z_T)^2]^{1/2}
 \end{aligned}$$

TABLE A-3. EPHEMERIS DATA UNITS AND ACCURACY

Item	Units (meters)	Accuracy (percent)
Satellite altitude from center of earth	10^6	0.0003
Transponder altitude from center of earth	10^6	0.0003
Distance from ground control center to satellite	10^6	0.0003
Satellite direction cosines	—	0.001



124083

Figure A-12. Ephemeris Coordinate System

The mechanism for entering the calculated ephemeris data into the on-line software program is presented in the acceptance test procedure (Texas Instruments Drawing No. SK714211). However, the acceptance test procedure does not describe which entry is applicable to the ATS-3 satellite and which entry is applicable to the ATS-1 satellite. The listing below presents the order in which the data must be entered in response to the various questions asked by the software program. All numbers entered via the teletype for the ephemeris data are decimal numbers.

AC 1 and 2 ALT

1. Enter distance from center of earth to aircraft transponder.
2. Enter distance from center of earth to reference transponder or second aircraft transponder.

SAT 1 and 2 ALT

1. Enter distance from center of earth to ATS-3 satellite.
2. Enter distance from center of earth to ATS-1 satellite.

SAT 1 D COS

1. Enter D_1 for ATS-3 satellite.
2. Enter D_2 for ATS-3 satellite.
3. Enter D_3 for ATS-3 satellite.

SAT 2 D COS

1. Enter D_1 for ATS-1 satellite.
2. Enter D_2 for ATS-1 satellite.
3. Enter D_3 for ATS-1 satellite.

SAT 1 and 2 Ranges from OCC

1. Distance from Ground Control Center to ATS-3 satellite.
2. Distance from Ground Control Center to ATS-1 satellite.

3. Geographic-Dependent Software Constants

In the position location algorithm there are certain fixed constants which are unique to the geographic location of the Ground Control Center. These constants are described in detail in Appendix B and are listed below.

Latitude of Ground Control Center + offset

Longitude of Ground Control Center + offset

Conversion of differences in longitude to nautical miles for a full-scale reading of 70 nautical miles

Conversion of differences in longitude to nautical miles for a full-scale reading of 35 nautical miles.

The development of the equations for calculating the geographic constants are also presented in Appendix B and are listed below:

$$\text{Conversion Factor}_{70 \text{ mile}} = 12,543.68 \cos (\text{latitude}_{\text{Ground Control Center}})$$

$$\text{Conversion Factor}_{35 \text{ mile}} = 2 \text{ Conversion Factor}_{70 \text{ mile}}$$

$$\text{Latitude} + \text{Offset} = \text{Latitude of Ground Control Center in radians} - 0.01016$$

$$\text{Longitude} + \text{Offset} = \text{Longitude of Ground Control Center in radians} + 0.01016/\cos (\text{latitude}_{\text{GCC}})$$

Again, it is emphasized that in utilizing the above equations a left-handed coordinate system is used where angles designating west longitude are positive angles. The location of these constants in the on-line software program and the accuracy to which they must be calculated are presented in Table A-4. Each constant is entered into the software program as a binary floating number, thus the requirement for two memory locations per constant. The

TABLE A-4. GEOGRAPHIC CONSTANTS, MEMORY LOCATIONS, AND ACCURACY

Constant	Memory Locations	Accuracy (percent)
Conversion Factor ₇₀ mile	10614 ₈ and 10615 ₈	0.0003
Conversion Factor ₃₅ mile	10612 ₈ and 10613 ₈	0.0003
Latitude + Offset	10542 and 10543	0.0003
Longitude + Offset	10540 and 10543	0.0003

TABLE A-5. FORMAT FOR ENTERING CONSTANTS

Bit No.	15	14	13	12	11	10	9	8	7	6	5	4	3	2	1	0
Word 1	S	Exponent + 0200 ₈									High Mantissa					
Word 2	0	Low Mantissa														

format for entering the constants as floating point binary numbers is shown in Table A-5. An example to demonstrate the procedure for converting a decimal number to the above floating point format is presented as follows for the decimal number 10529.8.

First convert the integer part of the decimal number to an octal number

$$10,529_{10} = 24,441_8$$

Convert the fractional part of the decimal number to an octal number

$$0.8_{10} = 0.63146_8$$

Thus the mantissa for the number is

$$2444163146_8$$

or

$$\frac{2}{10} \quad \frac{4}{100} \quad \frac{4}{100} \quad \frac{4}{100} \quad \frac{1}{001} \quad \frac{6}{110} \quad \frac{3}{001} \quad \frac{1}{001} \quad \frac{4}{100} \quad \frac{6}{110}$$

The exponent is determined by counting the number of binary bits that are required to represent the integer part of the octal number ($24,441_8$)

$$\text{No. of bits} = 14_{10} = 16_8$$

$$\text{Then the exponent} + 0200_8 = 0216_8$$

Thus the floating point number is:

$$\begin{array}{cccccccccccccccc} \text{word 1} = & 15 & 14 & 13 & 12 & 11 & 10 & 9 & 8 & 7 & 6 & 5 & 4 & 3 & 2 & 1 & 0 \\ & 0 & 1 & 0 & 0 & 0 & 1 & 1 & 1 & 0 & 1 & 0 & 1 & 0 & 0 & 1 & 0 \\ & & \underbrace{}_{2'} & & \underbrace{}_1 & & \underbrace{}_6 & & \underbrace{}_2 & & \underbrace{}_4 & & \underbrace{}_4 & & & & \end{array}$$

$$\begin{array}{cccccccccccccccc} \text{word 2} = & 0 & 0 & 1 & 0 & 0 & 0 & 0 & 1 & 1 & 1 & 0 & 0 & 1 & 1 & 0 & 0 \\ & & & \underbrace{}_4 & & \underbrace{}_1 & & \underbrace{}_6 & & \underbrace{}_3 & & & & & & & \end{array}$$

or expressing the result in octal we have

$$\text{word 1} = 043522$$

$$\text{word 2} = 020714$$

APPENDIX B

SOFTWARE DESCRIPTION

I. General

This appendix describes and contains flow charts for both the on-line and off-line VHF Range/Range programs. The on-line VHF Range/Range program does not provide for on-line printout of data because of time limitations. Since a new position-location calculation is performed every 5 seconds, it would not be feasible to both continuously input raw phase data and compute position and at the same time output the raw data and the calculated data. Thus, the raw and calculated data gathered during an on-line experiment is stored on magnetic tape for subsequent printout by an off-line program. The on-line program will be first discussed, followed by a description of the off-line program.

II. On-Line Program Description

A flow diagram of the on-line program is presented in Figure B-1. The program inputs digitized raw phase data from the OPLE Receivers and from this data computes the location of the transponder(s) relative to the location of the Ground Control Center or reference transponder. Provision is also made for inputting radar data to serve as "truth" measurements. The position-location algorithm will be first discussed, followed by an operations procedure for the on-line software program.

A. Position-Location Algorithm

The equations relating position location to the appropriate input measurement parameters for both absolute and differential ranging are developed in this section. Three parameter measurements are required: the range from each of the two satellites to the aircraft and the aircraft altitude above the earth's surface. For the VHF Satellite Navigation Experiment the aircraft altitude is a predetermined constant parameter. Additionally, parameters defining the position of both satellites with respect to the Ground Control Center and the distance from the earth's center to the two satellites are required.

The ranging equations may be divided into two major subsections; phase angle difference calculations, and position location calculations. A simplified flow diagram of the position location algorithm is presented in Figure B-2.

1. Phase Angle Difference Calculations

To calibrate the system, phase measurements for each tone and each receiver must be made from the GCC to the reference terminal. To obtain an accurate set of calibration data, the sines and cosines for each tone and receiver are summed for 12 samples. The 12 calibration angles (three tones and four receivers) are calculated as follows:

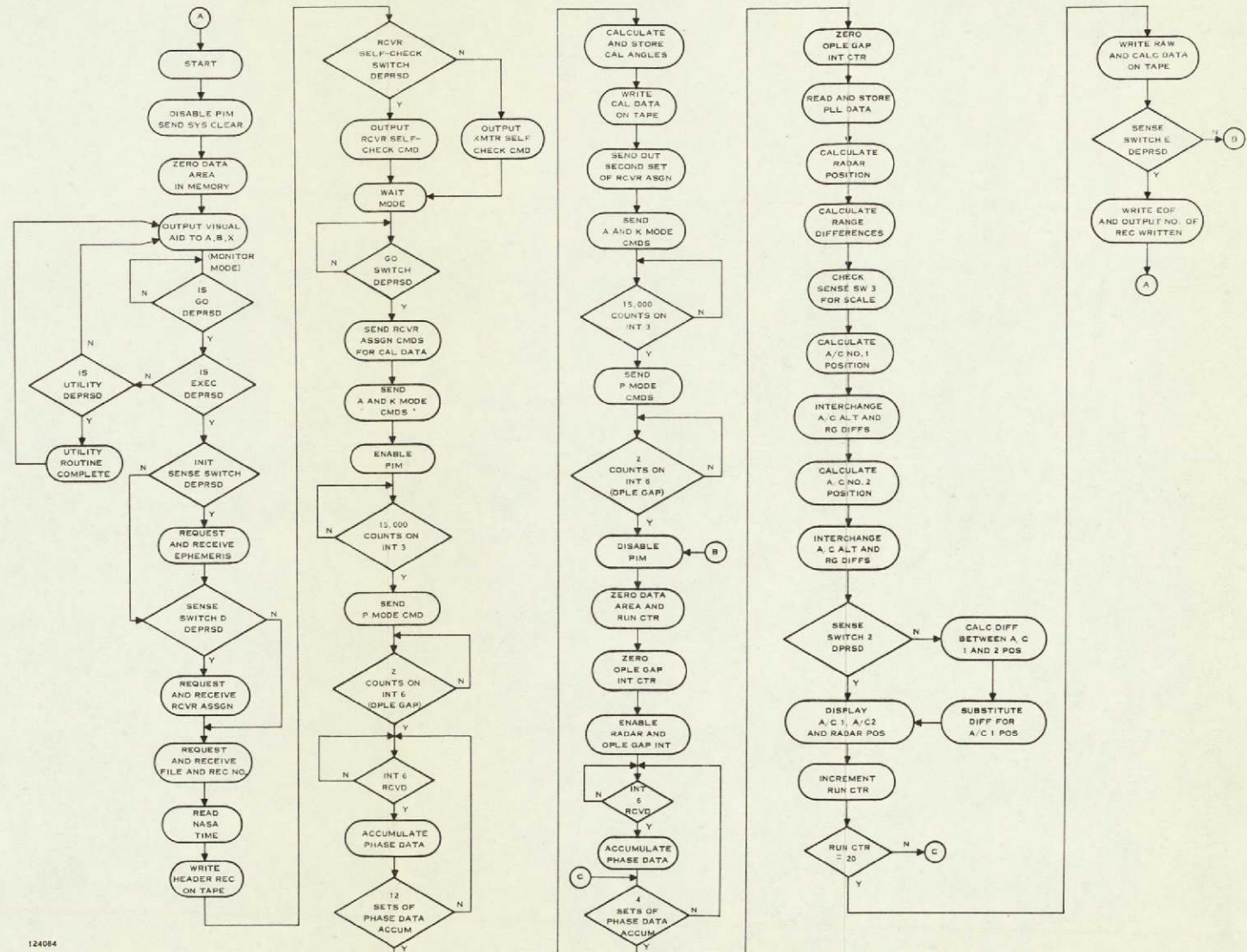
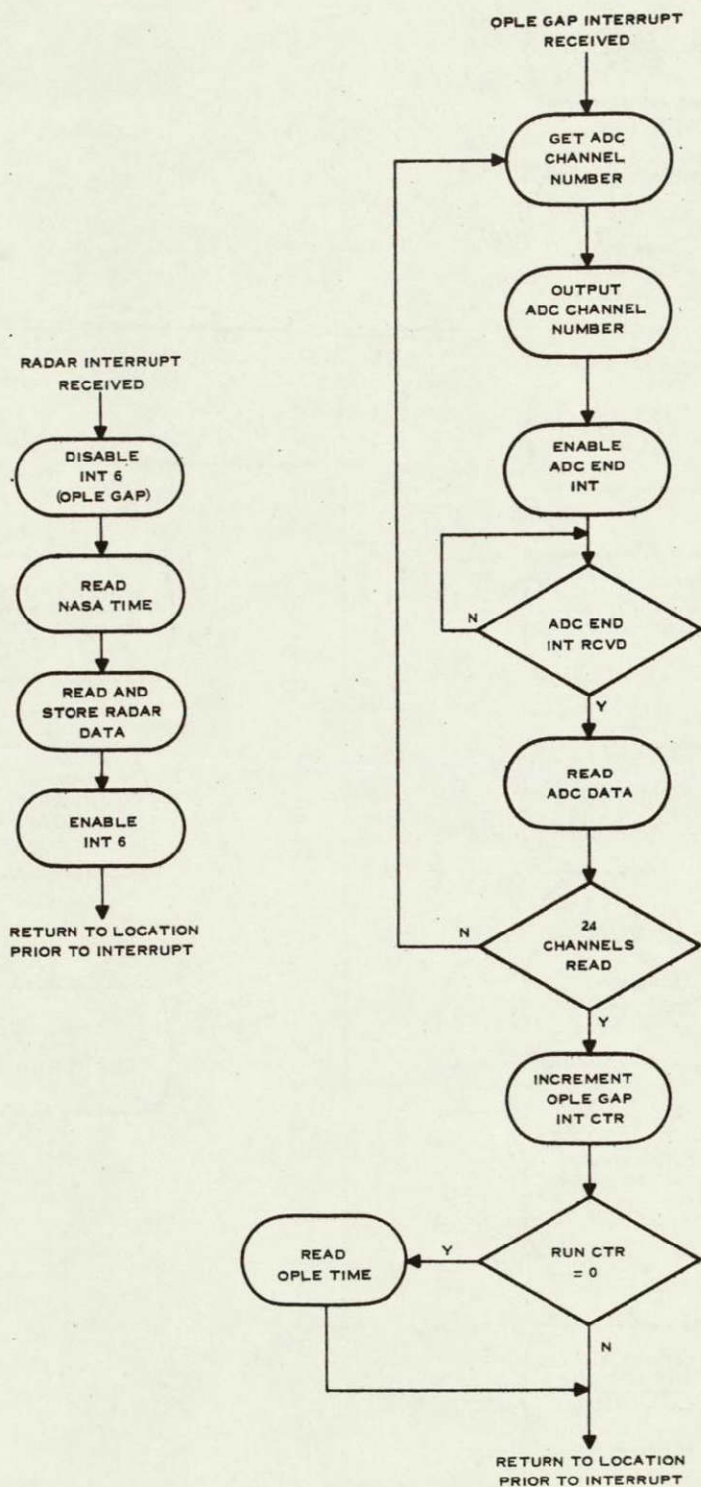
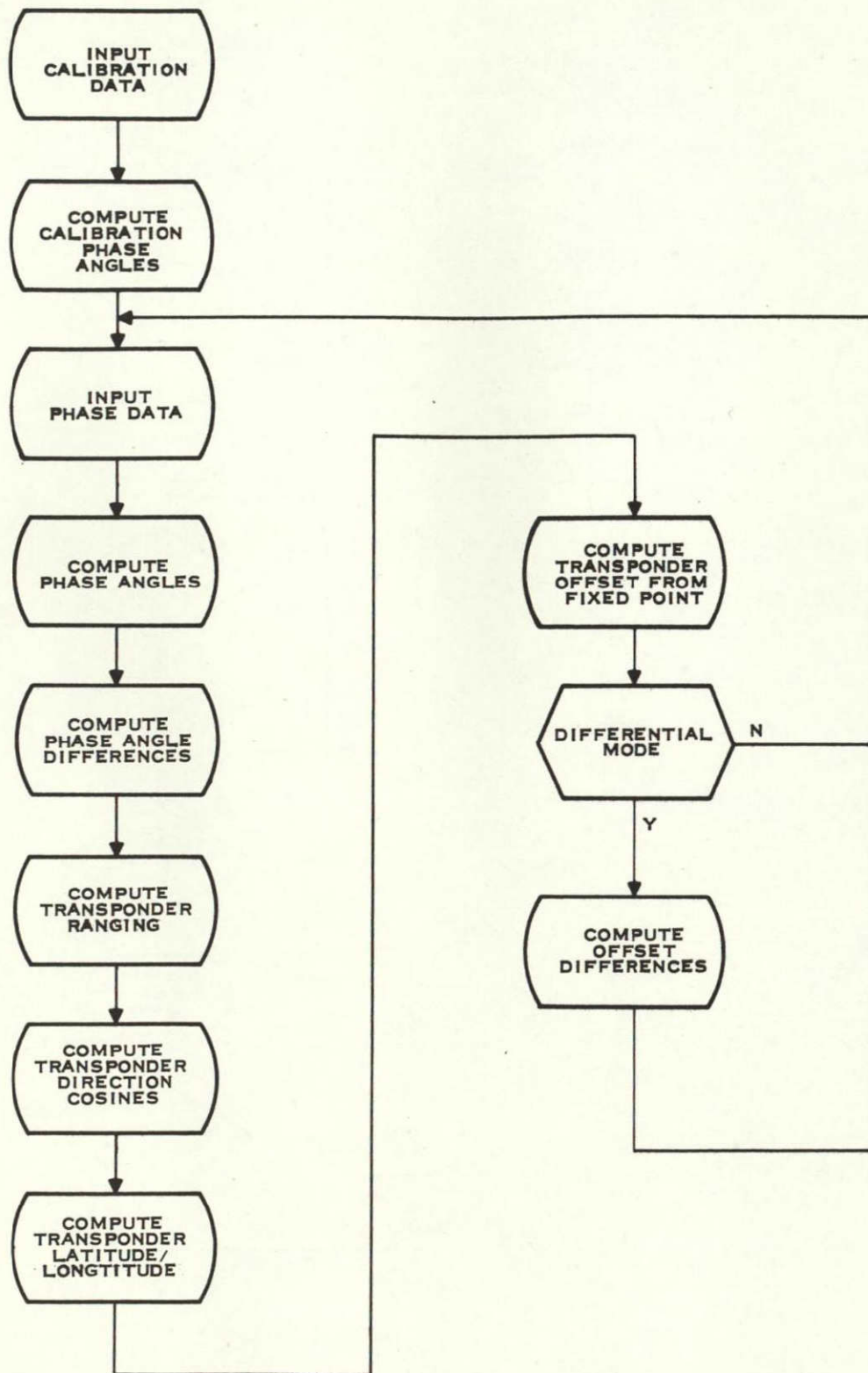


Figure B-1. On-Line Program, Flow Diagram (Sheet 1 of 2)



124085

Figure B-1. On-Line Program, Flow Diagram (Sheet 2 of 2)



124086

Figure B-2. Simplified Flow Diagram of the Position Algorithm

$$\phi_{cnm} = \tan^{-1} \frac{\sum_{i=1}^{12} S_{nmi}}{\sum_{i=1}^{12} C_{nmi}} \text{ radians}$$

where

n = 1-3 tones

m = 1-4 receivers

c = calibration data.

The arctan is accomplished by a table loop-up procedure using a 127-word table for 45 degrees. Should

$$\sum_{i=1}^{12} S_{nmi} \text{ be greater than } \sum_{i=1}^{12} C_{nmi}$$

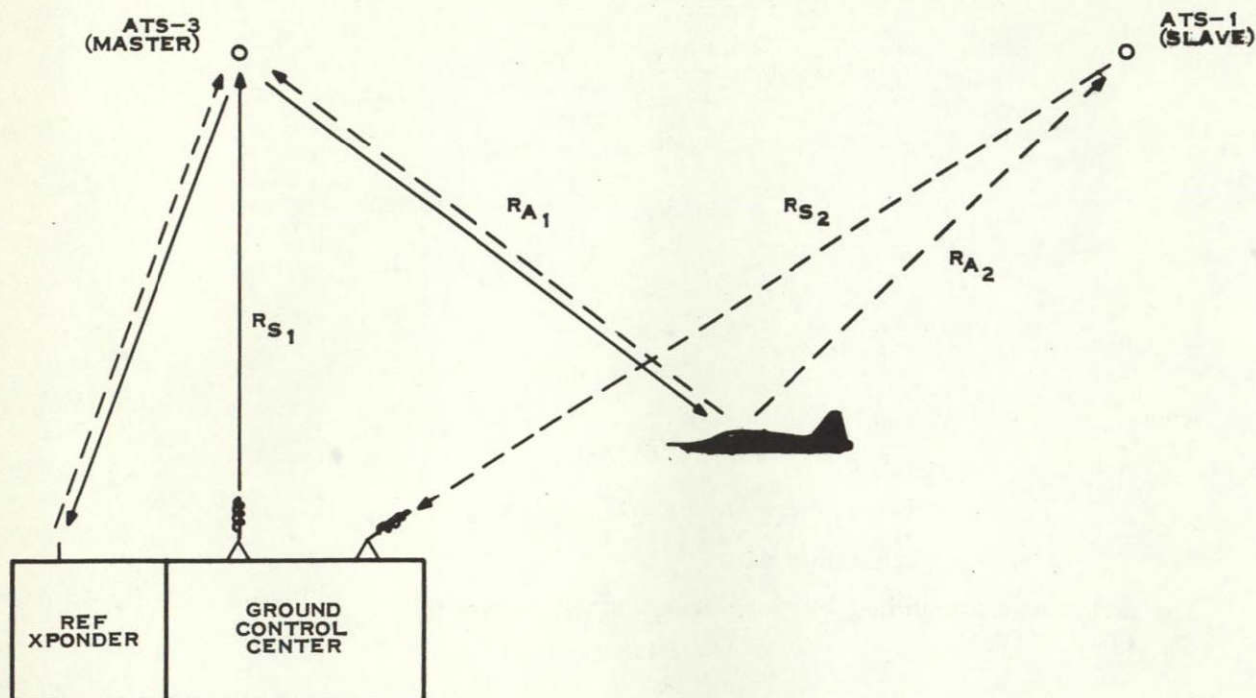
Then the calibration angle is determined as follows:

$$\phi_{cnm} = \pi/2 - \tan^{-1} \frac{\sum_{i=1}^{12} C_{nmi}}{\sum_{i=1}^{12} S_{nmi}} \text{ radians}$$

The quadrant information is determined prior to the table loop-up procedure. The output ϕ_{cnm} is from 0 to 2π radians.

After the calibration angles are calculated and the phase mode is initiated, four phase data sets are read every 5 seconds. The 12 phase angles ϕ_{nm} are calculated in the very same manner as were the calibration angles.

Before initiating the position location calculations, it is necessary to determine the range from the aircraft to the satellite via phase difference calculations. The diagram in Figure B-3 illustrates the principle of the phase difference calculations. The calibration angle measurements involve transmitting a tone package from the Ground Control Center to the master



124087

Figure B-3. Principle Phase Difference Calculations

satellite, from the master satellite to the reference transponder located at the Ground Control Center, from the reference transponder to both satellites, and from both satellites back to the Ground Control Center. Thus the calibration angles pertain to the distance from the OCC to the master or slave satellites. In particular, since phase-lock loop receivers No. 1 and No. 2 are assigned to the master (ATS-3) satellite and receivers No. 3 and No. 4 are assigned to the slave (ATS-1) satellite, it follows:

$$\phi_{cn_1} \text{ and } \phi_{cn_2} = 4 R_{s_1}$$

$$\phi_{cn_3} \text{ and } \phi_{cn_4} = 2 R_{s_1} + 2 R_{s_2}$$

The phase angle measurements involve transmitting a tone package from the Ground Control Center to the master satellite, from the master satellite to both the reference and aircraft transponders, from the reference and aircraft transponders to both satellites, and from both satellites to the Ground Control Center. The four phase-lock loop receivers in the Ground Control Center are assigned as follows:

Receiver No. 1—aircraft transponder-master satellite

Receiver No. 2—reference transponder-master satellite

Receiver No. 3—aircraft transponder-slave satellite

Receiver No. 4—reference transponder-slave satellite.

With the above assignments, it follows that:

$$\phi_{n_1} = 2R_{s_1} + 2R_{A_1}$$

$$\phi_{n_2} = 4R_{s_1}$$

$$\phi_{n_3} = R_{s_1} + R_{A_1} + R_{A_2} + R_{s_2}$$

$$\phi_{n_4} = 2R_{s_1} + 2R_{s_2}$$

By taking the difference between the calibration angles and the phase angles for each tone and receiver, the phase difference can be calculated. From the phase difference the range difference is calculated from the formula

$$R = \frac{C}{f} \alpha$$

where R is the range difference, C is the speed of light, f is the tone frequency, and α is the phase difference. However, care must be exercised in calculating the phase differences to ensure that the geographic location of the tone ambiguity limits do not vary from calibration run to calibration run. Moreover, it is necessary that the center point of nonambiguous ranging coverage is the same for all three tones. The problem that can arise by simply taking phase difference measurements without regard to ambiguity limits is illustrated by the following example. Assume

$$\phi_{C_{13}} = 1.99\pi \text{ radians}$$

Assume the aircraft is flying in the vicinity of the Ground Control Center and at two different points in time the following phase measurements are made:

$$\phi_{13}(t_1) = 1.97\pi \text{ radians}$$

$$\phi_{13}(t_2) = 2.01\pi \text{ radians} = 0.01\pi \text{ radians}$$

since the phase angle resolution is only 0 to 2π radians. Taking phase differences gives

$$\Delta\phi(t_1) = \frac{1.97\pi - 1.99\pi}{2\pi} = -0.01$$

$$\Delta\phi(t_2) = \frac{0.01\pi - 1.99\pi}{2\pi} = -0.99$$

It can be seen in the above example that the two phase difference calculations are radically different, although the aircraft was in the same geographic vicinity. The problem arises in that since the calibration angle ϕ_{13} was measured to be 1.99π , the Ground Control Center becomes a limiting point on the nonambiguous ranging coverage.

To establish the Ground Control Center as the center point for nonambiguous ranging coverage for all three tones, the following phase differencing equation is used:

$$\alpha_{nm} = \text{fractional part of} \left(\frac{\phi_{nm} - \phi_{cnm}}{2\pi} + 1.5 \right) - 0.5$$

Having made the phase difference calculations, the range difference calculations are now made. The best weighted average of the three measurements is computed to minimize the range error. This minimum error is attained by applying weighting functions proportional to the measurement accuracies which, in the case of constant phase jitter caused by noise, becomes proportional to the sidetone frequencies. The general weight average and range is expressed by the equation:

$$R_m = \frac{C \left[\frac{\alpha_{1m}}{f_1} K_1 + \frac{\alpha_{2m}}{f_2} K_2 + \frac{\alpha_{3m}}{f_3} K_3 \right]}{K_1 + K_2 + K_3}$$

using the weighting values of $K_1 = f_1$, $K_2 = f_2$, $K_3 = f_3$

$$R_m = \frac{C}{f_1 + f_2 + f_3} [\alpha_{1m} + \alpha_{2m} + \alpha_{3m}]$$

$$R_m = 0.144495 [\alpha_{1m} + \alpha_{2m} + \alpha_{3m}] \times 10^6 \text{ meters}$$

For just the 941 tone

$$R_m = \frac{C}{f_1} \alpha_{1m} = 0.318426 \alpha_{1m}$$

The resulting range difference measurements contain the following ranging information, ignoring ambiguity for the moment.

$$R_1 = 2R_{A_1} - 2R_{s_1}$$

$$R_2 = 0$$

$$R_3 = R_{A_1} + R_{A_2} - R_{s_1} - R_{s_2}$$

$$R_4 = 0.$$

Thus the range from the aircraft to each of the two satellites may be found as follows:

$$R_{A_1} = \frac{R_1}{2} + R_{s_1}$$

$$R_{A_2} = R_{s_1} + R_{s_2} + R_3 - R_{A_1}$$

$$R_{A_2} = R_{s_1} + R_{s_2} + R_3 - \frac{R_1}{2} - R_{s_1}$$

$$R_{A_2} = R_3 - \frac{R_1}{2} + R_{s_2}$$

It is to be noted at this point that the problem of ambiguity resolution has not been resolved. Thus if the aircraft is not within approximately 70 miles of the Ground Control Center (reference transponder), so that $R_{A_1} - R_{s_1}$ and $R_{A_2} - R_{s_2}$ are within the ambiguity range limits, then additional a priori knowledge must be furnished.

Having established R_{A_1} and R_{A_2} , the position-location equations are now utilized to determine the geographic location of the aircraft transponder.

2. Position-Location Computation

Before discussing the position-location equations, a brief review of directional cosines and their application is first given. Refer to Figure B-4.

Given the vectors \vec{R}_1 and \vec{R}_2 , it is the purpose of the example to find $|\vec{R}_3|$. The Cartesian components of vectors \vec{R}_1 and \vec{R}_2 may be written as:

$$R_1(X_1) = R_1 \cos \phi_1 \cos \psi_1 = R_1 b_{11}$$

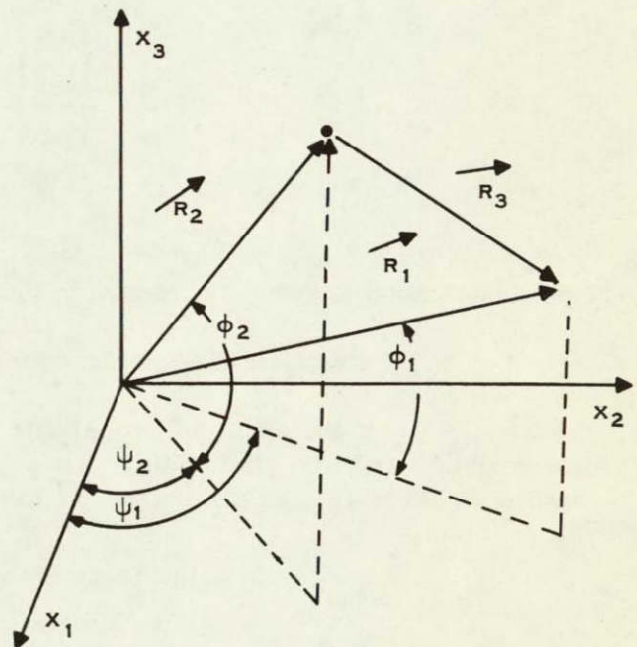
$$R_1(X_2) = R_1 \cos \phi_1 \sin \psi_1 = R_1 b_{21}$$

$$R_1(X_3) = R_1 \sin \phi_1 = R_1 b_{31}$$

$$R_2(X_1) = R_2 \cos \phi_2 \cos \psi_2 = R_2 b_{12}$$

$$R_2(X_2) = R_2 \cos \phi_2 \sin \psi_2 = R_2 b_{22}$$

$$R_2(X_3) = R_2 \sin \phi_2 = R_2 b_{32}$$



124088

Figure B-4. Direction Cosines Geometry

Therefore

$$\begin{aligned}
 |R_3| &= \left\{ [R_1(X_1) - R_2(X_1)]^2 + [R_1(X_2) - R_2(X_2)]^2 + [R_1(X_3) - R_2(X_3)]^2 \right\}^{1/2} \\
 |R_3| &= \left\{ R_1^2(X_1) + R_1^2(X_2) + R_1^2(X_3) + R_2^2(X_1) + R_2^2(X_2) + R_2^2(X_3) \right. \\
 &\quad \left. - 2[R_1(X_1)R_2(X_1) + R_1(X_2)R_2(X_2) + R_1(X_3)R_2(X_3)] \right\}^{1/2} \\
 |R_3| &= \left\{ R_1^2 + R_2^2 - 2R_1R_2(b_{11}b_{12} + b_{21}b_{22} + b_{31}b_{32}) \right\}^{1/2}
 \end{aligned}$$

Now the "b" terms are the direction cosines and may be expressed as vectors where

$$\vec{b}_1 = \begin{bmatrix} b_{11} \\ b_{21} \\ b_{31} \end{bmatrix}, \vec{b}_2 = \begin{bmatrix} b_{12} \\ b_{22} \\ b_{32} \end{bmatrix}, \text{ and } \vec{b}_1^T = [b_{11} \ b_{21} \ b_{31}]$$

Since

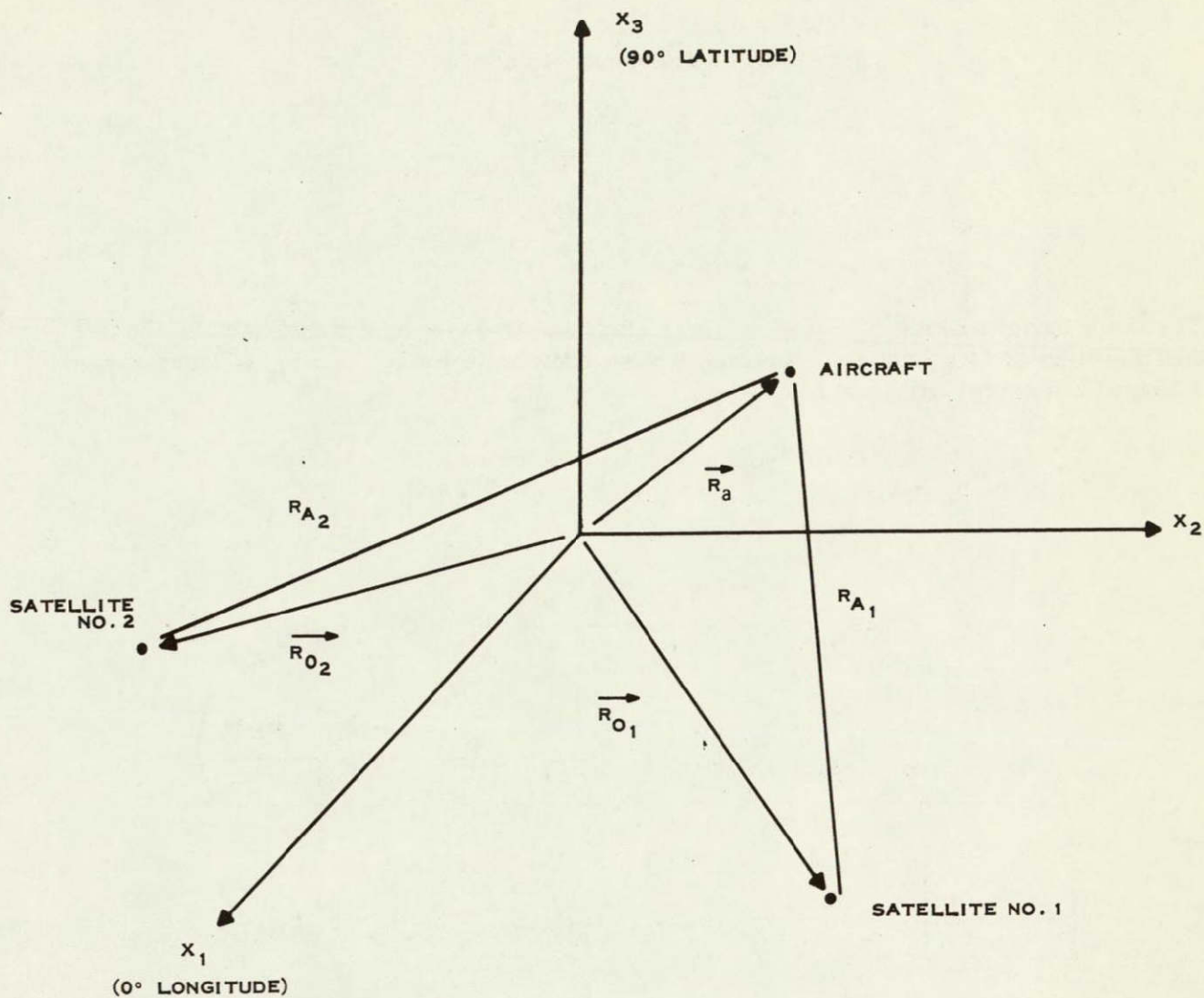
$$\begin{aligned}
 \vec{b}_1^T \vec{b}_2 &= [b_{11} \ b_{21} \ b_{31}] \begin{bmatrix} b_{12} \\ b_{22} \\ b_{32} \end{bmatrix} = b_{11}b_{12} + b_{21}b_{22} + b_{31}b_{32} \\
 |R_3|^2 &= R_1^2 + R_2^2 - 2R_1R_2 \vec{b}_1^T \vec{b}_2
 \end{aligned}$$

The position-location problem is illustrated in Figure B-5.

a. Absolute Position-Location Computations

If the orthogonal coordinate system X_1, X_2, X_3 is aligned such that the X_3 axis corresponds with the North/South axis of the earth and the X_1 axis passes through the Greenwich meridian (0° longitude), then the direction cosine vectors \vec{b} for the two satellites are defined as follows:

$$\begin{aligned}
 b_{1n} &= \text{cosine (angle between } \vec{R}_{on} \text{ and } X_1 \text{ axis)} \\
 &= \text{cosine (latitude) cosine (longitude)} \\
 b_{2n} &= \text{cosine (angle between } \vec{R}_{on} \text{ and } X_2 \text{ axis)} \\
 &= \text{cosine (latitude) sine (longitude)} \\
 b_{3n} &= \text{cosine (angle between } \vec{R}_{on} \text{ and } X_3 \text{ axis)} \\
 &= \text{sine (latitude)}
 \end{aligned}$$



GIVEN:

R_{A1} (MEASURED RANGE BETWEEN AIRCRAFT AND SATELLITE 1)

R_{A2} (MEASURED RANGE BETWEEN AIRCRAFT AND SATELLITE 2)

R_h (MEASURED ALTITUDE OF AIRCRAFT)

\vec{R}_{01} (VECTOR TO SATELLITE 1)

\vec{R}_{02} (VECTOR TO SATELLITE 2)

FIND:

\vec{R}_a (VECTOR TO AIRCRAFT)

124089

Figure B-5. Geometry of Position Location Problem

Utilizing direction cosine vector notation yields

$$R_{A_1}^2 = R_{O_1}^2 + R_a^2 - 2R_{O_1} R_a \cos b_1 \quad (B-1)$$

$$R_{A_2}^2 = R_{O_2}^2 + R_a^2 - 2R_{O_2} R_a \cos b_2 \quad (B-2)$$

Also we know

$$1 = b_{a_1}^2 + b_{a_2}^2 + b_{a_3}^2 \quad (B-3)$$

The simultaneous solution of Equations (B-1), (B-2) and (B-3) for b_a is complicated by the fact that Equation (B-3) is nonlinear. However, we can easily solve for b_{a_1} and b_{a_2} in terms of the measured and known terms and b_{a_3} .

$$\begin{aligned} b_{11} b_{a_1} + b_{12} b_{a_2} &= \frac{R_{O_1}^2 + R_a^2 - R_{A_1}^2}{2R_{O_1} R_a} - b_{13} b_{a_3} = D_1 - b_{13} b_{a_3} \\ b_{21} b_{a_1} + b_{22} b_{a_2} &= \frac{R_{O_2}^2 + R_a^2 - R_{A_2}^2}{2R_{O_2} R_a} - b_{23} b_{a_3} = D_2 - b_{23} b_{a_3} \\ b_{a_1} &= \frac{D_1 - b_{13} b_{a_3} - b_{12} b_{a_2}}{b_{11}} = \frac{D_1 - b_{13} b_{a_3} - b_{12} \left(\frac{D_2 - b_{23} b_{a_3} - b_{21} b_{a_1}}{b_{22}} \right)}{b_{11}} \\ \left[1 - \frac{b_{12} b_{21}}{b_{11} b_{22}} \right] b_{a_1} &= \frac{1}{b_{11} b_{22}} (b_{22} D_1 - b_{22} b_{13} b_{a_3} - b_{12} D_2 + b_{12} b_{23} b_{a_3}) \\ b_{a_1} &= \frac{1}{\Delta} (b_{22} D_1 - b_{12} D_2) + \frac{b_{a_3}}{\Delta} (b_{12} b_{23} - b_{22} b_{13}) \end{aligned} \quad (B-4)$$

where $\Delta = b_{11} b_{22} - b_{12} b_{21}$

$$\begin{aligned} b_{a_2} &= \frac{D_2 - b_{23} b_{a_3} - b_{21} b_{a_1}}{b_{22}} = \frac{D_2 - b_{23} b_{a_3} - b_{21} \left(\frac{D_1 - b_{13} b_{a_3} - b_{12} b_{a_2}}{b_{11}} \right)}{b_{22}} \\ \left[1 - \frac{b_{21} b_{12}}{b_{11} b_{22}} \right] b_{a_2} &= \frac{1}{b_{11} b_{22}} [b_{11} D_2 - b_{21} D_1 + b_{a_3} (b_{21} b_{13} - b_{11} b_{23})] \\ b_{a_2} &= \frac{1}{\Delta} (b_{11} D_2 - b_{21} D_1) + \frac{b_{a_3}}{\Delta} (b_{21} b_{13} - b_{11} b_{23}) \end{aligned} \quad (B-5)$$

Now let us assume that both satellites are in the equatorial plane. Thus we can rewrite Equations (B-4) and (B-5) as follows:

$$b_{a_1} = \frac{1}{\Delta} (b_{22} D_1 - b_{12} D_2) \quad (B-6)$$

$$b_{a_2} = \frac{1}{\Delta} (b_{11} D_2 - b_{21} D_1) \quad (B-7)$$

Having solved for b_{a_1} and b_{a_2} via Equations (B-6) and (B-7), we can now solve for b_{a_3} as follows:

$$b_{a_3} = \pm(1 - b_{a_1}^2 - b_{a_2}^2)^{1/2} \quad (B-8)$$

The solution for b_{a_3} via Equation (B-8) is only approximate, since the solutions for b_{a_1} and b_{a_2} were obtained by assuming the two satellites were in the equatorial plane. However, an iterative process can be initiated at this point to obtain the desired degree of computational accuracy. A flow diagram of this iterative process is presented in Figure B-6. As shown in the flow diagram, the iteration is repeated 10 times, which has been found to be more than adequate for the computational accuracy required.

The plus and minus signs in Equation (B-8) correspond to symmetric locations in the northern and southern hemispheres, respectively. Thus a priori knowledge of the aircraft location is needed to determine the sign of b_{a_3} .

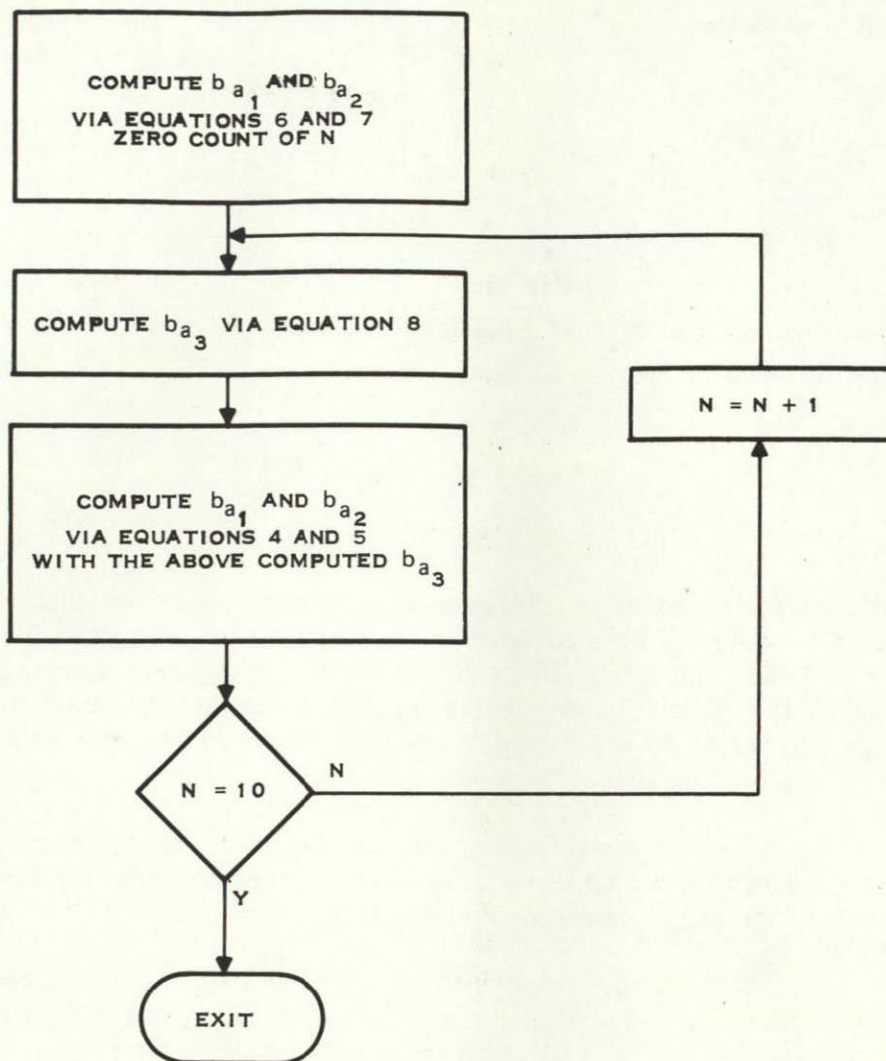
Now, having determined b_{a_1} , b_{a_2} , and b_{a_3} , it is necessary to calculate the latitude and longitude of the aircraft. Again, assume the orthogonal coordinate system X_1 , X_2 , X_3 is aligned such that the X_3 axis corresponds with the North/South axis of the earth sphere and the X_1 axis passes through the Greenwich meridian (0° longitude). The longitude is determined as follows:

$$\text{longitude} = \tan^{-1} \left\{ \frac{\text{the projection of } \vec{R}_a \text{ on the } X_1 \text{ axis}}{\text{the projection of } \vec{R}_a \text{ on the } X_2 \text{ axis}} \right\} = \tan^{-1} \left\{ \frac{|R_a| b_{a_2}}{|R_a| b_{a_1}} \right\}$$

$$\text{longitude} = \tan^{-1} \left\{ \frac{b_{a_2}}{b_{a_1}} \right\}$$

The latitude is defined as the angle between the vector R_a and the $X_1 X_2$ plane; therefore, the latitude is:

$$\text{latitude} = \sin^{-1} (b_{a_3})$$



124090

Figure B-6. Iteration Loop, Flow Diagram

It would be convenient to have an on-line display device, such as an X-Y plotter, to display the aircraft's distance from a known and fixed geographic point. The problem then is to convert differences in latitude and longitude between the aircraft transponder and a fixed reference point to X-Y differences in, say, nautical miles. Assuming the circumference of the earth is 21,639.34 nmi, then a degree change in latitude is equivalent to $21639.34/360 = 60.109$ nmi, regardless of longitude. However, the amount that a degree change in longitude represents in nautical miles is directly dependent on latitude. For purposes of illustration, the coordinates of Texas Instruments, Dallas, will be utilized to convert differences in longitude to nautical miles where:

$$\text{longitude}_{\text{Texas Instruments Dallas}} = 96^{\circ}45'1.8'' \text{ W} = 96.7505^{\circ} \text{ W}$$

$$\text{latitude}_{\text{Texas Instruments Dallas}} = 32^{\circ}55'57'' \text{ N} = 32.9325^{\circ} \text{ N}$$

If an orthogonal coordinate system X, Y, Z is aligned such that the Y-axis corresponds with the North/South axis of the earth and the X-axis passes through the Greenwich meridian (0° longitude), then the amount that a degree change in latitude represents in nautical miles can be found as follows:

$$D_X = R_E \cos(\text{latitude}) \sin(\Delta \text{ longitude})$$

where

D_X = distance in X direction in nautical miles

R_E = radius of earth in nautical miles

latitude = latitude at Texas Instruments, Dallas

$$D_X = \frac{21639.34}{2\pi} \times \cos 32.9325^\circ \times \sin 1^\circ$$

$$D_X = \frac{21639.34}{2\pi} \times 0.8393 \times 0.01745$$

$$D_X = 50.44 \text{ nautical miles/degree of longitude}$$

For latitude the conversion is simply

$$D_Y = \frac{2\pi R_E}{360} = \frac{21639.34}{360}$$

$$D_Y = 60.109 \text{ nautical miles/degree of latitude.}$$

The data processor in the Ground Control Center outputs digital data in a 16-bit word format. Thus, to enable outputting the data in one digital word, 8 digital bits will be assigned to latitude information and 8 digital bits will be assigned to longitude information. Furthermore, since the nonambiguous distance is approximately 70 nmi, the full 8-bit count will be made equivalent to 70 nmi or

$$X = D_X \frac{255}{70}$$

$$X = 183.745 \text{ digital counts/degree of longitude at } 32.9325^\circ \text{ latitude}$$

$$Y = D_Y \frac{255}{70}$$

$$Y = 218.968 \text{ digital counts/degree of latitude}$$

Converting to radians

$$X = 183.745 \times \frac{360}{2\pi}$$

$$X = 10527.8 \text{ digital counts/radian of longitude at } 32.9325^\circ \text{ latitude}$$

$$Y = 218.968 \times \frac{360}{2\pi}$$

$$Y = 12545.9 \text{ digital counts/radian of latitude.}$$

To ease the complexity of converting the digital latitude and longitude words to analog signals for presentation to the display unit, the digital output words will be restricted to always being positive numbers. Also, it is desirable to have the reference point (which in this example will be Texas Instruments, Dallas) in the center of the display. To accomplish both outputting positive numbers and placing the reference point in the center of the display, the following latitude and longitude differencing equations can be used, assuming full scale represents 70 nmi.

$$\Delta \text{ latitude} = \text{latitude}_{\text{Aircraft Transponder}} - (\text{latitude}_{\text{Reference Point}} - \phi_c)$$

where

ϕ_c = number of radians required to offset display 127.5 digital counts or 35 nautical miles

$$\phi_c = \frac{1 \text{ radian}}{12545.9 \text{ digital counts}} \times 127.5 \text{ digital counts}$$

$$\phi_c = 0.01016 \text{ radian}$$

For Texas Instruments, Dallas

$$\text{latitude}_{\text{Reference}} - \phi_c = 0.564066$$

Thus

$$\Delta \text{ latitude} = \text{latitude}_{\text{Aircraft Transponder}} - 0.564066$$

In the very same manner

$$\Delta \text{ longitude} = 1.7007353 - \text{longitude}_{\text{Aircraft Transponder}}$$

Finally, the equations to convert from latitude and longitude in radians to nautical mile displacement from Texas Instruments, Dallas, are as follows:

$$Y_{\text{Latitude}} = (\text{latitude}_{\text{Aircraft Transponder}} - 0.564066) 12545.9$$

$$X_{\text{Longitude}} = (1.7007353 - \text{longitude}_{\text{Aircraft Transponder}}) 10527.8$$

To convert from latitude and longitude in radians to nautical mile displacement from Texas Instruments with a full scale of 35 nmi the following equations hold.

$$Y_{\text{Latitude}} = (\text{latitude}_{\text{Aircraft Transponder}} - 0.564066) 25092 - 127.5$$

$$X_{\text{Longitude}} = (1.7007353 - \text{longitude}_{\text{Aircraft Transponder}}) 21059.6 - 127.5$$

b. Differential Position-Location Computations

Although the preceding section is entitled Absolute Position-Location Computations, it is in truth a diluted form of differential position-location computations. That is, any fixed delays (or phase errors) in the Ground Control Center transmit or receive subsystems, in the satellites and in the aircraft transponder, and any fixed bias effects in the propagation media are cancelled in the phase angle difference calculations between the current phase data and the previously recorded calibration data. However, any time-varying effects are not cancelled.

Now if the position of the reference transponder, as calculated by the absolute position-location computations utilizing phase-lock loop receivers No. 2 and No. 4, is subtracted from the position of the aircraft transponder, again as calculated by the absolute position-location computations utilizing phase-lock loop receivers No. 1 and No. 3, the common mode time varying effects are cancelled. The equations utilized in determining the position of the aircraft transponder in the differential mode is as follows:

$$\begin{array}{rclcl} X_{\text{Lat.}} & X_{\text{Lat.}} & X_{\text{Lat.}} & & +127.5 \\ \text{Diff.} & = & \text{ABS} - & \text{ABS} & \\ \text{A/C} & & \text{A/C} & & \text{Ref.} \end{array}$$

$$\begin{array}{rclcl} Y_{\text{Lon.}} & Y_{\text{Lon.}} & Y_{\text{Lon.}} & & +127.5 \\ \text{Diff.} & = & \text{ABS} - & \text{ABS} & \\ \text{A/C} & & \text{A/C} & & \text{Ref.} \end{array}$$

B. Operators Instructions, On-Line Program

The program initialization procedure, receiver assignments, and ephemeris data entry are all discussed in the Acceptance Test, Part I, Individual Test for Ground Control Center-VHF Satellite Navigation Experiment (Texas Instruments Drawing No. SK714211). Additional information concerning ephemeris data is presented in Appendix A. However, not discussed in the above references are the various tasks and options that can be performed using the sense switches on the OPLE Control Console in conjunction with the sense switches on the DMI DATA 620 Computer. Table B-1 lists the tasks and options with the appropriate sense switch pattern. The instructions for using the utility programs are presented below.

1. Magnetic Tape Read-Write

Upon entering this program, the following message will be typed on ASR-35 Teletype Unit.

SS1 ON = WRT, OFF = RD

TAPE FILE AND RECORD NUMBER.

One responds by typing:

N1
N2
\$

TABLE B-1. ON-LINE PROGRAM TASKS AND OPTIONS

Utility Task	Sense Switch Pattern
1. Magnetic Tape Read	Utility, F, Go
2. Magnetic Tape Write	Utility, F, SS-1, Go
3. Help (Debug aid)	Utility, H, Go
4. Binary Paper Tape Loader	Utility, D, Go
5. Off-Line Floating Point Input	Utility, G, Go
6. Close File On Magnetic Tape	Utility, E, Go
VHF Range/Range Program Task	Sense Switch Pattern
1. Data Entry (No Receiver Assignments)	Execute, Init, Go
2. Receiver Assignments	Execute, D, Go
3. Data Entry and Receiver Assignments	Execute, Init, D, Go
4. No Data Entry or Receiver Assignments	Execute, Go
5. Take Out of Wait Loop	Go
6. 35-Mile Range	Any Range/Range Pattern
7. 70-Mile Range	SS-3 and any Range/Range Pattern
8. 1 A/C (Differential Mode)	Any Range/Range Pattern
9. 2 A/C or Absolute Mode	SS-2 and any Range/Range Pattern
10. Normal Termination	E. and any Range/Range Pattern

where N1 is the file number, N2 is the record number and \rightarrow is a carriage return which terminates the number. A leading 0 for N1 or N2 indicates an octal input and no leading zero indicates a decimal input. Hence, a zero must be entered as 00. The \$ terminates the input mode.

Once the input mode is terminated, the ASR-35 Teletype Unit responds by typing:

START AND FINAL ADDRESS

One responds by typing:

N1 \rightarrow
N2 \leftarrow

where N1 is the start address and N2 is the final address. Again, the octal/decimal convention discussed above holds. To prevent program overlay while reading, the following criteria should be followed:

If $N1 > 16711_8$ then $N2 \leq 17777_8$

If $0 \leq N1 \leq 16500_8$ then $N2 \leq 16500_8$

The record is then read or written according to the setting of SS1.

2. Help (Debug Aid)

This subroutine is fully described in the OPLE Software Manual, HB4-A67, 15 February 1968.

3. Binary Paper Tape Loader

This subroutine is also fully described in the OPLE Software Manual, HB4-A67, 15 February 1968.

4. Off-Line Floating Point Input

This subroutine converts decimal numbers as entered via the ASR-35 Teletype Unit into floating point numbers and stores the resulting point numbers into previously designated locations in memory. This subroutine is especially useful in entering the geographic dependent software constants (Appendix A).

Upon entry the program will halt. The starting or first address of where the floating point numbers are to be stored is entered into the A Register. At this time, the RUN switch is pressed. The numbers are then entered via the ASR-35 Teletype Unit with or without a decimal point or a sign. When no sign is entered, the number is assumed to be positive. When no decimal point is entered, the decimal point is assumed to be at the far right of the word. A (carriage return) ends the word and a \$ sign ends the input mode and returns the system to the monitor mode.

III. Off-Line Program Description

The off-line program provides for printout on the ASR-35 Teletype Unit of the raw and calculated data gathered during the on-line experiment. A flow diagram of the off-line program is shown in Figure B-7. The off-line program performs no calculations, but rather simply formats the data stored on magnetic tape during the on-line run for presentation to the ASR-35 Teletype Unit.

The procedures for initializing, loading, and operating the program are presented in the Acceptance Test, Part I, Individual Test for Ground Control Center-VHF Satellite Navigation Experiment (Texas Instruments Drawing No. SK714211). However, not presented in the above reference are the various printout options available. Table B-2 lists the options with the appropriate sense switch patterns.

TABLE B-2. SENSE SWITCH SETTINGS—OFF-LINE PROGRAM

Sense Switch Settings	Function
SS "D" ON	Disables printout of header (ephemeris) data
SS "E" ON	Disables printout of OPLE Time (Time of OPLE Interrupt)
SS "F" ON	Disables printout of NASA time (time of Radar Interrupt)
SS "3" ON SS "G" OFF	Having performed the options of SS's "D," "E," and "F," skips to next run
SS "3" ON SS "G" ON	Having performed the options of SS's "D," "E," and "F," skips to next record
SS "H" ON	Disables printout of calibration data record
SS "1" ON	Disables printout of raw phase data
SS "2" ON	Enables printout of radar data

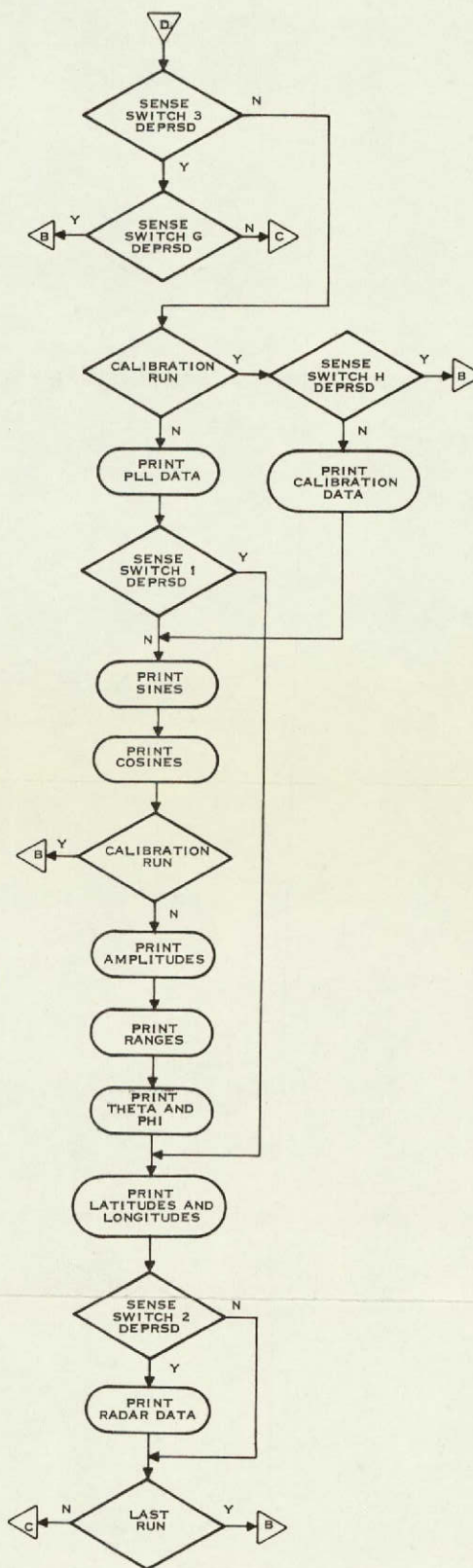
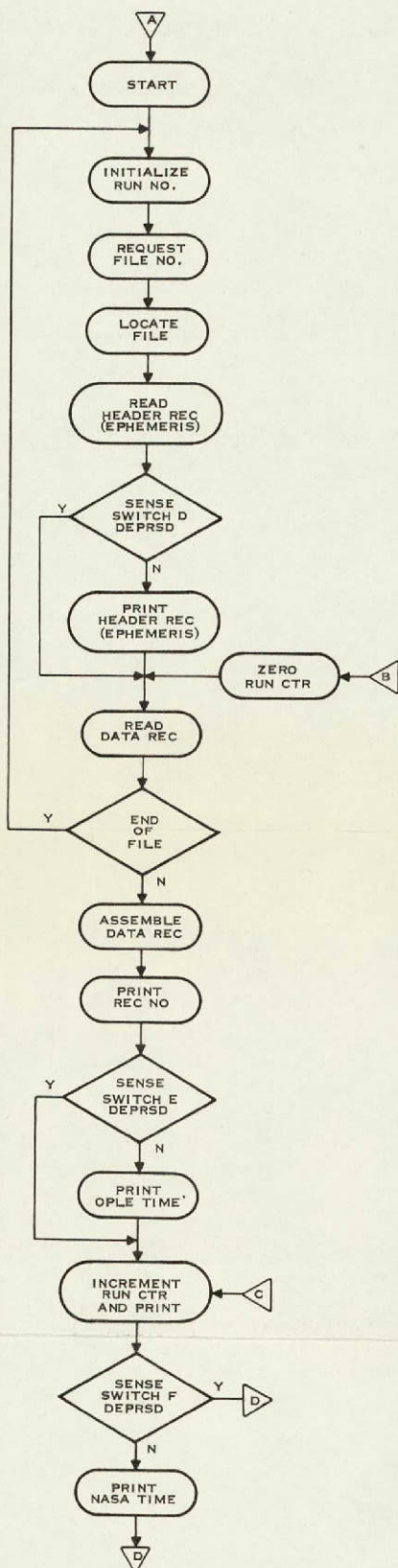


Figure B-1. Offline Program, Flow Diagram

B-23/B-24

The units associated with the various numbers printed are listed below:

Header (Ephemeris) Record

1. Receiver Assignments—octal if proceeded by a zero, decimal otherwise
2. Aircraft Altitude— 10^6 meters from the center of the earth
3. Satellite Altitude— 10^6 meters from the center of the earth
4. Satellite Range— 10^6 meters from GCC to satellite
5. Satellite Direction Cosines—unitless
6. Delta—unitless ($b_{11} b_{22} - b_{21} b_{12}$)

Calibration Record

1. Calibration Data—measured phase in radians
2. Sines—sum of 12 sine samples
3. Cosines—sum of 12 cosine samples

Data Records

1. PLL—number from 0 to 2 which represents the phase-lock loop correlation detector output voltage
2. Sines—sum of four sine samples
3. Cosines—sum of four cosine samples
4. Amplitudes—number from 0 to 5.66 which represents the amplitude of the signals out of the phase detector
5. Range—range difference for each receiver in 10^6 meters
6. Theta—longitude of A/C 1 in radians
7. Phi—latitude of A/C 1 in radians
8. Latitude 1—displacement of A/C 1 from reference point in Y-direction, scaled per setting of SS-3 during on-line experiment [see Appendix B.2.a.(2)]
9. Longitude 1—displacement of A/C 1 from reference point in X-direction, scaled per setting of SS-3 during on-line experiment [see Appendix B.2.a.(2)]
10. Latitude 2—same as latitude 1
11. Longitude 2—same as longitude 1
12. $R*\cos$ —displacement of radar track from Texas Instruments in the Y-direction plus 35 nmi, scaled to 255 equals 70 nmi
13. $R*\sin$ —displacement of radar track from Texas Instruments in the X-direction plus 35 nmi, scaled to 255 equals 70 nmi
14. Azimuth—azimuth of radar target from Texas Instruments in degrees referenced from true north
15. Range—range of radar target from Texas Instruments in nautical miles.

APPENDIX C

TRANSPONDER DESCRIPTION

I. Description of Transponder

The transponder was packaged in a standard ½-long Austin Trumbull Radio (ATR) case as shown in Figure 4-2. Twelve modules were used to house the circuits; Figure C-1 shows a typical module (the transmitter power amplifier) with its top cover removed. Figure C-2 depicts a top view of the transponder and the relative location of the modules.

The following paragraphs describe each of the 12 modules in the transponder as shown in Figure C-3. Schematic diagrams of these modules are included at the end of this appendix.

1. Diplexer (Figure C-4)

The purpose of the diplexer is to allow the transmitter and receiver section of the transponder to operate simultaneously from one antenna. This is accomplished by building two filters, both tied to the antenna port. One filter is in the receiver signal path and the other in the transmit signal path. The receiver path filter passes the receive frequency with a minimum amount of loss, while greatly attenuating the transmit frequency signal. The filter in the transmit path performs a similar function for the transmit signal, passing that signal and rejecting any signal at the receive frequency.

The transmit filter is a two-pole Butterworth filter with a 10-MHz bandwidth. The transmit-to-antenna loss at the transmit frequency is 2.0 dB and 67 dB at the receive frequency. The receive filter is a four-pole Tchebysheff filter with a 5-MHz bandwidth. The antenna-to-receiver loss is 3.0 dB at the receive frequency and 80 dB at the transmit frequency.

B. VHF Converter (Figure C-5)

The VHF converter receives the 135-MHz signal from the diplexer through a 3-dB noise figure Field Effect Transistor (FET) front end. This signal is mixed with a 205-MHz local oscillator down to 70 MHz. By using high-side conversion, image frequency rejection becomes a simpler problem. Gain of 30 dB is obtained in this module and then filtered before going to the second converter.

C. Pilot Tone Tracking Loop

The pilot tone tracking loop consists of several modules which comprise a phase-lock loop. It must first be realized that several signals are received simultaneously in this system. A pilot tone is received and converted down to 10.7 MHz for the transponder phase-lock loop. Also, a package of tones very close in frequency is received at 10.665 MHz. The package of tones is retransmitted while the pilot tone, locked in the phase-lock loop, holds the 10.665-MHz package in the center of that filter passband.

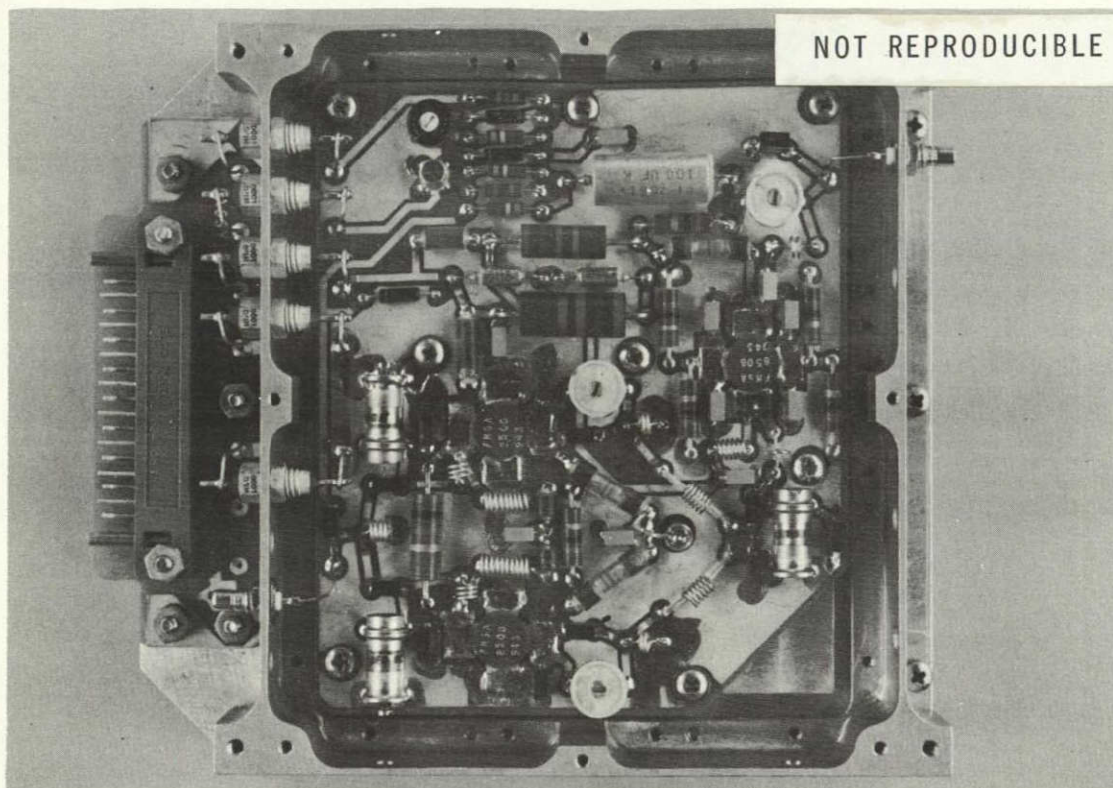
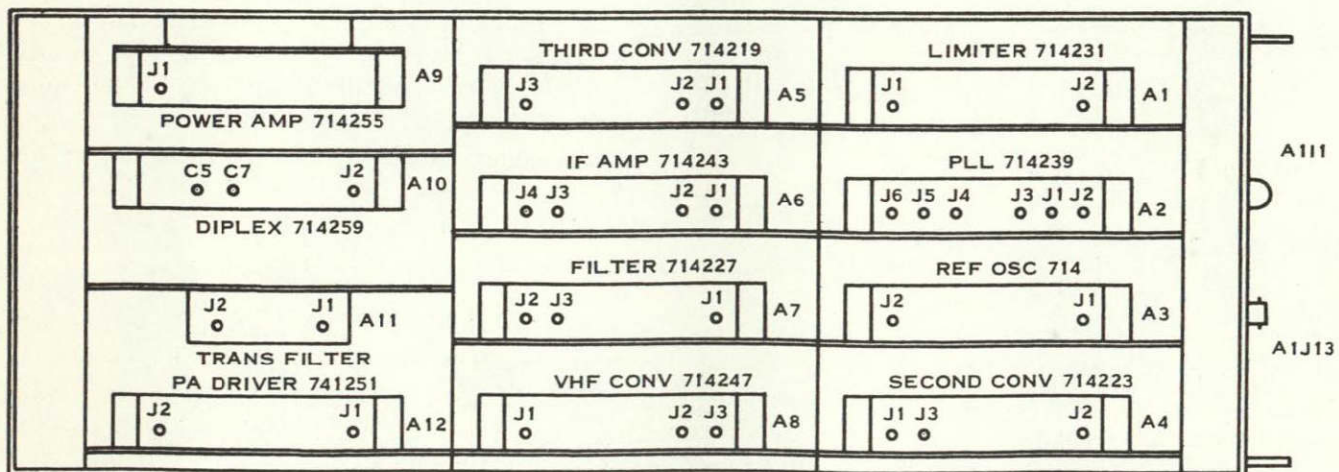
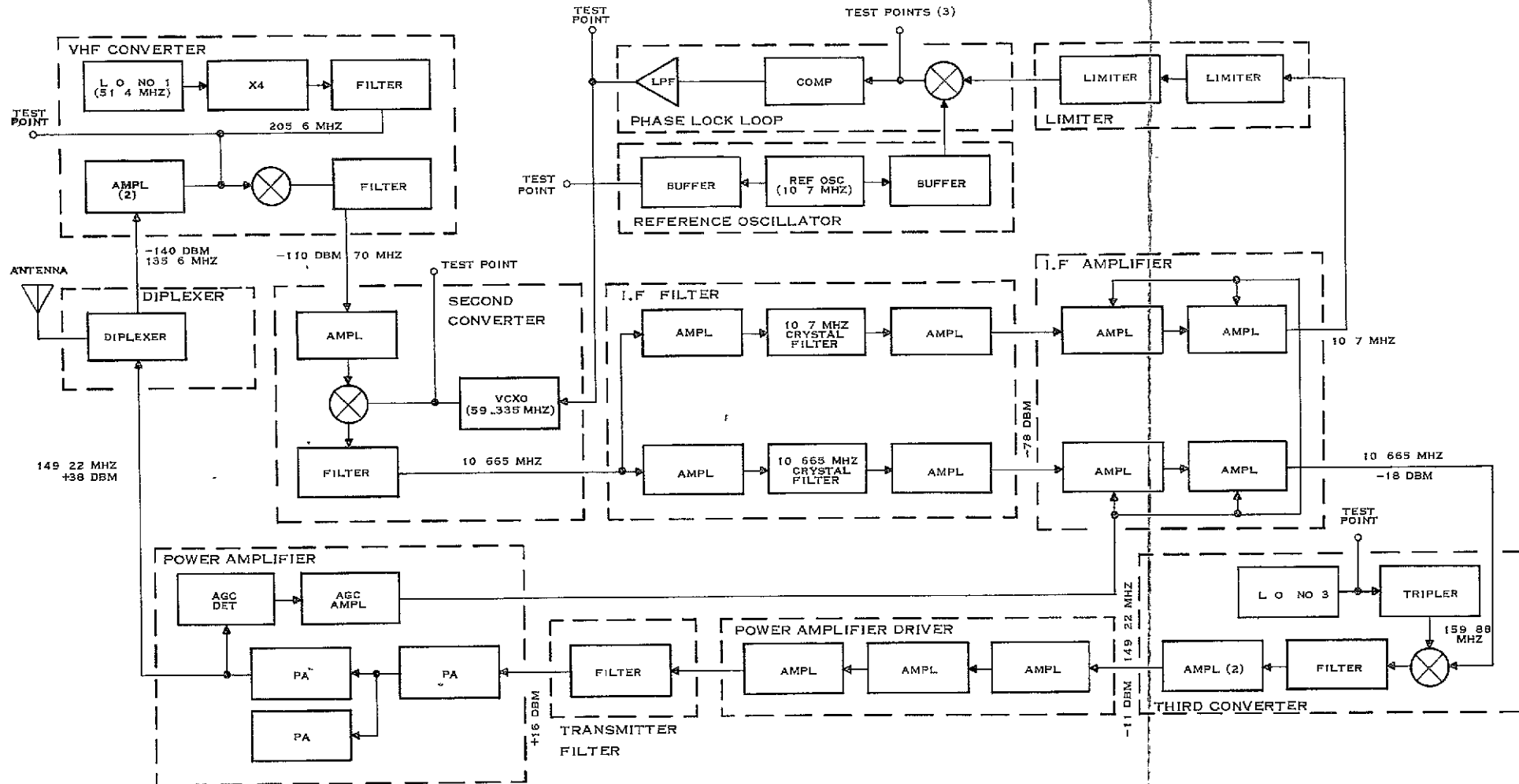


Figure C-1. Transmitter Power Amplifier Module



124093

Figure C-2. Transponder, Top View



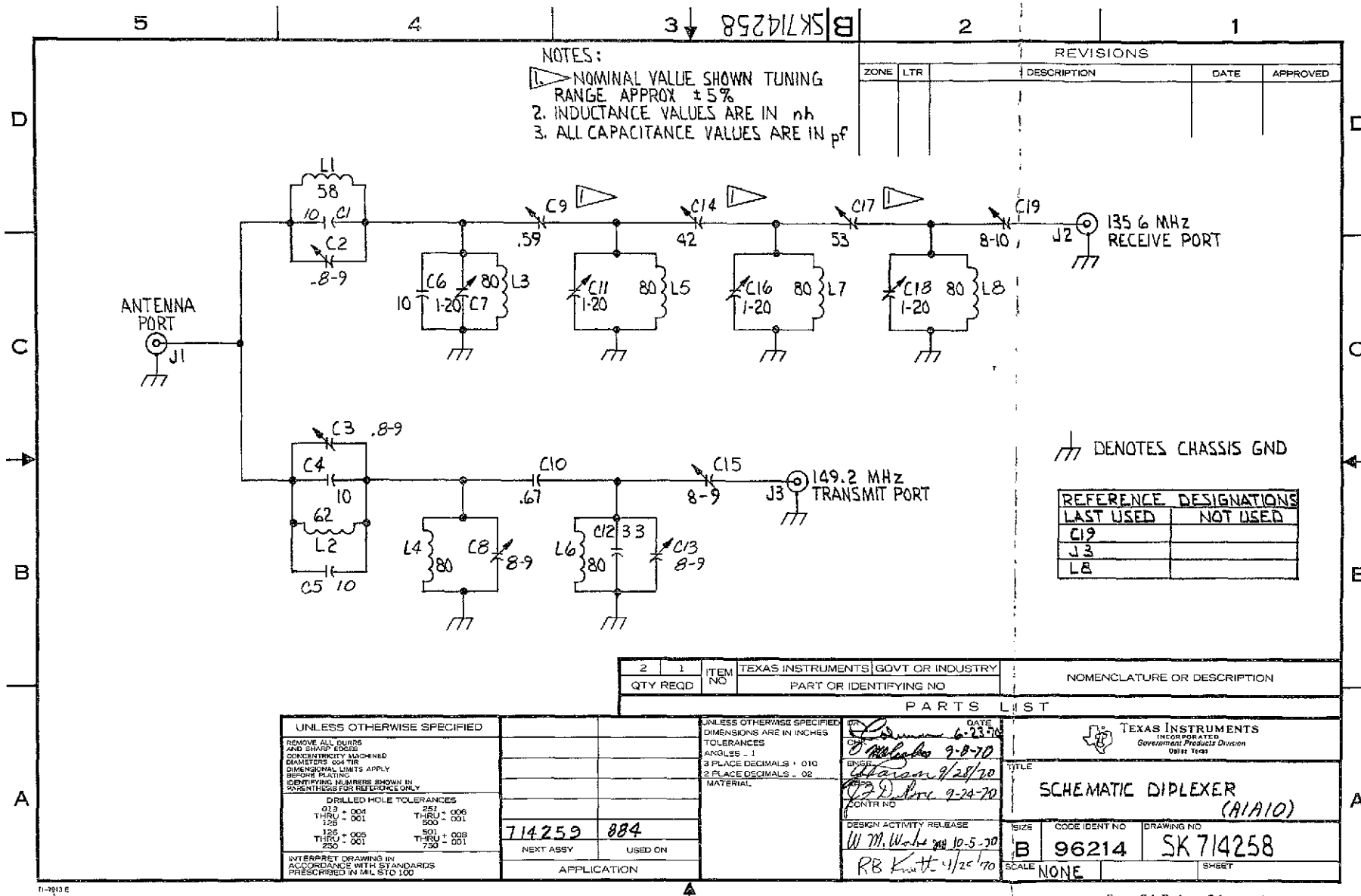


Figure C-4 Diplexer, Schematic Diagram

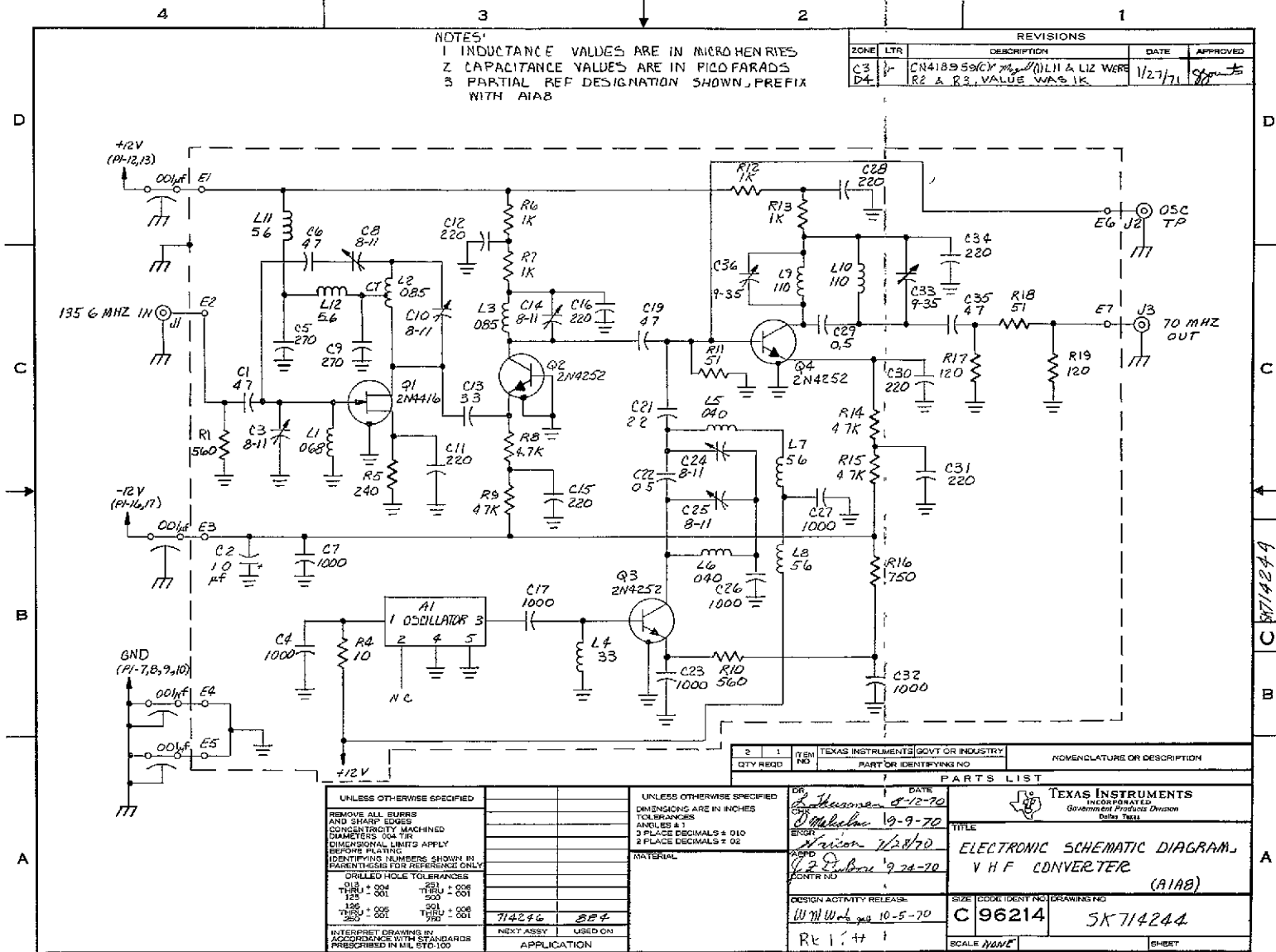


Figure C-5 VHF Converter, Schematic Diagram

All of the signals are received together through the second converter. They are then fed into an IF filter where the 10.7 and the 10.665 MHz are separated. Then, the 10.7-MHz signal goes through an IF amplifier into a limiter and to a phase detector where it is compared with a 10.7-MHz reference oscillator. The resulting error signal then varies the VCXO in the second converter to establish and maintain phase lock.

1 Second Converter

A schematic diagram of the second converter is shown in Figure C-6. The incoming 70-MHz signal from the VHF converter is at the -110 -dBm level. This signal is amplified, fed into a mixer along with a VCXO at 59.3 MHz, and passed through an L-C filter to the IF filters at a level of -93 dBm.

2 IF Filter

The IF filter module, shown in Figure C-7, consists of three sections: an amplifier, a crystal filter (6-kHz bandpass), and another amplifier. These two amplifiers, along with the filter loss, yield an overall gain of 15 dB.

3 IF Amplifier

The IF amplifier, Figure C-8, is a pair of cascaded MC1590 linear integrated circuits. The design is straightforward, producing 60-dB gain. With a -78 -dBm signal at the input, a -18 -dBm signal is obtained at the output. In this IF section, the automatic gain control (AGC) from the power amplifier is fed back to adjust the output to a constant level for varying incoming signal strengths.

4 Limiter (Figure C-9)

The limiter is a straightforward design using MC1590 IC's and produces 60 dB of limiting. This module is necessary to maintain a constant level of signal into the phase detector. The AGC response time is too slow for rapid variations in signals and primarily maintains a constant output from the IF amplifier for different incoming signal strengths. Also, in this transponder, the AGC operates from the power amplifier output level, which is dependent on the signal level. The level of the signal going through the transmitter may not necessarily be the same as that going to the phase detector.

5 Phase-Lock Loop (Figure C-10)

The phase-lock loop module contains a phase detector which feeds a compensated operational amplifier and then a low-pass filter. When the phase-lock loop is locked, both the incoming signal from the limiter and a reference oscillator are on the same frequency and in phase. If the incoming signal shifts slightly in frequency, the phase detector produces an error signal which in turn varies the VCXO. When the incoming signal first appears and the loop is trying to acquire phase lock, there is a considerable frequency and phase difference between that and the reference oscillator. When this situation occurs, a low-frequency output is obtained from the phase detector. This signal is then compensated, amplified, and filtered, producing a distorted sine wave. The distorted sine wave contains a dc component which slews the VCXO until phase lock is acquired.

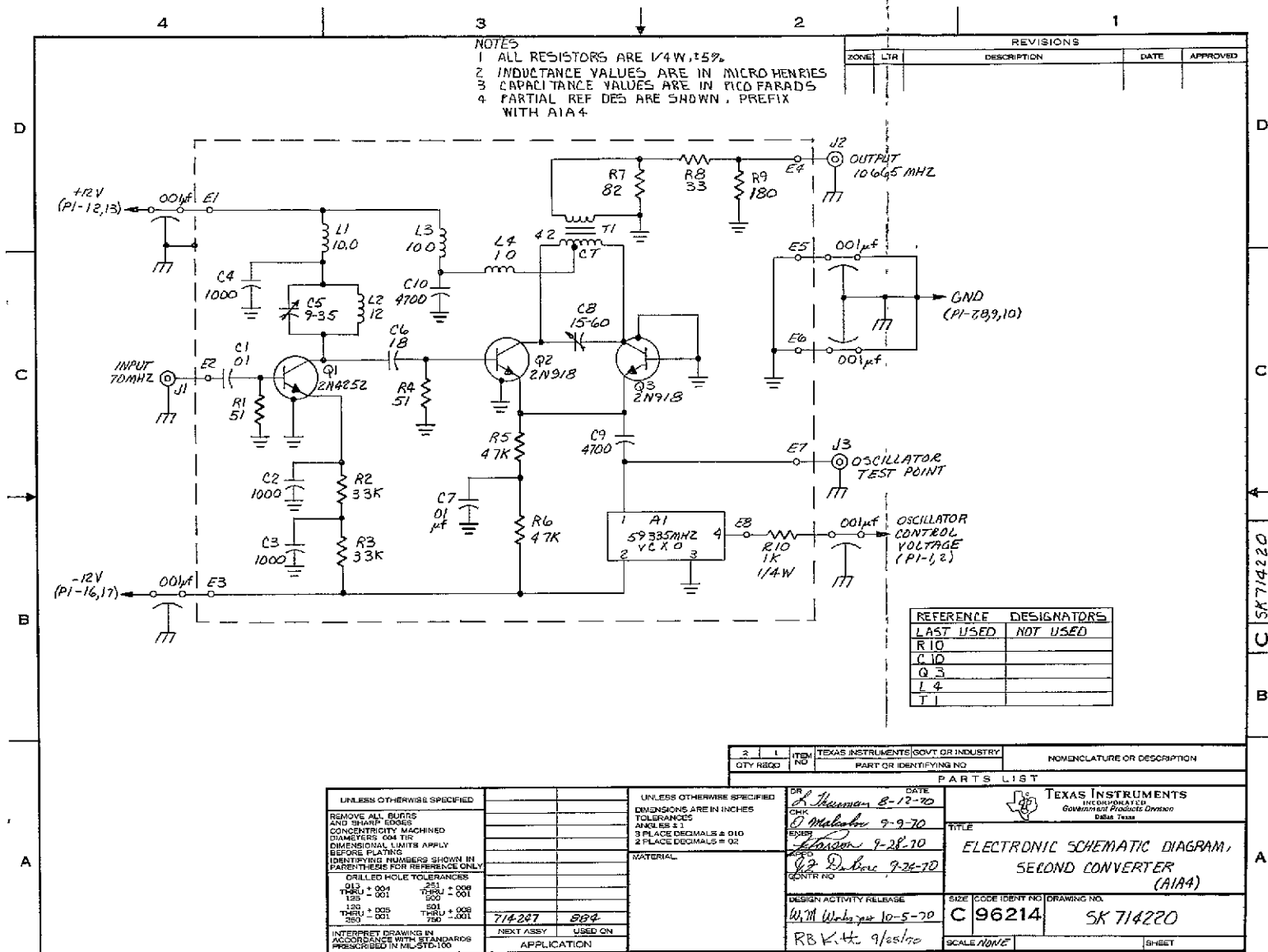
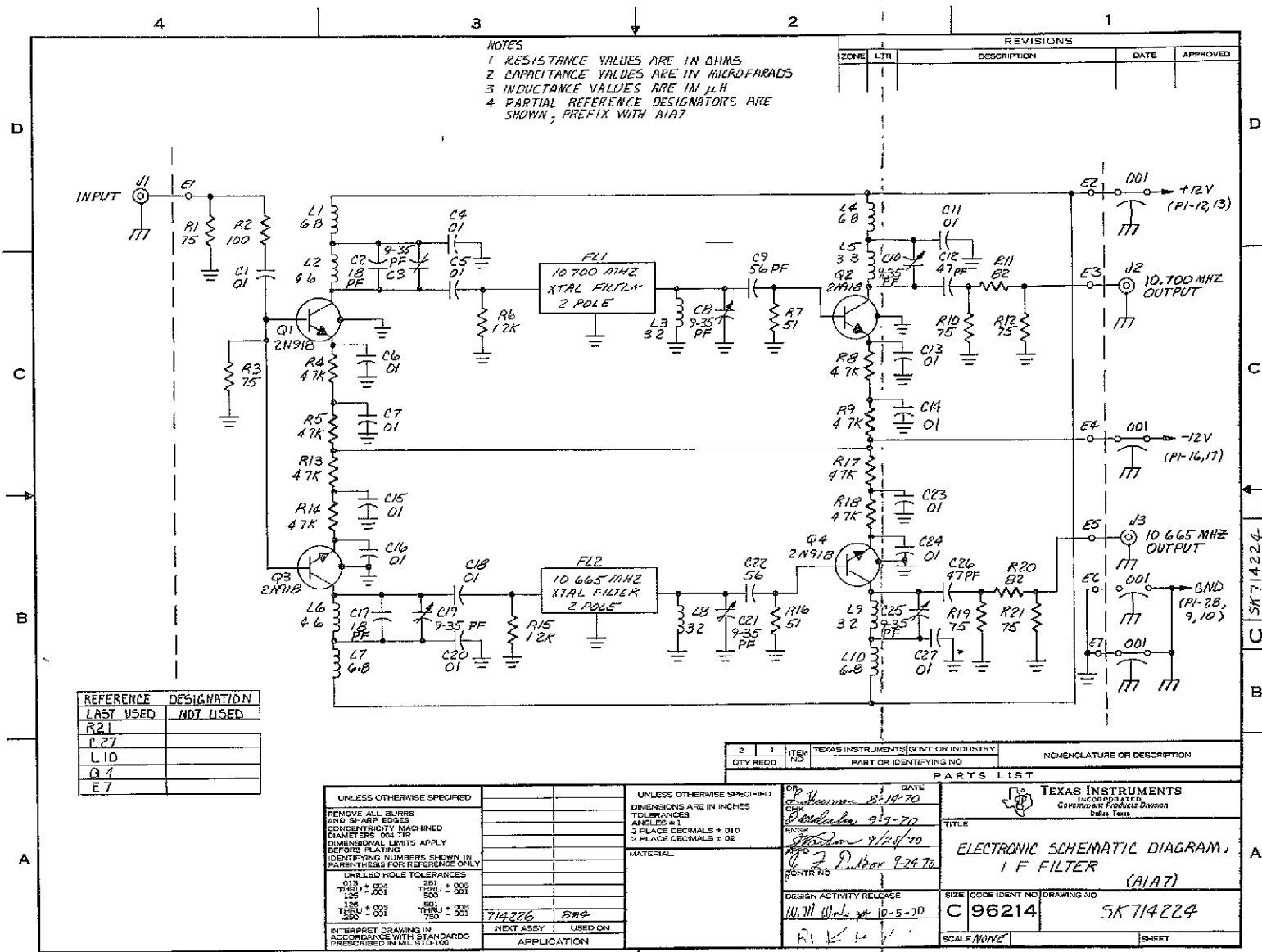


Figure C-6 Second Converter, Schematic Diagram



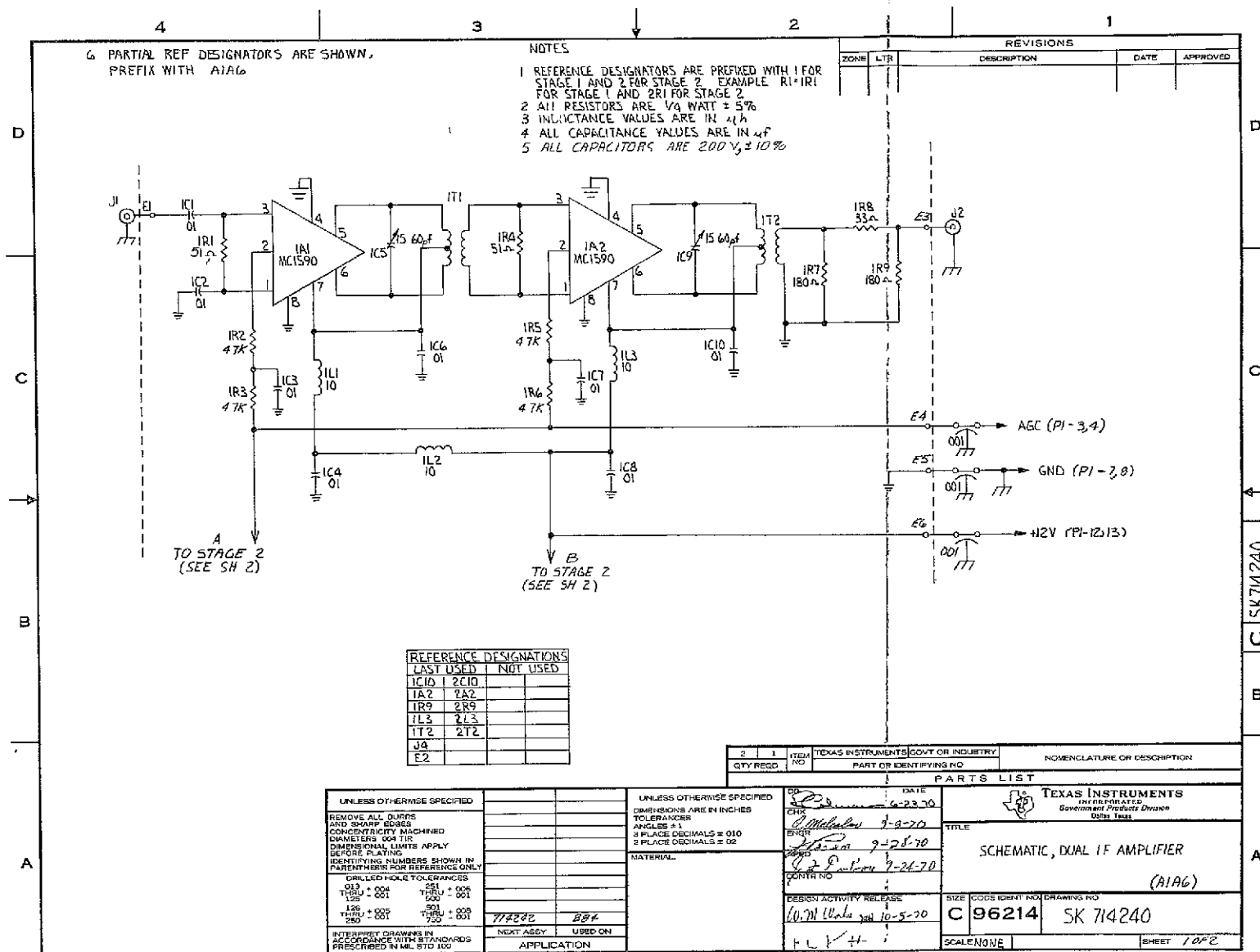


Figure C 8 Dual IF Amplifier,
Schematic Diagram (Sheet 1 of 2)

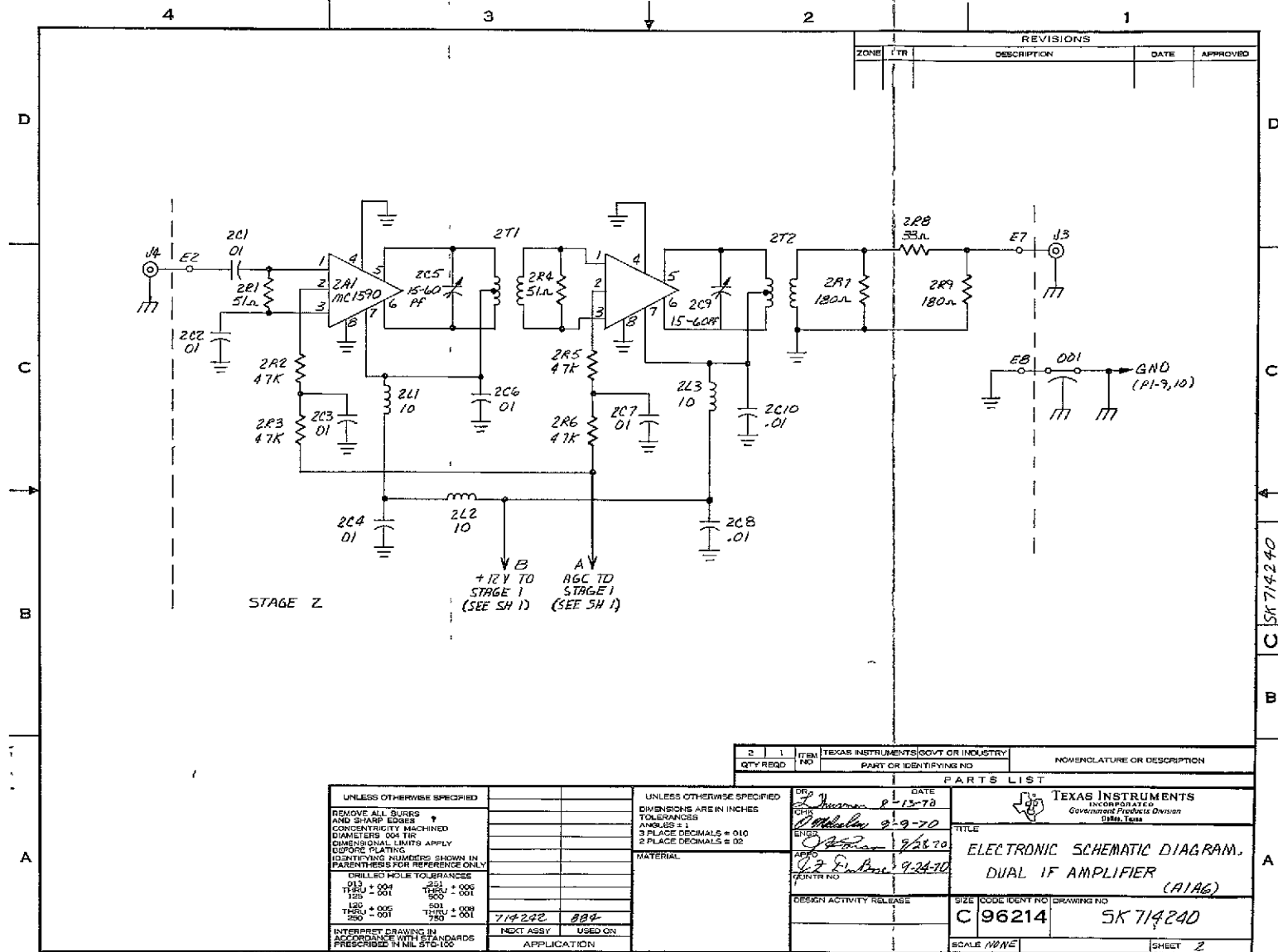
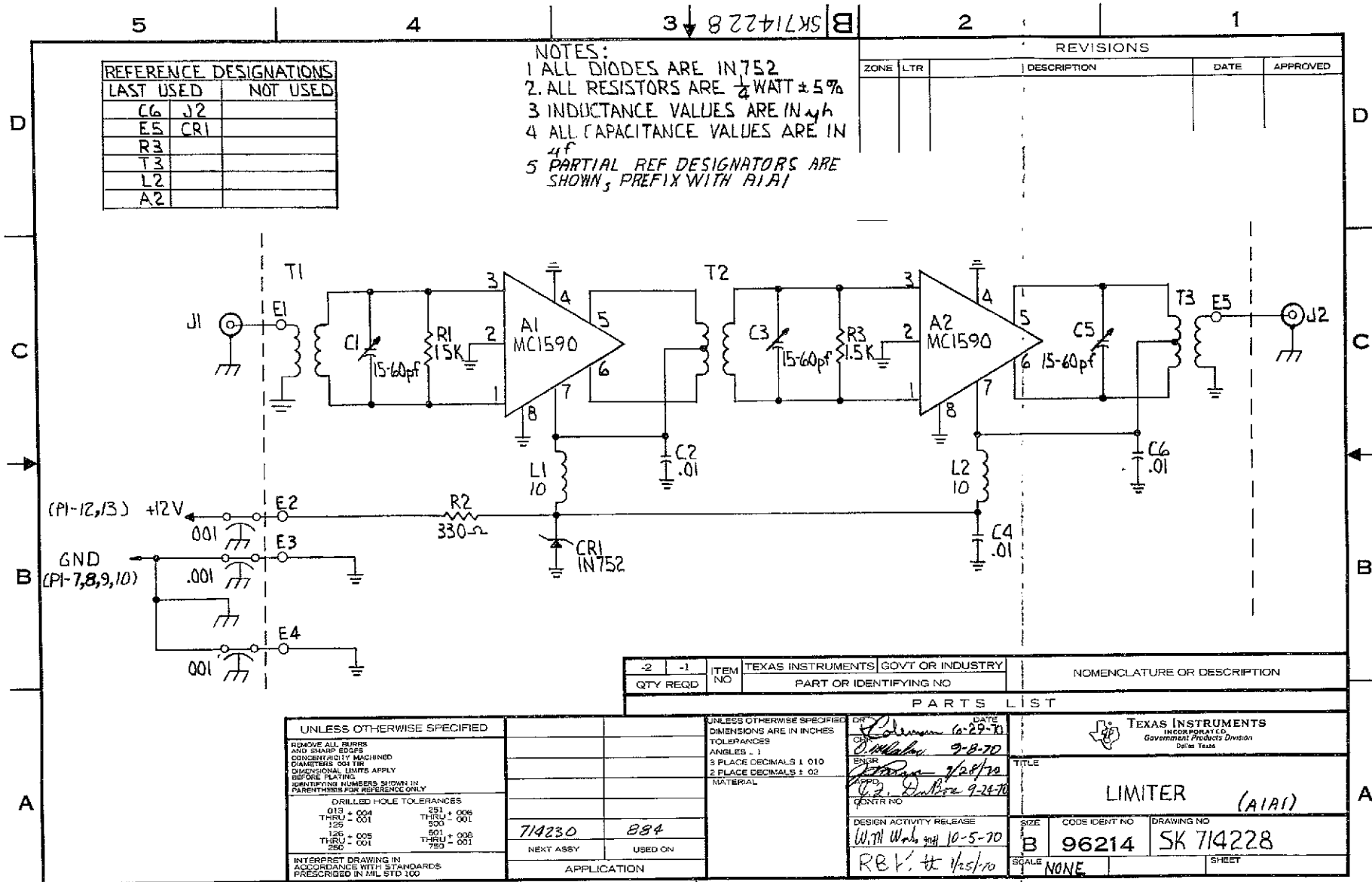


Figure C8 Dual IF Amplifier, Schematic Diagram (Sheet 2 of 2)



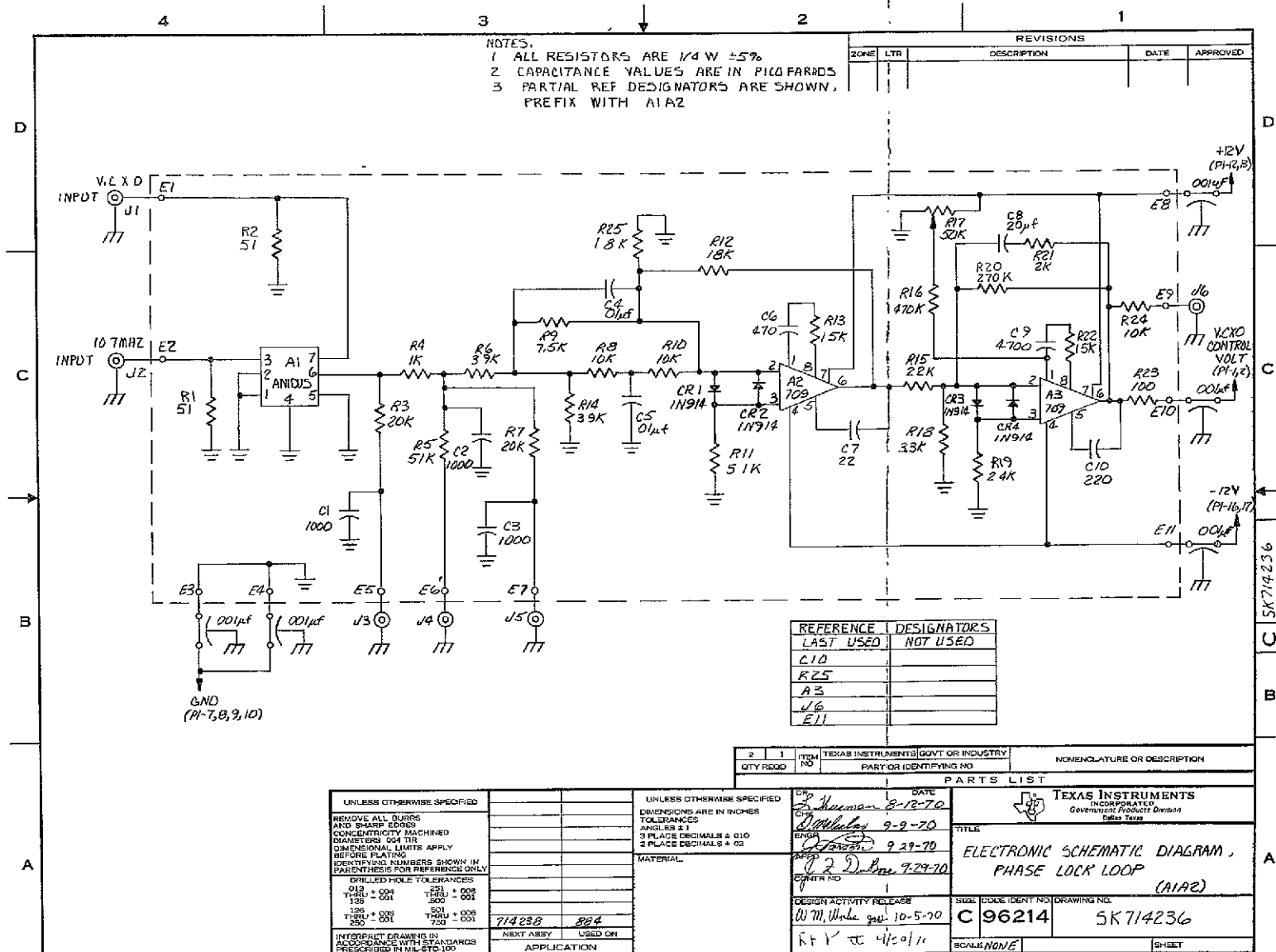


Figure C 10 Phase-Lock Loop, Schematic Diagram

6 Reference Oscillator (Figure C-11)

The reference oscillator is a crystal oscillator at 10.7 MHz. Two buffer stages are used to isolate the oscillator from load variations.

D Transmitter

The transmitter portion of the transponder accomplishes the following:

- Converts the incoming ranging signal to another frequency from the receive frequency.

- Amplifies the ranging signal to a usable level for transmission to the satellites.

In addition, the power amplifier section of the transmitter has to provide an automatic gain control output to feed back to the receiver. All stages in the transmitter signal path must operate linearly.

1 Third Converter (Figure C-12)

The IF amplifier output is at a frequency of 10.665 MHz, with the package of several tones on or adjacent to this frequency. The third converter takes the output of a local oscillator, triples it to 159 MHz, and feeds this into a mixer along with the 10.665-MHz output from the IF amplifier. The mixer output is filtered and then amplified for an output of -11 dBm at 149.22 MHz.

2 Power Amplifier Driver (Figure C-13)

The Power Amplifier (PA) driver section is an intermediate module between the third converter and the power amplifier. Its purpose is to boost the signal from the third converter to a sufficient level to drive the power amplifier. Since the output of this module is still at a relatively low level, +18 dBm, class A amplifier stages can still be used. Although the efficiency of each stage is not high (about 20 percent), the linearity is very good. The specification for the transmitter output linearity is an intermodulation distortion product suppression of 20 dB. Normally, there is a degradation of 6 dB in intermodulation distortion (IMD) per stage in a transmitter system. This implies that the first stage of the power amplifier module must have 26 dB of IMD suppression. For the PA driver, the third, second, and first stages must have 32-dB, 38-dB, and 44-dB IMD suppression, respectively. To achieve this kind of linearity, the use of class A amplifier stages is a necessity.

3 Power Amplifier (Figure C-14)

The power amplifier consists of a two-stage amplifier and an AGC detector and amplifier. As in the PA driver, the first stage of amplification is achieved using a class A amplifier. To obtain the required linearity at the output and still maintain a reasonable efficiency at an output power level of 4 watts, the final stage is operated in class AB. Along with yielding the linearity, these two stages together have enough gain to amplify the +16-dBm output from the PA driver to +38 dBm, this includes 2-dB loss in a bandpass filter inserted in the transmitter signal paths (Figure C-15). A level of +38 dBm must be obtained at the output to overcome another 2-dB loss in the duplexer.

TABLE C-1 TRANSPONDER SCHEMATIC DIAGRAMS

Diagram	Drawing Number	Figure
Third Converter	SK714216	C-12
Second Converter	SK713220	C-6
IF Filter	SK714224	C-7
Limiter	SK714228	C-9
Reference Oscillator	SK714232	C-11
Phase-Lock-Loop	SK714236	C-10
Dual IF Amplifier	SK714240	C-8
VHF Converter	SK714244	C-5
PA Driver	SK714248	C-13
Power Amplifier	SK714252	C-14
Transmitter Filter	SK714256	C-15
Duplexer	SK714258	C-4
DC Wiring	SK714266	C-16

The signal from the power amplifier output is detected and then amplified to provide a slow-release, dc, AGC control level to control the entire receiver-transmitter loop gain. The AGC circuit is designed with a long time constant so that the PA output level can go through a zero point with modulation and still not allow the loop gain to increase. If a weak signal is received in the receiver, the AGC control circuitry allows the loop gain to increase to compensate for the weak signal.

4 External Power Amplifier

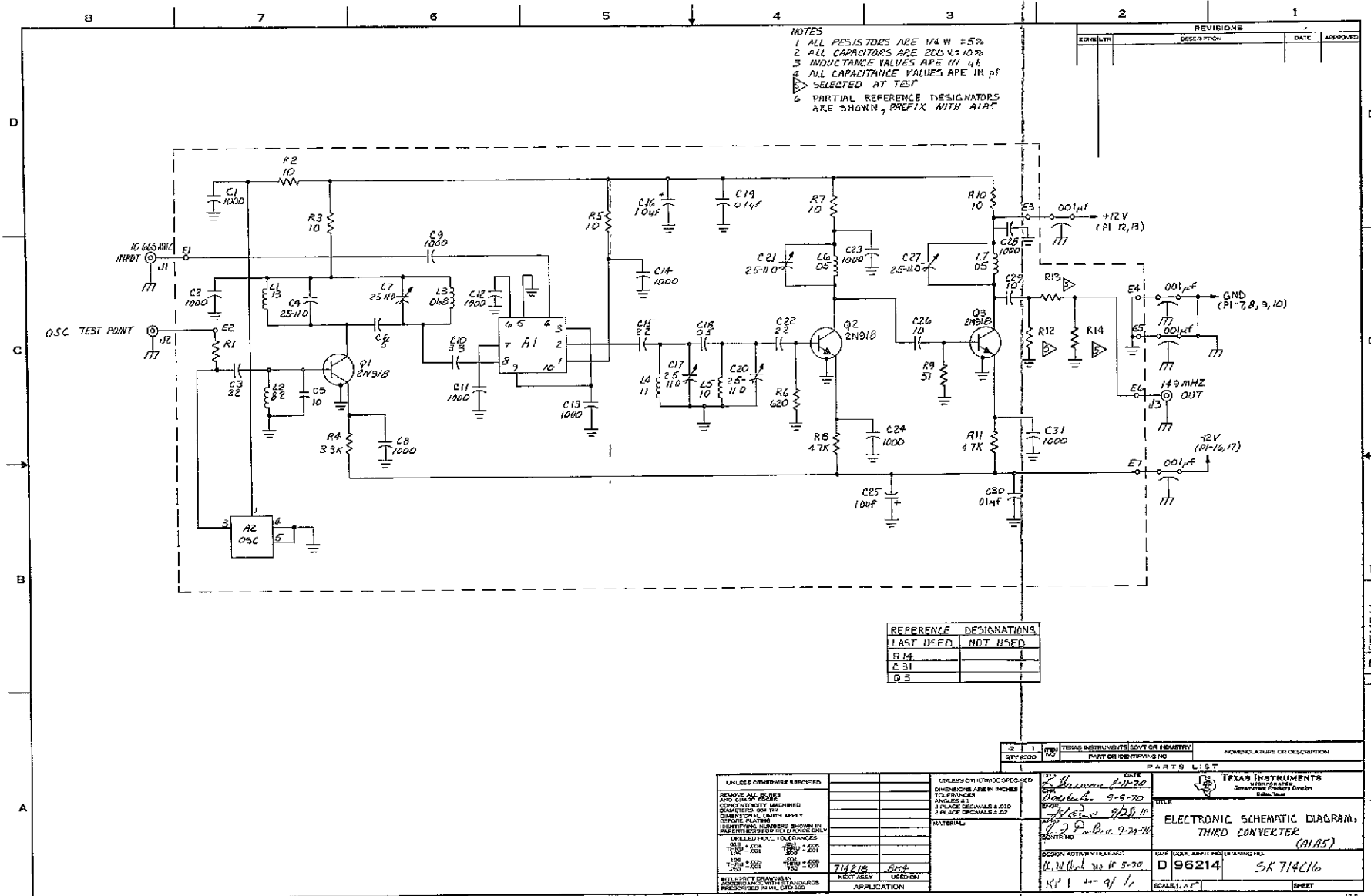
To improve the overall link for system tests, an external power amplifier was added to the basic transponder. This external PA was an unmodified commercial item produced by the Gonset Company. It is capable of 500 watts dc input power with better than 50-percent efficiency. The basic transponder output is more than adequate to drive the Gonset PA to the desired output. It was empirically determined that 30 watts into the antenna provided ample signal for the system link.

The Gonset PA has a 4 X 150 tube-type amplifier and was originally designed for 144- to 148-MHz service. A check with the manufacturer showed the PA to be operational up to 152 MHz.

II Transponder Schematic Diagrams

Schematic diagrams of the 12 modules are included in the following pages. A listing of the schematics is given in Table C-1.





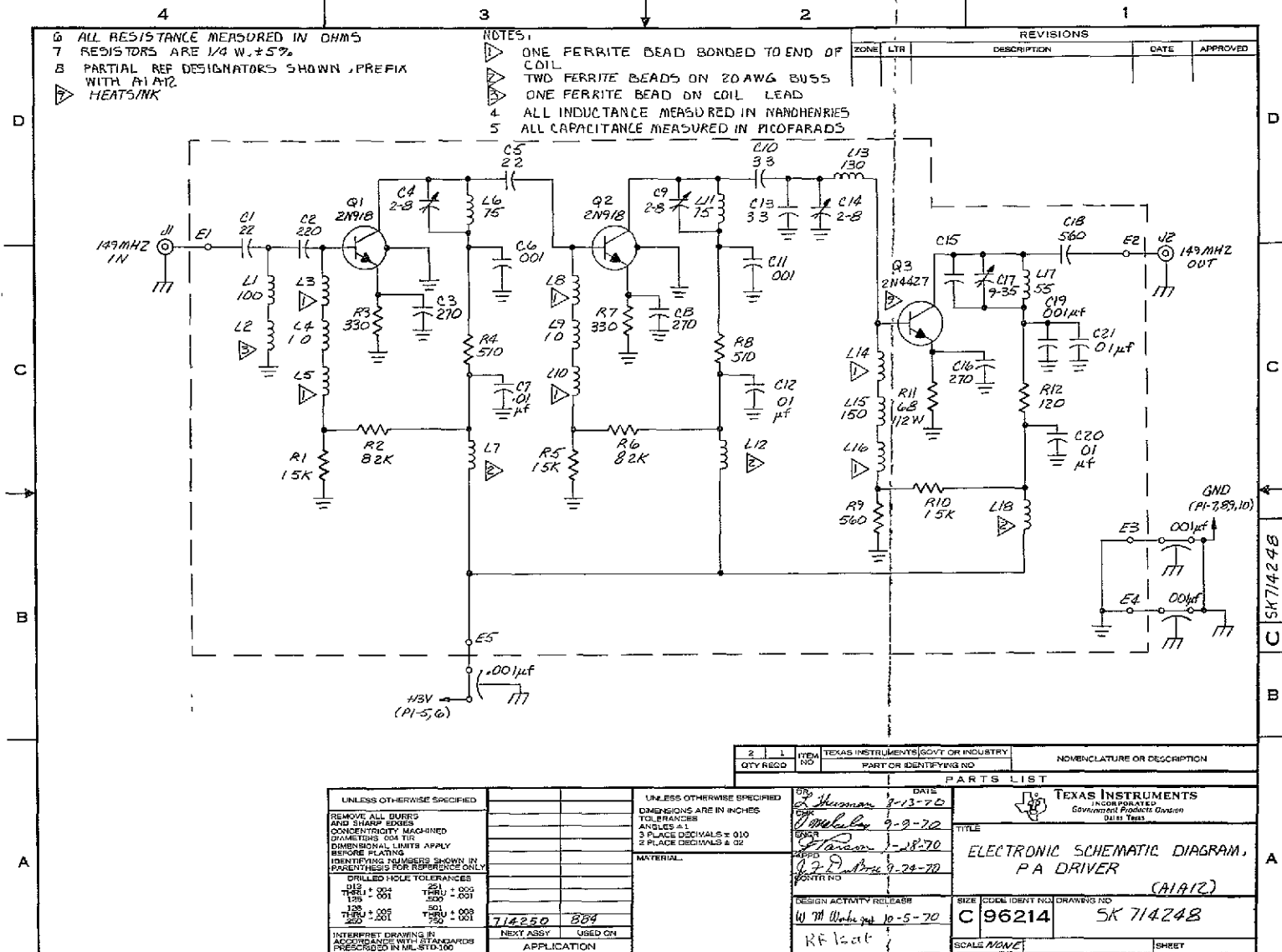
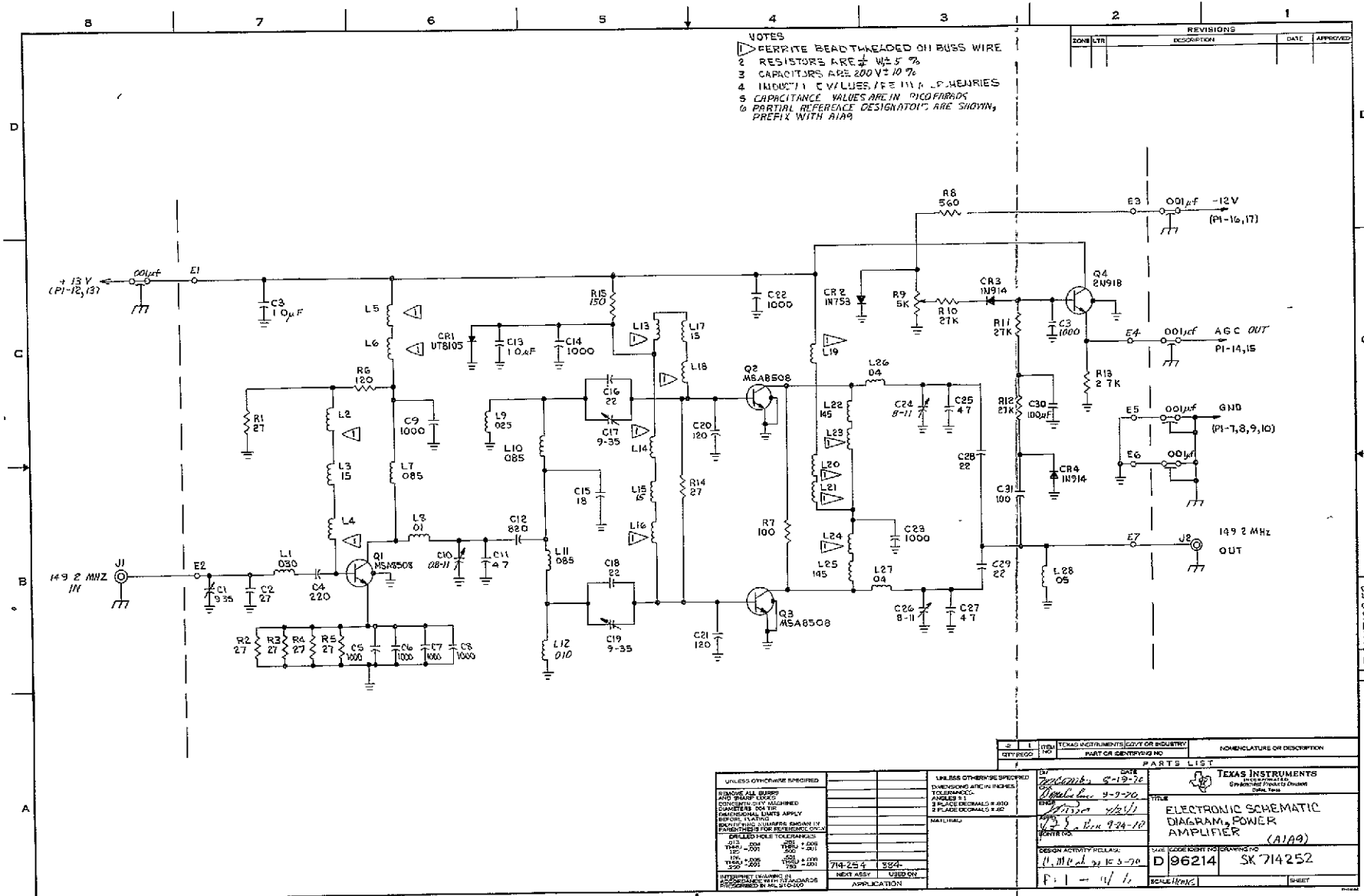
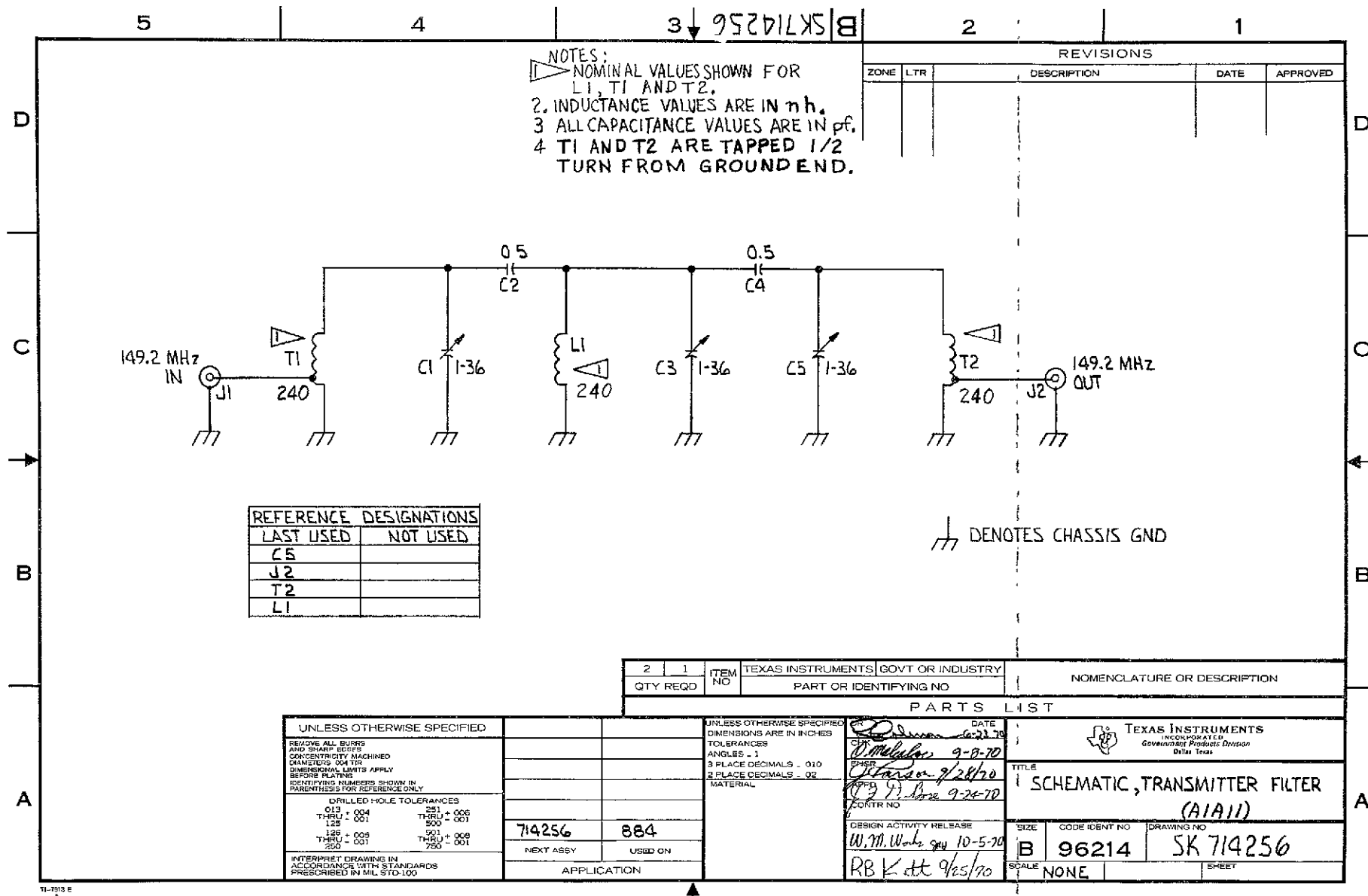
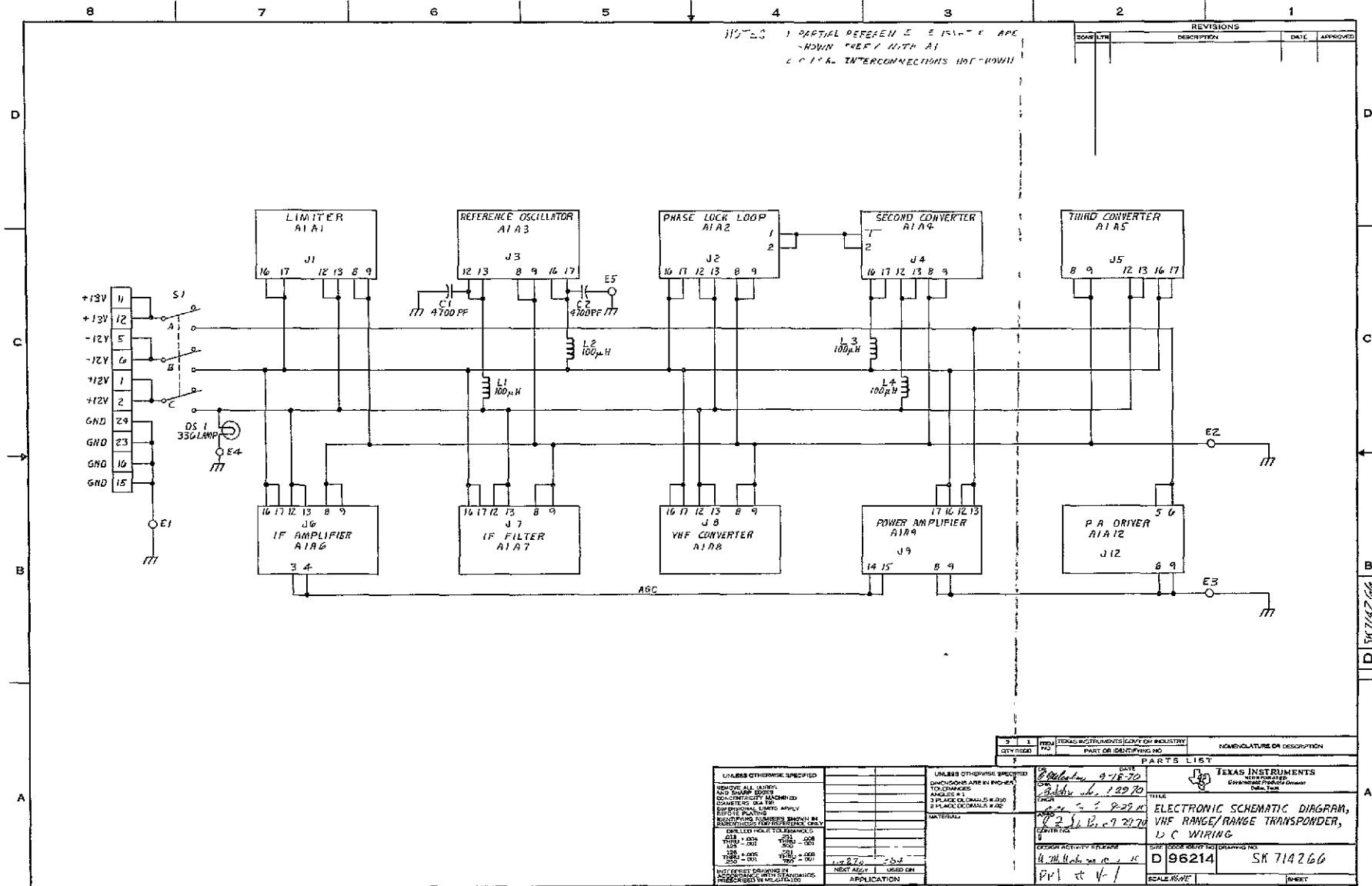


Figure C-13 Power Amplifier Driver, Schematic Diagram







APPENDIX D

POSITION ERROR ANALYSIS

As explained in Section III, the position of the aircraft is determined as the intersection of three spheres whose centers are located as follows: one sphere centered at ATS-1, one centered at ATS-3, and one centered at the earth's center. The parameters required for this position determination are the distances from the aircraft to each satellite and altitude of the aircraft. Errors in measuring or estimating these parameters lead to errors of position location, and the extent of these position errors is influenced by the system geometry through the Geometric Dilution of Precision (GDOP) Factor.

It is the purpose of this appendix to examine qualitatively and quantitatively the sources of error in the range determination and the ranging sensitivity to the various error sources for the position location technique using differential range measurements. These then lead to estimates of the position location errors, using calculated GDOP factors for the ATS-1 and ATS-3 satellites with an aircraft in the vicinity of Dallas, Texas.

I Sources of Error in Range Determination

The principal sources of error may be considered in four categories:

- 1 Propagation errors consisting of ionospheric and tropospheric effects and multipath effects
- 2 Measurement errors caused by system noise and ground processor inaccuracies
- 3 Delay errors caused by uncompensated delays of aircraft transponder, reference transponder, satellite transponders, and the ground processor
- 4 Satellite position uncertainty

A Propagation Errors

1 Ionospheric Effects

The effect of the ionosphere is to reduce the group velocity of the propagated wave and hence increase the path delay compared with that experienced in free space. The ranging error is a function of integrated electron density (I) and has been treated in detail in Reference 1 from which Table D-1 has been taken, showing the one- and two-way path errors produced at various satellite elevation angles over a range of integrated electronic densities. These are the errors to be expected in absolute ranging techniques, but this effect is largely removed if differential techniques are used.

Irregularities in the structure of the ionosphere also introduce signal amplitude fluctuations or scintillations. Midlatitude scintillations have been measured by Aarons and Whitney². Their data gives a 90 percentile/scintillation fade margin of 1.3 dB and 99 percentile value of 9.4 dB. The fading periods are distributed approximately as in Table D-2. Fading periods of several seconds are therefore to be expected frequently in the present experiment.

TABLE D-1 IONOSPHERIC RANGING ERROR

Satellite Elevation Angle (ϵ)	$I = 2 \times 10^{16} \frac{\text{elec}}{\text{m}^2}$		$I = 3 \times 10^{17} \frac{\text{elec}}{\text{m}^2}$		$I = 8.6 \times 10^{17} \frac{\text{elec}}{\text{m}^2}$	
	One-Way Path Error	Two-Way Path Error	One-Way Path Error	Two-Way Path Error	One-Way Path Error	Two-Way Path Error
$\epsilon = 20^\circ$	-0.16 km	-0.32 km	-2.6 km	-5.1 km	-6.5 km	-13.0 km
$\epsilon = 45^\circ$	-0.12 km	-0.25 km	-2.0 km	-4.0 km	-5.3 km	-10.7 km

TABLE D-2 MULTIPATH FADING PERIODS

Fading Period	Percentage of Occurrences
$T_s \leq 5$ seconds	43
$5 \text{ seconds} \leq T_s \leq 14$ seconds	29
$15 \text{ seconds} \leq T_s \leq 59$ seconds	28

2 Tropospheric Effects

For elevation angles (Ψ) greater than 10 degrees, the tropospheric refraction error is given to within 3 percent by

$$\Delta R_{\text{TROPO}} = \int (10^{-6} / \sin \Psi) N(h) dh$$

where $N = (n - 1) \times 10^6$, n being the index of refraction for air. For an aircraft at

5000 feet, and for $N_{\text{surface}} = 400$, the maximum tropospheric range error is 6 meters for satellite elevations of about 20 degrees, and hence is entirely negligible.

3 Multipath Effects

As described in Reference 3, multipath interference introduces both amplitude and frequency modulation to the direct path signal. The net result is amplitude fading and a time-varying phase shift that introduces a ranging error. For the satellite elevation angles of 20 to 40 degrees applicable to the present experiment in the vicinity of Dallas, Texas, the expected multipath ranging errors are approximately as shown in Table D-3.

These values were computed assuming the characteristics of the Dorne and Margolin Satecom antenna for reception of the direct and multipath signals.

TABLE D-3 MULTIPATH RANGING ERROR

Satellite Elevation	Type of Fading	Nominal Ranging Error for 941 Hz Tone
0-30 degrees	Specular	1.3 km
30-50 degrees	Diffuse	4.8 km

B Measurement Errors

1 System Noise Effects

Because of various noise sources in the ranging system and limitations of available signal power from the aircraft and satellite (principally the latter), limits

exist on the available signal-to-noise power density of the ranging signal returned to the ground station.

As described in Section III, the ranging method employed in this experiment involves measuring the delay imparted to the sidetone ranging signal (941 Hz) over the two-way ranging path (GCC-satellite-aircraft-satellite-GCC).

The variance of the estimate of the phase delay may be expressed as

$$\sigma_{\phi}^2 = \frac{1}{(2E/N_o)}$$

where

E = energy of sidetone integrated by the phase detection process

N_o = noise power density appearing at phase detector from all noise sources in the system

For a 1-second integrate and dump process

$$E/N_o = C/N_o$$

where C/N_o is the expected sidetone carrier to noise power density. The predicted values of C/N_o derived in Appendix E are shown in Table D-4 and have been converted to phase error and range error, using the fact that 1 degree represents 0.81 km for a 941-Hz tone. The values of phase error and ranging error shown in Table D-4 result from the integration of four 1-second samples of the expected signal at the output of the phase detectors.

TABLE D-4 SYSTEM NOISE RANGING ERROR

Predicted C/N _o	ϕ_{rms} (4 samples)	rms Range Error (941 Hz)
27 dB Hz (nominal)	0.86 degrees	0.7 km
23 dB Hz (threshold)	1.0 degree	0.81 km

2 System Instrumentation Effects

The phase detection process described in Section III has implicit measurement error due to departure of the phase detector characteristic from the theoretical. For the in-phase and quadrature analog phase detectors of the GCC (modified OCC)

a phase error of approximately 2 degrees may be attributed to this error source—instrumentation error. This is by no means the state-of-the-art accuracy of phase detectors, 0.1 degree being obtainable using digital phase detectors.

For the present application existing phase detectors (having 2-degree error) were available in the OPLE equipment. The range error due to this phase error decreases as frequency increases and for the 10.2-kHz tone used in OPLE, the error contributed was negligible. For the 941-Hz sidetone of the VHF Range/Range Experiment, the error in range due to the 2 degrees is

$$\begin{aligned} 2 \times 0.81 \text{ km} &= 1.62 \text{ km peak} \\ &= 1.2 \text{ km rms (approximately)} \end{aligned}$$

3 Delay Errors

a Aircraft Terminal Uncompensated Delay Effect

The effect of uncompensated time delay and phase shift variations expected to occur in the aircraft transponder is a ranging error of approximately 60 meters. This is the assumed random delay variations not removed by the differential techniques described earlier, which compensate for large static bulk delay differences between the aircraft transponder and reference transponders.

b Satellite Transponder Uncompensated Delay Effect

The nominal value of the satellite transponder group delay will be removed through simultaneous aircraft and reference terminal range measurements. The residual or uncompensated time delay which is caused by variations in the signal amplitude and frequency is conservatively estimated to be 0.1 microsecond corresponding to a range error of 30 meters.

c Ground Processor Delay Uncertainty

In a properly implemented differential ranging system (using TDM techniques) the uncertainty in ground processor delay would be similar to the residuals for aircraft transponder and satellite transponders. However, because of the frequency division multiplex scheme required for the present experiment, removal of bulk delay differences is not possible continuously. Therefore, the delays attributed to the GCC processing chain for the VHF R/R experiment are estimated to comprise a mean delay error effect of up to 1.5 km with standard deviation delay value of approximately 0.1 km. The mean effect can be viewed as slow drift in delay differences between receivers removed only in the calibration phase of the measurement; the variation of delay of 0.1 km is due to fluctuations in each channel, over the period of the measurement. In estimating the error from this source, only the rms error will be considered and the bias effect will be removed in the experimental data.

4 Satellite Position Uncertainty

Approximations to the satellite position error are made as follows:

Satellite Position Error, Latitude = 2 km

Satellite Position Error, Longitude = 1 km

This position uncertainty is resolved into along-range and cross-range error giving the following values:

Along range = 0.4 km

Across range = 2.0 km

II Range Error Budget

The budget of errors in the computed satellite-to-aircraft ranges is derived by

Computing sensitivity factors relating satellite-A/C range to the error sources for the differential master/slave configuration.

Applying the sensitivity factors to the source error allocations to determine error in computed range

A Error Sensitivity Factors

Reference is made to the Texas Instruments System Study report for Position Location and Aircraft Communications Equipment (PLACE)⁴ where the error sensitivity factors are computed in Appendix B Table D-5 of error sensitivity factors applies for the differential master/slave satellite configuration used in the VHF R/R experiment

TABLE D-5 ERROR SENSITIVITY FACTORS

Error Source	Sensitivity Factor	
	Satellite 1	Satellite 2
Link Noise	0.707	1.58
Terminal Delay	0.707	0.707
Ground Processor Delay	0.707	0.707
Satellite Transponder Delay	1.0	1.73
Satellite Position		
Along Range	0.008	0.008
Across Range	0.13	0.13
Atmospheric Effects	1.41	1.41
Multipath Effects		
Satellite-to-A/C	0.5	0.5
A/C to-Satellite	0.5	1.1

b RMS Errors in Derived Satellite-to-Aircraft Ranges

The errors are obtained by applying the sensitivity factors of Table D-5 to the allocated values of source errors discussed in Section I of this Appendix. The rms errors are summarized in Table D-6. It should be noted that two error totals are included. The first excludes atmospheric and multipath effects and will apply to static experiments in which the bias term is removed and the deviation of the error measured. The second total applies to flight tests in which the bias errors are removed.

III Position Location Errors

A Geometric Dilution of Precision (GDOP) Factors

Errors in the derived aircraft-to-satellite ranges are reflected as position location errors in latitude and longitude. The relationship between these two is referred to as GDOP effect. The GDOP factors are most easily computed by calculating first the equivalent radial errors of the two circles of position centered at the subsatellite points, and then resolving these two errors into latitude and longitude errors using results for the intersection of two circles.

The ratio of radial error from the subsatellite point along a great circle, to the satellite-to-aircraft range error is given by

$$\frac{\text{Radial error}}{\text{Range error}} = \frac{1}{\cos \psi}$$

where ψ = elevation angle of the satellite. Resolving this error into latitude and longitude components gives the following relationships

$$\frac{[\text{Latitude Error}]_1}{\Delta R_1} = \frac{1}{\cos \psi_1} \frac{\cos \beta_2}{\sin (\beta_1 + \beta_2)}$$

$$\frac{[\text{Longitude Error}]_1}{\Delta R_1} = \frac{1}{\cos \psi_1} \frac{\sin \beta_2}{\sin (\beta_1 + \beta_2)}$$

where

ΔR_1 = range error to satellite 1

β_1 = angle at the subsatellite 1 point between the equator and the aircraft

β_2 = angle at the subsatellite 2 point between the equator and the aircraft

For the period of the experiment, the values that applied to satellite 1 (ATS-3) and satellite 2 (ATS-1) from Dallas were

$\Psi_1 = 24$ degrees

$\beta_1 = 33.5$ degrees

$\Psi_2 = 21$ degrees

$\beta_2 = 32$ degrees

The GDOP factors for each satellite are thus approximately the same and are equal to

$$\frac{\text{Latitude Error}}{\Delta R} = 1.02$$

$$\frac{\text{Longitude Error}}{\Delta R} = 0.64$$

These factors are expressed without sign, however, the direction of the position errors depends on the direction of the ranging errors. Signs can be ignored for estimating rms errors, however, the direction of residual bias errors and their magnitude depends on the polarities of range errors for each satellite.

B Predicted Position Location Errors

The rms position errors can be estimated using the predicted range errors shown in Table D-6 and the appropriate GDOP factors. These results for flight experiments are

Satellite 1

Latitude error = 2.85 km = 1.5 nm

Longitude error = 1.8 km = 1.0 nm

Satellite 1

Latitude error = 4.3 km = 2.3 nmi

Longitude error = 2.7 km = 1.5 nmi

Assuming independence for these position errors, the expected latitude and longitude errors for a flight experiment are

Latitude error = 2.75 nmi

Longitude error = 1.75 nmi

For static tests, it can be assumed that ionospheric and multipath terms will appear as bias effects, and hence in evaluating the deviation of position error with respect to the mean position error, these error sources can be neglected. In this case, the composite errors are

Latitude error = 1.50 nmi

Longitude error = 0.93 nmi

TABLE D-6 PREDICTED RMS ERRORS IN SATELLITE TO-AIRCRAFT RANGES

Error Source	Sensitivity Factors		Error Allocation (km)		RMS Error (km)	
	Sat 1	Sat 2	Sat 1	Sat 2	Sat 1	Sat 2
Link Noise	0.707	1.58	0.81	0.81	0.56	1.25
Instrumentation Error	0.707	1.58	1.2	1.2	0.84	1.9
Terminal Delay	0.707	0.707	0.06	0.06	—	—
Ground Processor Delay (excluding residual bias)	0.707	0.707	1.0	1.0	0.7	0.7
Satellite Transponder Delay	1.0	1.73	0.03	0.03	—	—
Satellite Position						
Along Range	0.008	0.008	0.4	0.4	—	—
Across Range	0.13	0.13	2.0	2.0	0.26	0.26
RMS Error for Static Experiments* →					1.25 km	2.4 km
Atmospheric Effects	1.41	1.41	1.3	1.3	1.82	1.82
Multipath Effects (30°)						
Satellite to A/C	0.5	0.5	2.5	2.5	1.25	1.25
A/C-to-Satellite	0.5	1.1	2.5	2.5	1.25	2.75
RMS Error for Flight Experiments* →					2.8 km	4.2 km

* This neglects bias effects, see text

APPENDIX E

RF LINK ANALYSIS

I Introduction

The components of the RF links in the VHF Navigation Experiment include the GCC transmitter and receivers, the ATS-1 and ATS-3 VHF repeaters, and the aircraft and reference transponders. The performance of the RF system is determined primarily by the power levels of the transmitted signal, the output power of the repeaters, the noise characteristics of the receivers, and the effective link losses between the different components of the system. Figure E-1 illustrates these components and their relationship to the various link losses found in this experiment configuration. This analysis includes a listing of the individual losses and gains which comprise each link loss, the derivation of power sharing equations and calculation of expected C/N values at the transponders and GCC receivers. The determination of the C/N values at the GCC receivers facilitates the prediction of noise-related errors in the measured sidetone phase.

II Link Losses

The predicted nominal worst case up-link losses are listed in Table E-1 and the down-link losses are listed in Table E-2. To reduce the number of uncertainties from the loss budget parameters, such uncertainties as diplexer loss and cable loss were measured rather than estimated. The aircraft antenna data was taken from the manufacturers' data³ as were the characteristics of the reference transponder Loop-vee Antenna⁴. The fade margins included in the losses account for multipath and ionospheric scintillation effects and were taken from the ATS-1/ATS-3 Dual Satellite Navigation Study⁵. The free space losses between the transponders and both satellites were assumed to be the same. Since the transponder power was measured after the diplexer, the diplexer loss is not included in the transponder/satellite up-link loss.

III Power Sharing

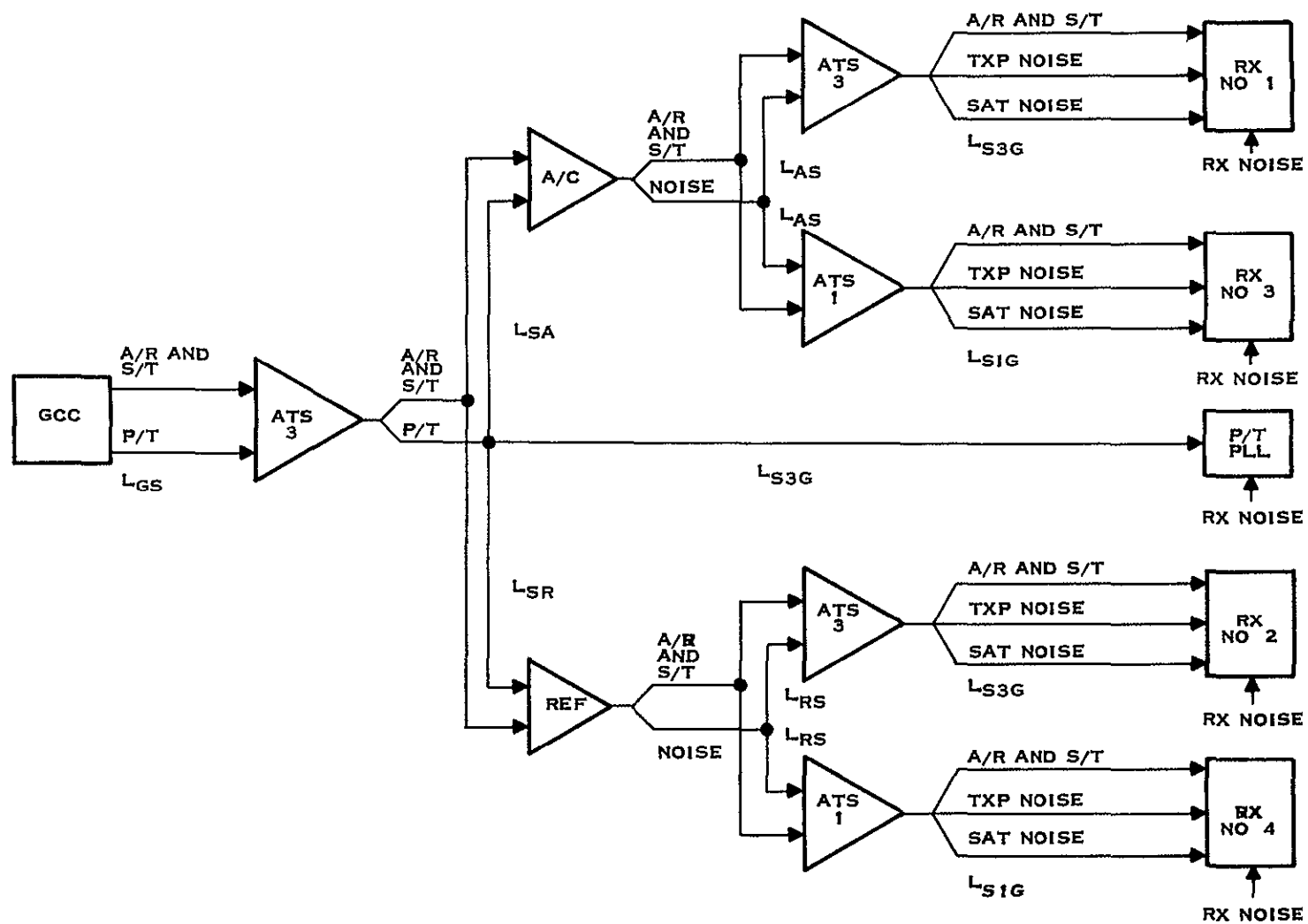
The total IF output power available from each repeater is divided among all input signals and receiver noise. As shown in Figure E-1, the input signals to each of the four repeaters are as follows:

ATS-3

- A/R sidetone, and pilot tone, signals transmitted by the GCC
- A/R sidetone signals relayed by both transponders
- Transmitted transponder noise
- Satellite noise and interference

ATS-1

- A/R and sidetone signals relayed by both transponders
- Transmitted transponder noise
- Satellite noise and interference



Transponders

Satellite relayed A/R and sidetone signals

Receiver noise

Satellite transmitted noise

Because of the relatively high link loss between the ATS-3 and the transponders, the transmitted satellite noise can be neglected in determining the total input power to the transponders

TABLE E-1 UP LINK LOSSES (149.2 MHz)

Parameter	Nominal (dB)	Worst Case (dB)
Common Losses		
Path Loss	-168.5	-169.7
Polarization Loss	- 3	- 4
Satellite Receiver Antenna Gain	8	8
Satellite Receiver Losses	- 1.8	- 1.8
TOTAL	-165.3	-167.5
GCC-to ATS 3 (L _{GS})		
Cable Loss	- 1.7	- 1.7
Diplexer Loss	- 2	- 2
GCC Antenna Gain	13	13
Fade Margin	- 1	- 3
TOTAL	-157.0	-161.2
Aircraft-to-Satellites (L _{AS})		
Cable Loss	- 1	- 1
Aircraft Antenna Gain	0	0
Aircraft Antenna Ellipticity	- 3	- 3
Fade Margin (includes multipath)	- 2	- 7
TOTAL	-171.3	-178.5
Reference-to-Satellites (L _{RS})		
Cable Loss	- 2	- 2
Loop-Vee Antenna Gain	0	0
Loop-Vee Antenna Ellipticity	- 4	- 4
Fade Margin	- 1	- 3
TOTAL	-172.3	-176.5

It was assumed that the RF output power of each repeater is constant. Thus, if the repeater has a power output of P_R and has no input signal, the repeater transmits P_R watts of noise.

Based on the assumptions in the previous paragraph, the power of a transponded signal is related to its received power by

$$P_o = \frac{P_i P_R}{P_T} \quad (E-1)$$

where

P_o = power level of the output signal

P_i = power level of the input signal

P_T = sum of all input signals including receiver noise

P_R = repeater output power

TABLE E-2 DOWN LINK LOSSES (135.6 MHz)

Parameter	Nominal (dB)	Worst Case (dB)
Common Losses		
Path Loss	-167	-168
Polarization Loss	- 3	- 4
Satellite Transmitter Antenna Gain	8.5	8.5
Satellite Transmitter Losses	- 1.7	- 1.7
TOTAL	-163.2	-165.2
ATS-3-to-GCC (L_{S3G})		
Fade Margin	- 1	- 3
GCC Antenna Gain	+ 13	+ 13
Diplexer Loss	- 4.5	- 4.5
TOTAL	-155.7	-159.7
ATS-1-to-GCC (L_{S1G})		
Fade Margin	- 1	- 3
GCC Antenna Gain	+ 13	+ 13
Diplexer Loss	- 3	- 3
TOTAL	-154.2	-158.2
ATS-3 to Aircraft (L_{SA})		
Fade Margin (includes multipath)	- 2	- 7
Aircraft Antenna Gain	0	0
Aircraft Antenna Ellipticity	- 3	- 3
Cable Loss	- 1	- 1
Diplexer Loss	- 2	- 2
TOTAL	-171.2	-178.2
ATS-3-to Reference (L_{SR})		
Fade Margin	- 1	- 3
Loop-Vee Antenna Gain	0	0
Loop-Vee Antenna Ellipticity	- 2.5	- 2.5
Cable Loss	- 2	- 2
Diplexer Loss	- 2	- 2
TOTAL	-170.7	-174.7

If the powers are expressed in dBm, Equation (E-1) can be written as

$$P_o(\text{dBm}) = (P_i(\text{dBm}) + P_R(\text{dBm}) - \dot{P}_T(\text{dBm})) \quad (\text{E-2})$$

Developing this expression further, it can be shown that the dBm level of a signal at any point in the link is given by

$$P_{sig} = P_{trans} + \Sigma P_R - \Sigma L - \Sigma P_{it} \quad (\text{E-3})$$

where all powers are expressed in dBm and losses in dB and

P_{trans} = the power level of the signal at its source

ΣP_R = summation of the output power of all the repeaters through which the signal has passed

ΣP_{it} = summation of the total input power to each of the repeaters

ΣP_L = summation of the link losses through which the signal has passed

In determining the total noise power density at the four GCC receivers, the transponder noise was treated as a separate signal transmitted from the transponder and Equation (E-3) was applied to determine the transponder noise level at the GCC. The satellite internal noise was treated in the same manner. The dBm levels of satellite, transponder, and receiver noise power densities were converted to watts/Hz, summed and then reconverted to a dBm/Hz value. The internal noise power density in the transponders and GCC receivers was calculated by

$$N_o = K/L [T_s + T_o (LF - 1)] \text{ (watts/Hz)} \quad (\text{E-4})$$

$$= k T_{eq} \text{ (dBm)} - L(\text{dB}) \text{ (dBm/Hz)} \quad (\text{E-5})$$

where

K = Boltzmann Constant

$$= 1.37 \times 10^{-23} \text{ J/}^\circ\text{K}$$

T_s = antenna temperature

$$= 2.61 \times 10^7 / f^2 \text{ MHz (}^\circ\text{K)}$$

T_o = standard temperature

$$= 290^\circ\text{K}$$

L = attenuation between the antenna output and the preamplifier

F = noise figure of the preamplifier

$$T_{eq} = T_s + T_o (LF - 1)$$

This expression assumes that the attenuator (duplexer and cables) are at standard temperature. The satellite noise power density is composed of thermal noise in addition to interference. Past experience has indicated that for power-sharing purposes the total noise power in the satellite 100-kHz bandwidth is approximately -113 dBm which corresponds to a noise power density of

TABLE E-3 POWER SHARING PARAMETERS

Parameter	Value	Units
Satellite Output Power (P_s)	46	dBm
Satellite Noise Power Density (N_{OS})	-163	dBm/Hz
Satellite Bandwidth (100 kHz)	50	dB Hz
Transponder Output Power (P_T)	43	dBm
Transponder Noise Power Density (N_{OT})	-168	dBm/Hz
Transponder Bandwidth (8 kHz)	39	dB Hz
GCC Pilot Tone Power (P_{PT})	44	dBm
GCC Acquisition A/R Tone Power (P_{AR})	47.4	dBm

-163 dBm/Hz The actual noise power density in certain sections of the bandwidth can be less than this figure since the noise power contributed by interference tends to be concentrated in certain channels within the total bandwidth. The parameters used in conjunction with the link losses to determine power sharing are listed in Table E-3.

The components of the total input power to ATS-3 (P_{IS3}) are given by

$$\text{GCC Transmitted Tones} = P_{GCC} - L_{GS} \quad (E-6)$$

Aircraft Transponder

$$\text{Signal} = P_T - L_{RS} \quad (E-7)$$

Reference Transponder

$$\text{Signal} = P_T - L_{AS} \quad (E-8)$$

$$\text{Satellite Noise} = N_S$$

where P_{GCC} = power transmitted by the GCC. The components of the total input power to ATS-1 (P_{IS1}) are the same as for ATS-3 provided the GCC transmitted tones are deleted.

The amount of satellite power allocated to each input signal can be calculated once the total input power is known. The power levels of the A/R and pilot tone signals transmitted from ATS-3 can be expressed as

$$P_{ARS} = P_{AR} + P_S - L_{GS} - P_{IS3} \quad (E-9)$$

$$P_{PTS} = P_{PT} + P_S - L_{GS} - P_{IS3} \quad (E-10)$$

The power level of the A/R signal at the transponders can be determined by subtracting the appropriate link loss from P_{ARS} . The total input power to the aircraft transponder (P_{IA}) and to the reference transponder (P_{IR}) is the sum of the A/R signal and the transponder noise.

The effects on power sharing caused by variations in the link losses are illustrated in Table E-4. Table E-5 lists, for each repeater, the percentage of total power allocated to each input signal for nominal link losses. For the worst case link losses, the percentage of power allocated to each received signal would be slightly less since the received signals are attenuated by a larger factor while the input noise remains constant.

IV Carrier-to-Noise Ratios

The equations developed for calculating the carrier-to-noise ratio at the transponders and at the GCC are direct applications of Equation (E-3). As explained in the previous section, the only noise source considered at the transponder is the combined antenna and transponder noise. At the four GCC receivers, the total noise is the sum of receiver noise, satellite noise, and transponder noise.

TABLE E-4 EFFECTS OF LINK LOSSES ON POWER SHARING

Parameter	Nominal (dBm)	Worst Case (dBm)
ATS-3 Input Power		
GCC Tone Package	-108.3	-112.2
Aircraft Transponder Signal	-128.3	-135.5
Reference Transponder Signal	-129.3	-133.5
Satellite Noise	-113	-113
TOTAL (P_{IS3})	-107	-109.6
ATS-3 Output Power		
Pilot Tone	39.9	38.4
A/R Tone	43.3	41.8
Satellite Noise	40	42.6
Aircraft Transponder Signal	24.7	20.1
Reference Transponder Signal	23.7	22.1
ATS-1 Input Power		
Aircraft Transponder Signal	-128.3	-135.5
Reference Transponder Signal	-129.3	-133.5
Satellite Noise	-113	-113
TOTAL (P_{IS1})	-112.8	-113
ATS 1 Output Power		
Aircraft Transponder Signal	30.5	23.5
Reference Transponder Signal	29.5	25.5
Satellite Noise	45.8	45.9
Aircraft Transponder Input Power		
A/R Tone	-128.1	-136.4
Transponder Noise	-129	-129
TOTAL (P_{IA})	-126.4	-128.2
Aircraft Transponder Output Power		
A/R Tone	41.3	34.8
Transponder Noise	40.4	42.2
Reference Transponder Input Power		
A/R Tone	-127.4	-132.9
Transponder Noise	-129	-129
TOTAL (P_{IR})	-125	-127.4
Reference Transponder Output Power		
A/R Tone	40.6	37.5
Transponder Noise	39	41.4

The carrier-to-noise power ratio for the pilot and A/R tones at the aircraft are given by

$$C/N (A/R) = P_{ARS} - L_{SA} - N_{OT} - 39 \text{ dB-Hz} \quad (E-11)$$

$$C/N (PT) = P_{PTS} - L_{SA} - N_{OT} - 18.4 \text{ dB-Hz} \quad (E-12)$$

and at the reference terminal by

$$C/N (A/R) = P_{ARS} - L_{SR} - N_{OT} - 39 \text{ dB-Hz} \quad (E-13)$$

$$C/N (PT) = P_{PTS} - L_{SR} - N_{OT} - 18.4 \text{ dB-Hz} \quad (E-14)$$

**TABLE E-5 POWER ALLOCATION
(NOMINAL LINK LOSSES)**

Repeater/Input Signal	Percentage
ATS-3	
GCC A/R Tone	50
GCC Pilot Tone	25
Satellite Noise	23.5
Transponder Signals	1.5
ATS-1	
Transponder Signals	5
Satellite Noise	95
Transponders	
A/R Tone	50
Transponder Noise	50

Since the pilot tone C/N was to be experimentally determined by measuring the filtered rms phase detector output voltage in the pilot tone phase lock-loop, the 70-Hz bandwidth ($2 B_{AL}$) of the loop was used. For the A/R tone the C/N was calculated for the 8-kHz transponder IF bandwidth.

The power levels of the A/R tone at each of the four GCC receivers are given by the following four equations:

$$P_{AR1} = P_{ARS} + P_T + P_S - L_{SA} - L_{AS} - L_{S3G} - P_{1A} - P_{1S3} \quad (E-15)$$

$$P_{AR2} = P_{ARS} + P_T + P_S - L_{SA} - L_{AS} - L_{S1G} - P_{1A} - P_{1S1} \quad (E-16)$$

$$P_{AR3} = P_{ARS} + P_T + P_S - L_{SR} - L_{RS} - L_{S3G} - P_{1R} - P_{1S3} \quad (E-17)$$

$$P_{AR4} = P_{ARS} + P_T + P_S - L_{SR} - L_{RS} - L_{S1G} - P_{1R} - P_{1S1} \quad (E-18)$$

The dBm/Hz values of the transponder noise power density transmitted to the GCC receivers are as follows:

$$N_{OT1} = N_{OT} + P_T + P_S - L_{AS} - L_{S3G} - P_{1A} - P_{1S3} \quad (E-19)$$

$$N_{OT2} = N_{OT} + P_T + P_S - L_{RS} - L_{S3G} - P_{1R} - P_{1S3} \quad (E-20)$$

$$N_{OT3} = N_{OT} + P_T + P_S - L_{AS} - L_{S1G} - P_{1A} - P_{1S1} \quad (E-21)$$

$$N_{OT4} = N_{OT} + P_T + P_S - L_{RS} - L_{S1G} - P_{1R} - P_{1S1} \quad (E-22)$$

The transmitted satellite noise power density received by each of the GCC receivers can be determined by:

$$N_{OS1} = N_{OS2} = N_{OS} + P_S - L_{S3G} - P_{1S3} \quad (E-23)$$

$$N_{OS3} = N_{OS4} = N_{OS} + P_S - L_{S1G} - P_{1S1} \quad (E-24)$$

REFERENCES

- 1 Texas Instruments Incorporated, *Systems Study Report for the Position Location and Aircraft Communications Equipment (PLACE) Ground Equipment*, Report No DR 973040 2, Volume I, Dallas, Texas, 1970
- 2 J Aarons and H E Whitney, "Ionospheric Scintillation at 135 MHz from a Synchronous Satellite," *Planetary and Space Science*, Vol 16, 1968, pp 21-28
- 3 Dorne and Margolin, Inc , *Technical Data for Dorne and Margolin, Inc , Satcom Antennas DM C33-2 and DM C34-1*, D E Nelson, Report 300 115, Bohemia, N Y , 5 May 1968
- 4 Electronics Communications, Incorporated, *Final Report for Project QPLE*, Report to NASA/GSFC under Contract NAS 5-10447, St Petersburg, Florida, 28 January 1968
- 5 Texas Instruments Incorporated, *ATS-1/ATS-3 Dual Satellite Navigation Study*, Report to NASA/GSFC under Contract No NAS 5 21163, Dallas, Texas, January 1971

**TABLE E-6 DETERMINATION OF ANTICIPATED PILOT AND
A/R TONE C/N VALUES FOR ACQUISITION MODE**

Parameter	Nominal	Worst Case	Units
ATS-3 Transmitted Signals			
A/R Tone	43.3	41.8	dBm
Pilot Tone	39.9	38.4	dBm
Aircraft Transponder			
Noise Power Density	-168	-168	dBm/Hz
A/R Tone			
Received A/R Tone Power	-128.1	-136.4	dBm
C/N (8 Hz)	0.9	-7.4	dB
Pilot Tone			
Received Pilot Tone Power	-131.2	-139.8	dBm
C/N (70 Hz)	18.4	9.8	dB
C/N ₀	36.8	28.2	dB Hz
Reference Transponder			
Noise Power Density	-168	-168	dBm/Hz
A/R Tone			
Received A/R Tone Power	-127.4	-132.9	dBm
C/N (8 kHz)	1.6	-3.9	dB
Pilot Tone			
Received Pilot Tone Power	-130.7	-136.3	dBm
C/N (70 Hz)	18.9	13.3	dB
C/N ₀	37.3	31.7	dB Hz
GCC Pilot Tone			
Received Satellite N ₀	-165.7	-167.7	dBm/Hz
Internal N ₀	-168.1	-168.1	dBm/Hz
Total N ₀	-163.8	-164.8	dBm/Hz
Received Pilot Tone Power	-115.7	-121.9	dBm
C/N (300 Hz)	23.3	18.1	dB
C/N ₀	48.3	43.1	dB Hz
GCC A/R Tone			
Receiver No. 1			
Received Transponder N ₀	-172.6	-183	dBm/Hz
Received ATS-3 N ₀	-165.7	-167.7	dBm/Hz
Internal N ₀	-168.1	-168.1	dBm/Hz
Total N ₀	-163.2	-164.8	dBm/Hz
Received A/R Power	-132.4	-148.4	dBm
C/N (100 Hz)	10.8	-3.6	dB
C/N ₀	30.8	26.4	dB Hz
Receiver No. 2			
Received Transponder N ₀	-175	-178.6	dBm/Hz
Received ATS-3 N ₀	-165.7	-167.7	dBm/Hz
Internal N ₀	-168.1	-168.1	dBm/Hz
Total N ₀	-163.4	-164.6	dBm/Hz
Received A/R Power	-134.3	-143.7	dBm
C/N (100 Hz)	9.1	0.9	dB
C/N ₀	29.1	20.9	dB Hz
Receiver No. 3			
Received Transponder N ₀	-165.3	-174.5	dBm/Hz
Received ATS-1 N ₀	-158.4	-162.4	dBm/Hz
Internal N ₀	-167.5	-167.5	dBm/Hz
Total N ₀	-157.2	-161	dBm/Hz
Received A/R Power	-125.1	-142.9	dBm
C/N (100 Hz)	12.1	-1.9	dB
C/N ₀	32.1	18.1	dB/Hz
Receiver No. 4			
Received Transponder N ₀	-167.7	-173.3	dBm/Hz
Received ATS-1 N ₀	-158.4	-162.4	dBm/Hz
Internal N ₀	-167.5	-167.5	dBm/Hz
Total N ₀	-157.4	-161	dBm/Hz
Received A/R Power	-127.1	-138.2	dBm
C/N (100 Hz)	10.3	2.8	dB
C/N ₀	30.3	22.8	dB/Hz

The total noise power density is then the sum of the received and internal noise power densities. The application of the derived equations, considering both nominal and worst case link losses, is illustrated in Table E-6. Referring to the noise power density components for the four receivers, Table E-6 indicates that transmitted satellite noise is the major noise source and exceeds the receiver and antenna noise by a factor of 2 for the ATS-3 channel and by a factor of 10 for the ATS-1 channel.

The A/R and sidetone phase mode carrier-to-noise power ratio corresponding to the A/R acquisition mode carrier-to-noise power density ratios can be determined when necessary by noting that during the ranging mode, the total power in the A/R and sidetones is equal to the A/R tone power during the acquisition mode. In addition, the A/R tone power is set 2 dB below the sidetone power.